Synthesis, Characterization, and Application of Silicon and Cu/Ge Nanomaterials

by

Yi Zhai

A thesis submitted in partial fulfillment of the requirements for the degree of

Master of Science

Department of Chemistry
University of Alberta

Abstract

Silicon nanocrystals (SiNCs) have been suggested as promising candidates for bioimaging because of their abundance, biocompatibility, and stable photoluminescent properties. However, "naked" SiNCs are insoluble in water and very reactive. As a result, NC surface functionalization is necessary to induce stability – fortunately this also offers the opportunity to target specific cell structures for imaging. This present thesis describes the preparation of photoluminescent D-mannose and L-alanine functionalized SiNCs obtained from the chlorination of hydride-terminated Si-NCs followed by reaction with appropriate carbohydrate and amino acid modifiers. Detailed characterization of the prepared nanoparticles was performed. Water soluble mannose and alanine functionalized SiNCs can be internalized by MCF-7 human breast cancer cells as shown in the detailed cell imaging studies.

Copper germanide is an appealing metallization material for Si-based devices due to the low resistivity and oxidatively stable up to 520 °C. A synthetic method of copper-germanium alloy (Cu_3Ge and $Cu_{0.85}Ge_{0.15}$) nanocrystals is described within this thesis. Copper-germanium alloy nanocrystals have been prepared by synthesis of Cu/GeO_2 core shell nanocrystals ($Cu@GeO_2$) followed by reductive thermal annealing process. This method affords freestanding, diameters of 70-300 nm copper-germanium alloy nanocrystals depend on the annealing temperature.

This thesis is dedicated to my parents,
Jianchang Zhai and Xiaolin Sun

Acknowledgements

I would never have been able to finish my degree without the guidance of my supervisor and committee members, help from friends, and support from my family during these past three years.

First and foremost, I would like to express my sincere gratitude to my supervisor Dr. Jonathan Veinot for the continuous support of my Master study and research. His excellent guidance, caring, and patience were key motivations throughout my Master. Jon has been supportive and has given me the freedom to pursue various projects without objection. I wish to thank my supervisory committee members Drs. Arthur Mar and Mark McDermott for their great advice and insightful comments to help me make this thesis come together.

I would like to acknowledge academic and technical support from Wayne Moffat (Analytical Services), Kai Cui (TEM), Dmitri Karpuzov (XPS), Shihong Xu (AES), George Braybook (SEM) and Gareth Lambkin (Biological Services). It would not have been possible to write this thesis without your help and support.

I would like to thank Dr. Mita Dasog, Dr. Zhenyu Yang, Leah Coumont, Dr. Tapas Purkait, Christina Gonzales, Dr. Muhammad Iqbal, Regina Sinelnikov, Lida Hadidi, Maryam Aghajamali, Morteza JavadiCharani, and Krishna Ramachandran for their continued help and support throughout this process. I would especially like to thank Dr. Mita Dasog and Dr. Tapas Purkait, you are always there for my drop by questions and gave me so much support for my research.

I would like to thank chemistry department staff members, Anita Weiler, Bonnie Gover, Laura Pham, Bernie Hippel and Bonnie Gover, Ryan Lewis, and Esther Moibi for all their help.

I would also like to thank my collaborators - Ryan Snitynsky, Allison Hahn, Dr. Christopher Sturdy, and Dr. Todd Lowary. This work would not have been possible without the technical expertise of you.

Most importantly, I would like to thank my family for their endless love and unconditional support throughout my life. I am grateful to my parents, who supported me emotionally and financially. The every week video talks are our only connections in these past five years during my study in Canada, but the talk with you always make me feel warm and happy. I always knew that you believed in me and wanted the best for me. None of this would have been possible without the love and patience of my boyfriend, Long Jiang. He kept encouraging me when I encountered difficulties in research and life. Together we are waiting for the next wave, and we are curious where it is going to take us.

爸爸妈妈，我爱你们！

Table of Contents

List of Figures

List of Schemes

List of Symbols, Nomenclature, and Abbreviations.

^{o}C: Degrees Celsius

AES: Auger electron microscopy

AFM: Atomic force microscopy

AlGaN: Aluminum gallium nitride

au: Arbitrary units

BE: Binding energy

CB: Conduction band

CdS: Cadmium sulfide

CdSe: Cadmium selenide

CdTe: Cadmium telluride

Cu_2ZnSnS_4: Copper zinc tin sulfide

Cu/Ge: Copper germanium alloy

CuNPs: Copper nanoparticles

Cu_2O: Copper oxide

CuO: Cupric oxide

DLS: Dynamic light scattering

DOS: Density of states

e: Charge of an electron (1.602 x 10^{-19} C)

e-: Electron

FTIR: Fourier transform infrared spectroscopy

FWHM: Full-width at half maximum

g: Gram

GaAs: Gallium arsenide

hr(s): Hour(s)

HR-TEM: High-resolution transmission electron microscopy

HSQ: Hydrogen silsesquioxane

InAs: Indium arsenide

InP: Indium phosphide

IR: Infrared

K: Degrees Kelvin

K: Shape factor

min(s): Minute(s)

n: Number

NC: Nanocrystal

nm: Nanometer

PbS: Lead sulfide

PbSe: Lead selenide

PL: Photoluminescence

QD: Quantum dot

QY: Quantum yield

SEM: Scanning electron microscopy

SiNCs: Silicon nanocrystals

SnO_2: Tin oxide

SnS: Tin sulfide

SRO: Silicon-rich oxide

STM: Scanning tunneling microscopy

T: Temperature

TEM: Transmission electron microscopy

VB: Valence band

XPS: X-ray photoelectron spectroscopy

XRD: X-ray diffraction

ZnS: Zinc sulfide

ZnSe: Zinc selenide

Chapter 1

Introduction

1.1Nanoscale materials

1.1.1 A brief history of nanoscale materials

Nanoscale materials have attracted considerable interdisciplinary interest due to their unique mechanical,[1] magnetic,[2-4] electrical,[5] and optical[6-8] properties. The breadth of their size dependent properties has lead to a wide range of practical applications, including bioimaging,[9-13] drug delivery,[14-16] catalysis,[17-19] sensors,[20, 21] environmental remdiation, *etc*. In this context, the fundamental study of nanomaterials has become one of the fastest-growing fields in modern science and engineering. Fig 1.1 illustrates the number of publications related to "nanomaterials" and "nanotechnology" by searching these key words in topic per year to 2013.

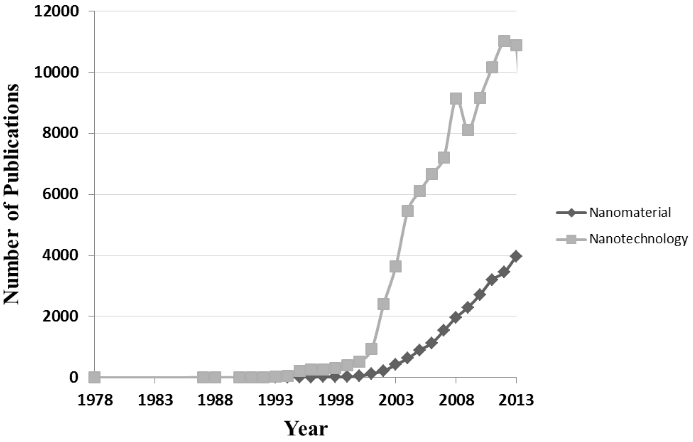

Fig. 1.1 The total number of research publications related to "nanomaterials" and "nanotechnology" per year. Data derived from Scopus (accessed Sept 03, 2014).

Even though modern nanotechnology has only a 55 year history, people have unknowingly exploited the properties of nanomaterials since the 4th century AD or before. One famous example is the Lycurgus Cup (Fig1.2). It appears green-yellow under reflected light, but when it is illuminated from within, the cup is red. This unique behavior is the result of small quantities of colloidal gold and silver in an approximate molar ratio of 1:14.[22, 23]

Fig. 1.2 Lycurgus Cup under reflected light (left) and transmitted light (right). (Reprinted with the permission from the British Museum).

Many feel the modern age of nanotechnology began in 1959 when Richard Feynman gave his lecture, “There’s Plenty of Room at the Bottom”; at that time he encouraged his audience and the scientific community to consider manipulation of single atoms and the behavior/properties of nanoscale materials.[24] It was not until 1974 that Norio Taniguchi first introduced the term "nanotechnology" which he defined as "*production technology to get extra high accuracy and ultra-fine dimensions, i.e., the preciseness and fineness on the order of 1 nm (nanometer), 10^{-9} m in length.*"[11]

From 1980s to the early 1990s, a number of revolutionary discoveries were made that saw many of Feynman's predictions become reality and stimulated rapid growth of a new scientific sub-discipline - nanotechnology. In 1982, Binnig and Rohrer invented scanning tunneling microscopy (Fig. 1.3), which allowed imaging and controlled manipulation individual atoms for the first time. [25] In 1983, Brus reported the discovery of quantum dots (QDs), a new nanoscale material for the first time.[26, 27] These discoveries were complemented by the invention of the atomic force microscope by Binnig, Quate, and Gerber in 1986.[28] In 1999, Mirkin *et al.* developed an atomic force microscope tip that can be used to write alkanethiols on a gold thin film,[29] which is what Feynman predicted in the year he indicated.

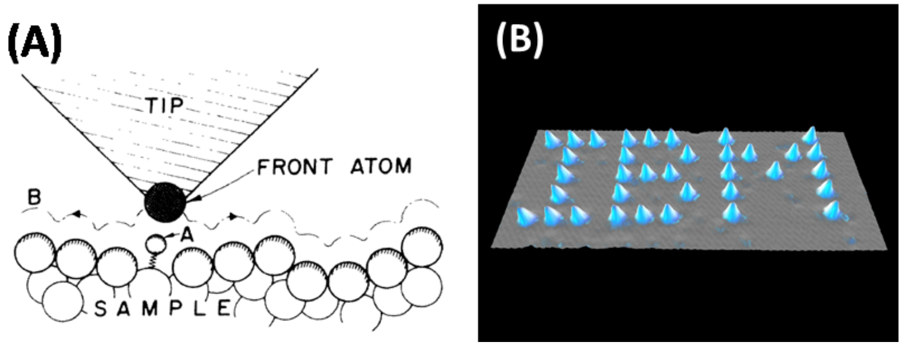

Fig. 1.3 (A) The principle operation of STM and AFM. (Image from reference 25) (B) 35 individual xenon atoms were manipulated by STM to spell out IBM logo. (Image from http://www.ibm.com/)

1.1.2 Unique properties of nanoscaled materials

The Lycurgus Cup qualitatively illustrates the unique size and material dependent optical properties of nanoscale materials. Noble metal (*e.g.*, gold and silver) nanoparticles are intensely colored because of light induced oscillations of the conduction band electrons - this is known as surface plasmon.[6, 30] In contrast, nanosized pieces of semiconductors (*e.g.,* CdSe,[31, 32] Si,[33] Ge,[34] Cu_2O,[35] SnO_2[36]) or QDs show size-dependent photoluminescence that is attributed to changes in the particle electronic structure. As particle sizes are decreased below the dimensions of the bulk Bohr exciton[A] radius, carriers (*i.e.*, electrons and holes) have a higher probability of recombining radiatively

---

[A] Exciton is an electron-hole pair that are attracted by Coulomb force.

leading to luminescence. The orbitals that are involved in band formation decrease in number as the number of atoms within a QD decreases and size of QDs shrinks from bulk to nanoscale. As a result, the band gap becomes larger with decreased particle size.[8, 37] Fig. 1.4 B schematically illustrates the influence of particle size effect on the band gap and by extension the photoluminescence maximum of QDs.[38] Fig. 1.5 shows the optical properties of QDs with different sizes and compositions. These unique optical properties expand biological applications (*e.g.*, biological labels,[11] bioimaging and cancer detection,[39] *etc.*) of nanoscale materials, which will be discussed in further detail in Section 1.2.3.

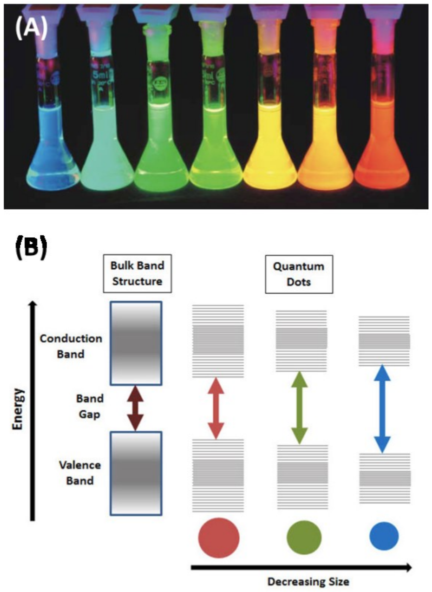

Fig. 1.4 (A) Fluorescence of CdSe@CdS core shell nanoparticles with diameters of 1.7 nm (left) to 6 nm (right). (Reprinted with permission from *J. Phys. Chem.*, 1996, **100**, 13226. Copyrigt 1996 American Chemical Society) (B) Schematic representation of quantum confinement effect in semiconductor nanoparticles. (Image from www.sigmaaldrich.com)

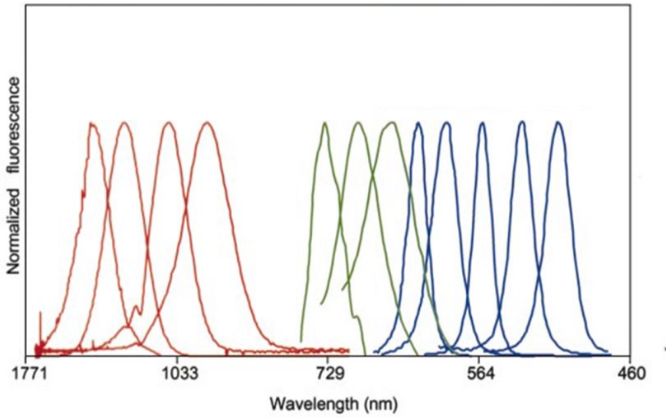

Fig. 1.5 The QD size and composition impact the optical properties. The blue series shows different sizes of CdSe QDs with diameter of 2.1 (right) to 4.6 nm (left). From right to left, the green series is of InP QDs with diameters of 3.0, 3.5, and 4.6 nm. The red series represents of InAs QDs with diameters of 2.8, 3.6, 4.6, and 6.0 nm. (Image adapted from *Chem. Soc. Rev.*, 2006, **35**, 583. Reproduced with the permission of The Royal Society of Chemistry)

In 1997, Trwoga *et al.* proposed a model for the luminescence spectrum called the effective mass approximation (EMA; Equation 1-1).[40] It remains one of the most widely used that relates nanoparticle size and band gap due to the simplicity of the equation. Fig. 1.6 shows the relationship between the calculated band gap for various Si crystals and the theoretical band gap. Various band gap energies of QDs with respect to the diameter have been analyzed by EMA.[41-44]

$$E(d) = E_g + \frac{\hbar^2\pi^2}{2d^2}\left(\frac{1}{m_e^*} + \frac{1}{m_h^*}\right) - \frac{1.786e^2}{\varepsilon_r d} + 0.284\, E_d \qquad \text{Equation 1-1}$$

In the above equation, d is the diameter of nanocrystal, E_g is the band gap of bulk nanocrystal, m_e^* and m_h^* represent effective mass of the electron and hole, respectively, e is the electron charge, ε_r is the relative permittivity, and E_d is the Rydberg energy for the bulk semiconductor (Equation 1-2):

$$E_d = \left(\frac{13.606\, m_0}{\epsilon_r^2\left(\frac{1}{m_e^*} + \frac{1}{m_h^*}\right)}\right) eV \qquad \text{Equation 1-2}$$

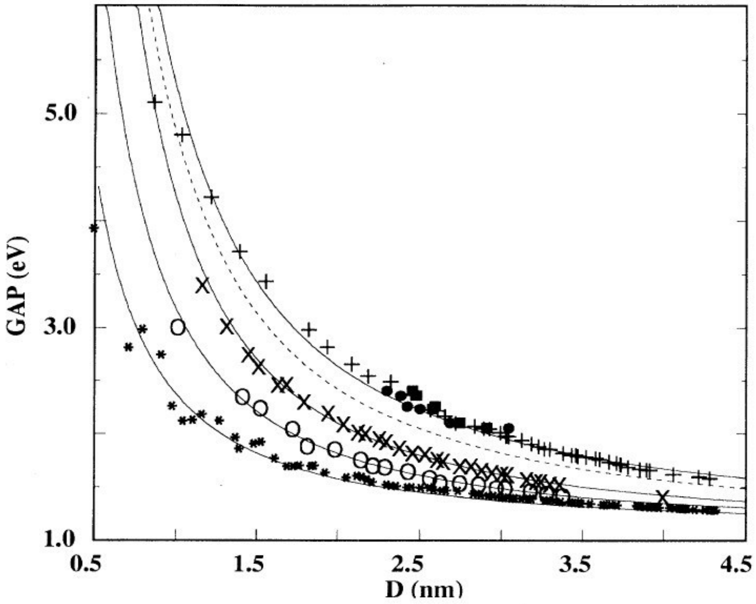

Fig. 1.6 Calculated optical band-gap energies for various silicon crystallites (+) or wires in 100 (X), 110 (+), and 111 (O) direction with respect to their diameter d. The dashed line is the theoretical band-gap energy for the crystallites. (Image from reference 44. Copyright 1993 The American Physical Society)

Another characteristic of nanoscaled materials that dominates their properties is their large surface area to volume ratio. Fig. 1.7 illustrates how preparing materials at the nanoscale influences surface area. This large surface area leads to unique reactivity; for example, nanoparticle-based catalysts have attracted considerable interest due to their enhanced reactivity and selectivity compared to their bulk material counterparts.[45] The increased surface area provides more available surface atoms, while surface defects (*e.g.*, corners, kinks, and edges) that often serve as reaction sites increase in concentration with decreasing of size. Other factors such as morphology (*i.e.*, size and shape) and chemical composition can also affect reactivity.[45]

Increasing particle surface area can also influence other physical properties (*e.g.*, melting point) of nanoscale materials. For example, the melting point of CdS changes from 1678 K to 673 K with the reducing size.[46] This size dependency results from surface atoms making up a larger proportion of the total atoms with decreasing particle size. Surface atoms tend to have higher energy than interior atoms, leading to a higher surface energy with decreasing surface area. Surface atoms move to minimize the surface energy to form a liquid state (dynamic favourable state). This fact decreases the melting point with the decreasing of crystal size.[37]

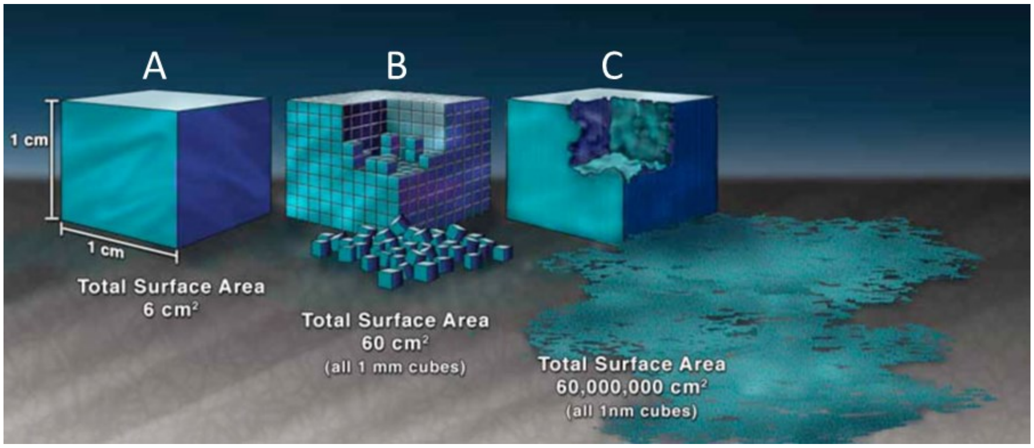

Fig. 1.7 A schematic representation of how preparing materials at the nanoscale influences the surface area. A cube of material 1x1x1 cm^3 (A) has a total surface area of 6 cm^2. If the same volume of material is prepared as 1x1x1 mm^3 cubes, 1000 cubes are required to fill the same volume leading to a total surface area of 60 cm^2 (B). If the materials is now divided into 1x1x1 nm^3 cubes, the total surface area comes to 6×10^7 cm^2 (C). (Image from www.nano.gov).

1.2 Silicon nanocrystals

Nanoscale particles of semiconductors, or QDs have been demonstrated for many materials including, II-VI (*e.g.*, CdSe, CdTe, ZnSe, *etc.*),[31, 32] III-V (*e.g.*, GaAs, InP, etc.),[47] Group IV (*e.g.*, Si, Ge, *etc.*),[33, 34] Group IV-VI (*e.g.*, SnS, PbTe, etc.),[48, 49] and alloy (*e.g.*, AlGaN, Cu_2ZnSnS_4, *etc.*) semiconductors.[50, 51] As noted above QDs exhibit size-dependent optical (Fig. 1.6) and electronic properties when the crystal size is below

Bohr radius. Prototype applications of QDs include bioimaging,[12, 52] photovoltaics,[53] sensing,[20] drug delivery,[54] *etc*. However, the fact that many are based upon heavy metal containing compounds raises significant concern.[55] In this context, it is useful to explore alternative non-toxic and abundant materials.

Silicon nanocrystals (SiNCs) have advantages over other QDs including low cost, abundance, biocompatibility, and stable electrochemical properties.[56] However, the electronic structure of Si differs substantially from direct band gap materials. Si is an indirect band gap semiconductor; hence the highest point of the valence band and the minimum point of the conduction band are not located at the same position in k-space (Fig. 1.8).[57] As a result, the vertical band gap optical transition is forbidden thus leading to bulk Si being non-luminescent – this has traditionally limited the optical applications of Si. [58] The electron is first captured by an interstitial defect, which makes the relaxation to the top of the valence band feasible. This process is usually accompanied by phonon emission or lattice vibrations. A detailed optical property of nanoscale Si materials will be discussed in Section 1.2.2.

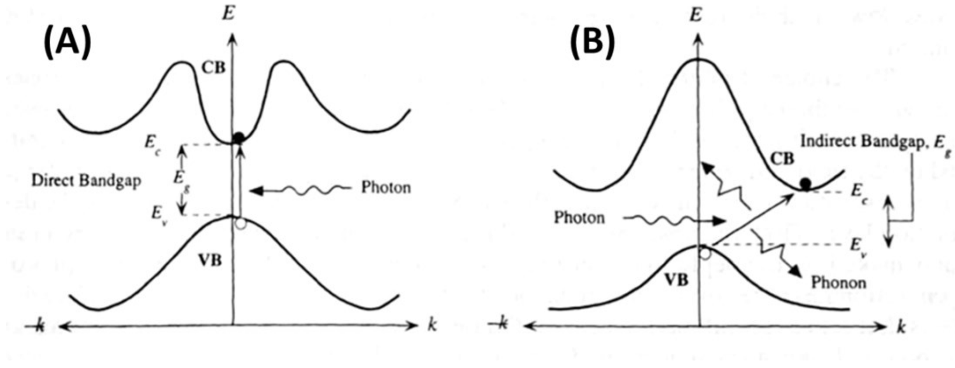

Fig. 1.8 Schematic band diagram showing direct (A) and indirect (B) band gap. (Image from reference 57)

1.2.1 Synthesis of SiNCs

A variety of synthetic methods have been developed to prepare SiNCs. In this section, key examples are summarized based on the four categories: solution-based, physical/ mechanical, solid-state, and gas-phase methods.[59]

Solution-based approaches. Solution-based methods involving precursor reduction are the most widely used procedures to prepare SiNCs.[59] It has been claimed that these approaches afford control of SiNC size and surface functionality.[60] The first report of SiNC synthesis drew inspiration from traditional compound semiconductor QD synthesis and involved the reduction of $SiCl_4$ and $RSiCl_3$ by Na at 385 °C at >100 atm for 3-7 days (Scheme 1.1 A).[60] The nanocrystals obtained from this reaction were polydispersed and exhibited diameters in the range of 2-9 nm; the yield was below 10%. In the years that followed numerous other methods requiring less harsh conditions appeared. Dhas *et al.* reported formation of SiNCs by reducing $Si(OEt)_4$ (tetraethoxysilane, TEOS) with sodium metal using ultrasonication at -70 °C. Further annealing of the product at 400 °C for 5 h under nitrogen was needed for the formation of SiNCs (Scheme 1.1 B).[61] Reactions of Zintl compounds (*e.g.,* KSi,[62] Mg_2Si,[63] and NaSi[64]) with $SiCl_4$ have been reported for the synthesis of SiNCs (Scheme 1.1 C). Another widely used synthetic method of SiNCs involved reaction of $SiCl_4$ with sodium naphthalide, the resulting product was chloride terminated SiNCs that were never isolated (Scheme 1.1 D).[65]

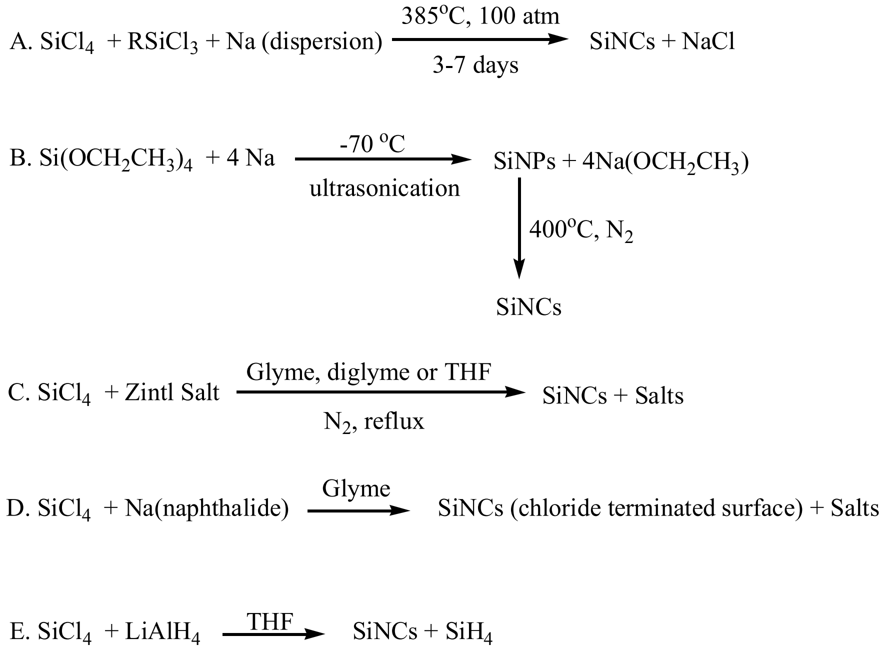

Scheme. 1.1 Solution-based synthetic methods for the preparation of SiNCs. (Image adapted from *Chem. Commun.*, 2006, 4160. Reproduced with the permission of The Royal Society of Chemistry)

Physical/ mechanical method. One top-down physical method of SiNCs synthesis is called high energy ball milling.[66] The biggest advantage of this method is simultaneous synthesis and surface functionalization by alkyl/alkenyl groups (Scheme 1.2). Another physical methods of SiNCs formation is by ultrasonic fracture.[67, 68]

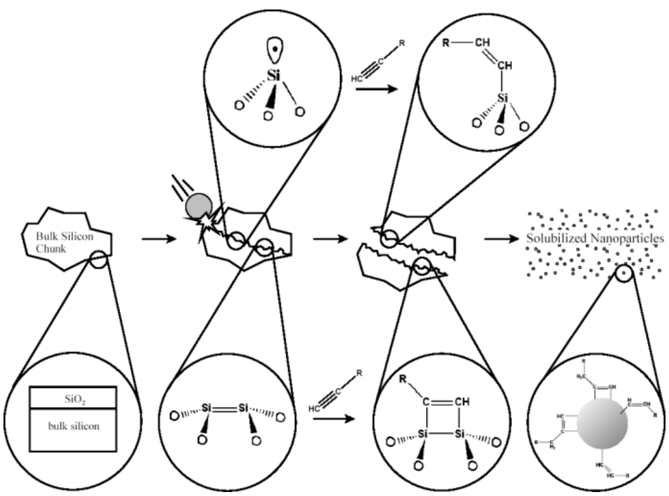

Scheme 1.2 Preparation of functionalized SiNCs using high energy ball milling. (Reprinted with permission from *Adv. Mater.,* 2007, **19**, 3984. Copyrigt 2007 WILEY-VCH Verlag GmbH & Co. KGaA, Weinheim)

Solid-state method. Silicon rich oxides (SROs) and other silicon rich structures (*e.g.*, sol-gel polymers $(HSiO_{1.5})_n$) are common solid-state precursors for preparing SiNCs. The thermal reduction (>1000 °C, inert or reduction condition) of these oxides or polymers yields SiNCs embedded in an oxide matrix.[69, 70] Subsequently, a hydrofluoric acid (HF) etching is needed to obtain freestanding SiNCs.[71, 72] The crystallinity and size of SiNCs can be tuned by annealing temperature and etching time.

Hydrogen Silsesquioxane (HSQ) is a commercially available SRO precursor. Hessel *et al.* reported the formation of SiNCs embedded in a silica matrix by a reductive thermal annealing process at 1100 °C in 4% H_2 and 96% N_2.[69] In order to obtain freestanding hydride-terminated SiNPs, the authors performed a HF acid etching to remove the silica matrix. It is believed that the cage network starts to redistribute with loss of SiH_4 at 250 °C-350 °C, and at 350 °C-450 °C Si rich oxide disproportionates to form Si(0) and SiO_2 (Fig. 1.9). An annealing temperature of at least 1100 °C is needed to obtain crystalline Si embedded in the oxide. Narrow particle size distribution (d = 3.14 nm, $2\sigma = 1.40$ nm) was obtained. The PL of hydride-terminated SiNC can be tuned by changing particle size upon HF etching of the SiNCs (Fig. 1.10).

250-350 °C:

(1) $2HSiO_{3/2} \longrightarrow H_2SiO + SiO_2$

(2) $H_2SiO + HSiO_{3/2} \longrightarrow H_3SiO_{1/2} + SiO_2$

(3) $H_3SiO_{1/2} + HSiO_{3/2} \longrightarrow SiH_4 + SiO_2$

350-450 °C:

(4) $4HSiO_{3/2} \longrightarrow 3SiO_2 + SiH_4$

(5) $SiH_4 \longrightarrow Si + 2H_2$

Fig. 1.9 Stages of HSQ thermal degradation in an inert atmosphere. (Reprinted with permission from *Chem. Mater.,* 2006, **18**, 6139. Copyrigt 2006 American Chemical Society)

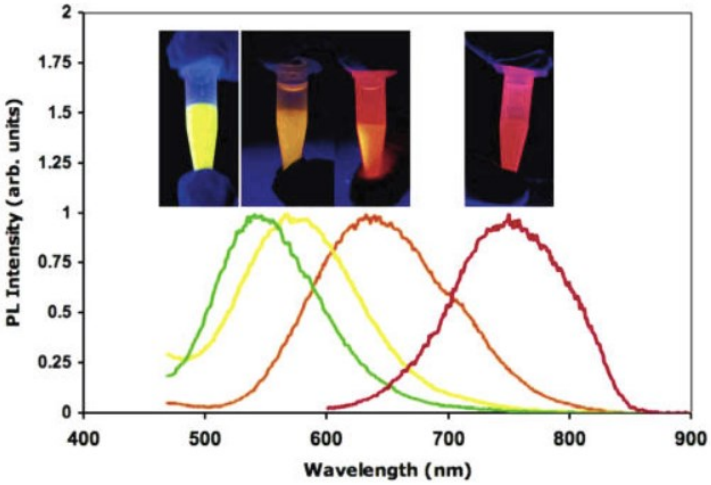

Fig 1.10 PL spectra of hydride-terminated SiNCs with different etching times. Solutions of SiNCs after 50 min etching (red), 85 min etching (orange), 115 min etching (yellow), and 135 min etching (green). Inset: Photographs of PL observed from SiNCs. (Reprinted with permission from *Chem. Mater.,* 2006, **18**, 6139. Copyrigt 2006 American Chemical Society)

Gas-phase methods. Gas-phase methods to prepare SiNCs frequently involve laser or microwave induced decomposition of silane (SiH_4). In 1976, Murthy *et al.* reported the synthesis of 30-80 nm octahedral SiNCs by thermal decomposition of silane in hydrogen at 1000-1100 °C.[73] One of the most commonly used gas-phase method involves pyrolysis of SiH_4 silicon precursor by CO_2 laser.[74] This method provides 5 nm SiNCs with red PL (Fig. 1.11). Similarly, instead of CO_2 laser, non-thermal plasma has also been used for pyrolysis of silane.[75]

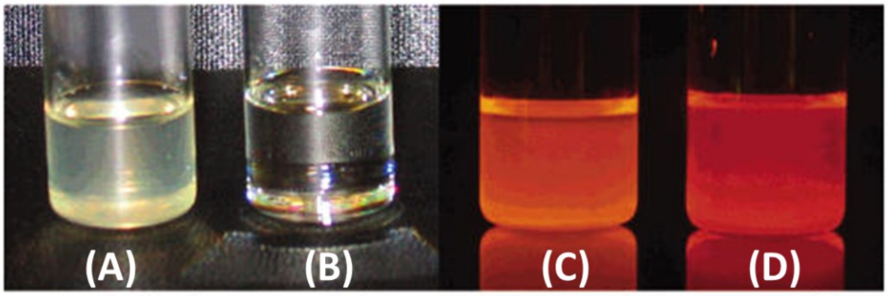

Fig. 1.11 Si nanoparticles (A) and octadecene treated Si nanoparticles (B) under room illumination and UV light (C) and (D). (Reprinted with permission from *Langmuir,* 2004, **20**, 4720. Copyrigt 2004 American Chemical Society)

1.2.2 Optical properties of SiNCs

After the discovery of the luminescence of porous silicon in 1991,[76] numerous prototype applications demonstrated including bioimaging,[77-79] and light-emitting devices.[80, 81] Despite these advances, the origin of SiNC luminescence remains the subject of controversy. In the following section, various explanations of the origin of SiNC PL are considered.

Surface states. Surface oxide defects have been proposed to be a dominant source of luminescence from Si. In 1999, Wolkin *et al.* observed a red-shift of PL after exposure to oxygen.[82] The authors claim oxide defects play an important role, especially for small particles (*i.e.,* d < 3 nm). They proposed electrons are trapped on the silicon of a Si=O species while the trapped hole is localized on the oxygen atom. This proposal is very controversial because no molecular equivalent of Si=O is known in the absence of substantial stabilization.[83, 84] Similar observations has been reported by Puzder *et al.*[85] Kanemitsu *et al.* have also observed strong PL from oxidized SiNCs and Si@SiO_2 core shell structures.[86] The authors proposed a model that explains the observed size independent and temperature dependent PL. They claimed the strong PL occurs from the radiative recombination process of localized excitons at the interfacial layer between the Si core and SiO_2 surface layer. In 2014, Dasog *et al.* exploited surface-emitting species and reported the PL of SiNCs can be effectively tuned across the entire visible spectral region through variation of surface functionalization without changing particle size (Fig. 1.12).[87] While the exact identity of the surface groups remains unknown, it is clearly possible to tailor SiNC PL by controlling surface chemistry.

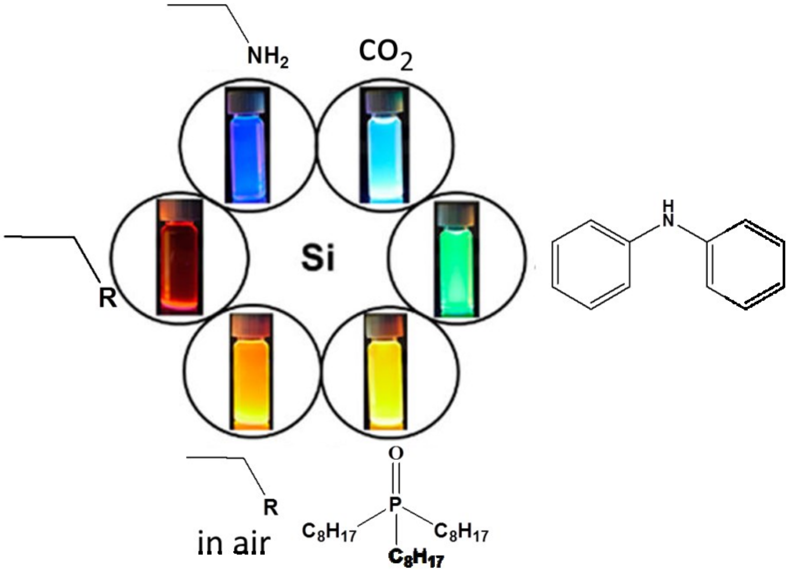

Fig. 1.12 SiNCs PL can be influenced by surface functionalization without changing particle size. (Reprinted with permission from *ACS Nano,* 2014, **8**, 9636. Copyrigt 2014 American Chemical Society)

Quantum confinement. As with other QDs, quantum confinement can play an important role in tuning the color of nanomaterials if the particle size is below the Bohr radius (*i.e.,* Bohr radius for Si is 4.5 nm). When the size of particles decrease from bulk to nanoscale, the number of orbitals that participating in bond formation decreases as well, leading to a removal of the orbital levels. As a result, the band gap becomes larger with a decrease in particle size.[88] Fig. 1.13 represents the band gap and PL maxima change as the function of particle size.

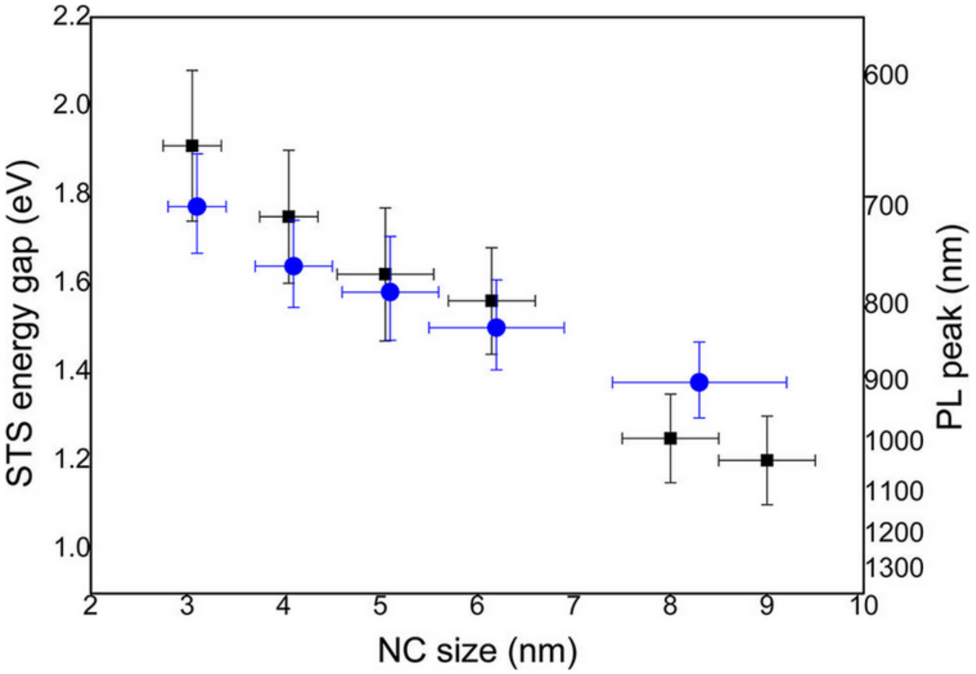

Fig. 1.13 Band gaps (black square) of dodecyl functionalized SiNCs and PL maxima (blue dots) with different particle size. (Reprinted with permission from *Nano Lett.,* 2013, **13**, 2516. Copyrigt 2013 American Chemical Society)

1.2.3 Bioimaging applications of SiNCs

Organic dyes have been reported as fluorescent probes for *in vivo* bioimaging due to their high tissue penetration, minimal photo-damage to biological samples, and reduced light scattering.[89, 90] Still, one of the most important challenges of organic dyes is they are not stable against photobleaching, which limits long-term bioimaging *in vitro* or *in vivo*.[91] QDs are photostable. Consequently, luminescent QDs have been proposed as alternative materials to fluorescent organic dyes for bioimaging applications[52, 92-95] due to their tunable optical properties[92] and tailorable surface chemistry.[96] However, II-VI QDs (*e.g.*, CdSe/ZnS QDs) and III-V (*e.g.*, InAs/GaAs QDs) are cytotoxic unless a biocompatible surface layer is coated to reduce the cytotoxicity of the QDs.[55] This alone limits practical utility for applications involving biological systems.[97-100]

McVey and Tilley's recent review highlights the bioimaging applications of SiNCs.[101] In terms of the toxicity of SiNCs, Zuihof *et al.* studied the rule of the surface functionalities and size on SiNCs.[102] They found that positively charged (amine) SiNCs showed more toxicity than negatively charged (carboxylic acid) and neutral (hydroxyl) SiNCs. In addition, smaller particles were found to be more toxic than larger ones.[102] Tilley *et al.* found that highly reactive surface functionalities (epoxides) are more toxic than amine or diol functionalities.[103] In 2004, Li *et al.* reported the synthesis of poly(acrylic acid) functionalized red luminescent silicon and their application as biological labels for fluorescence imaging of Chinese hamster ovary (CHO) cells, which is the first report of bioimaging using red PL SiNCs.[104] Luminescent porous silicon nanoparticles have also been demonstrated for *in vivo* imaging applications for tumors and other organs (Fig. 1.14).[105] In 2008, Erogbogbo *et al.* reported stable polyethylene glycol phospholipid micelles functionalized water-dispersible red luminescent Si QDs and their use as luminescent labels for pancreatic cancer cells.[106] Zhong *et al.* developed the proteins functionalized red and blue PL biocompatible SiNCs that serve as bioimaging applications of Hela cells.[107, 108] These examples indicate SiNCs could be potentially useful biological labels. Two examples of water soluble functionalized SiNCs and their application for bioimaging will be reported in detail in Chapter 2.

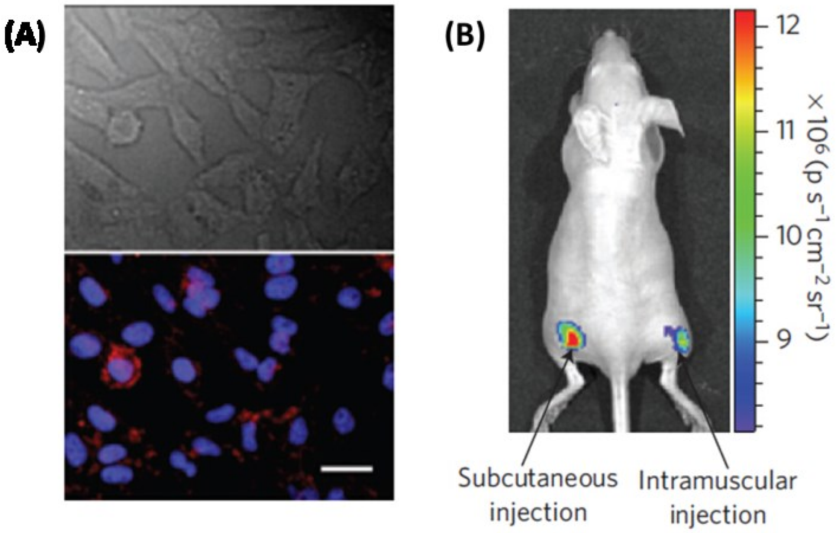

Fig 1.14 (A) Image of luminescent porous silicon nanoparticles with Hela cells. Red and blue indicate luminescent porous silicon nanoparticles and cell nuclei, respectively. The scale bar is 20 μm. (B) In vivo fluorescence image of LPSiNPs (20 μL of 0:1 mg/mL) injected subcutaneously and intramuscularly on each flank of a mouse. (Image from reference 105)

1.3 Copper, germanium, and Cu/Ge alloy nanoparticles

In materials science, using mixtures of elements to generate intermetallic compounds and alloys often leads to unique materials with far reaching applications including electronics,[109-111] magnets,[112, 113] and catalysts.[114-116] Alloys are attractive because of the synergistic effects of the components which lead to a rich diversity of compositions, structures, and properties.[117] These properties become even more significant when alloys are prepared on the nanoscale.[118, 119]

Copper nanoparticles are used as the metallization material for Si-based devices due to the low resistivity (~ 2 μΩ cm at 300 K), high-reliability, and low cost.[120-122] Germanium nanoparticles have the potential application for related optoelectronic devices due to the low cost and relative straightforward synthesis process.[123, 124] Cu/Ge alloys are of interest because of their low resistivity (5.5 μΩ cm),[125] and oxidatively stable up to 520 °C.[126] NPs of these alloys offer the potential for metallization material of choice for Si-based devices. Cu oxidize in air around 250 °C to form CuO and Cu_2O.[127] The oxidation rate of Cu was determined using *in situ* resistivity measurement and X-ray photoelectron spectroscopy (XPS). A 4 monolayer thickness of germanium oxide was obtained after 300 min oxidation treatment (temperature = 250 °C, under 0.5 atm of pure oxygen atmosphere).[128] The oxidation rate was studied using kinetic resolved

X-ray photoelectron spectroscopy and a two-step oxidation model was proposed by Tabet *et al.* in 1998.

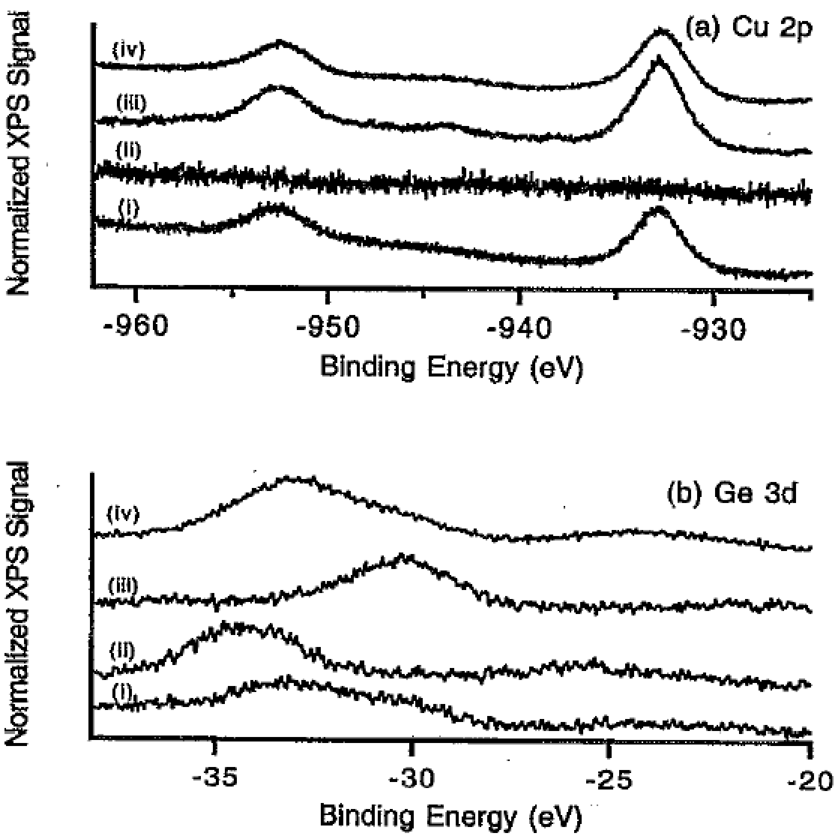

Fig. 1.15 (a) Cu 2p and (b) Ge 3d core levels XPS of (i) as-received Cu_3Ge, (ii) Cu_3Ge oxidized in air at 430 °C for 30 min, (iii) sputter-cleaned Cu_3Ge, and (iv) sample same as (iii) but exposed to air for 12 h at room temperature. (Reprinted with permission from *J. Appl. Phys.*, 1995, **77**, 5443. Copyrigt 1995 AIP Publishing LLC.)

The coating of Cu_3Ge by thin layer of GeO_2 protects Cu_3Ge from oxidation below 450 °C in air.[127] The oxidation of Cu_3Ge was studied using XPS (Fig. 1.15). The Cu 2p peak indicates that the Cu species was Cu(0) for samples (i), (iii), and (iv). However, there is no Cu signal for sample (ii); in this sample Ge oxidized and the layer of Ge oxide stops Cu being resolved by XPS. Since the temperature was low for sample (iv) (room temperature), the oxidation rate of Ge is slow and only a very thin layer of Ge oxide formed, as a result, Cu signal can be resolved by XPS. Ge formed oxide after exposure to air, which can be observed from the binding energy shift from sample (ii) to (iii) and (iii) to (iv). When the temperature is above 450 °C, the Ge oxide layer becomes thinner and thinner as evaporation rate is faster than growth rate. Consequently, at above 450 °C the oxidation protection is lost.

Copper germanide has attracted considerable interest as a promising candidate as metallization material for very large scale integration (VLSI) technology[125, 129] and metal oxide semiconductor field effect transistors (MOSFET) (Fig. 1.16).[130, 131] Part of its appeal arises from its low resistivity (5.5 μΩ cm)[125] compared to other metallization materials (*e.g.*, $CoSi_2$: 18–20 μΩ cm[126], Cu_3Si: ~ 60 μΩ cm[132, 133]). The resistance of the metallization material is inversely proportional to the thickness of the metallization layer; nanoparticles make it possible to have very thin layers.

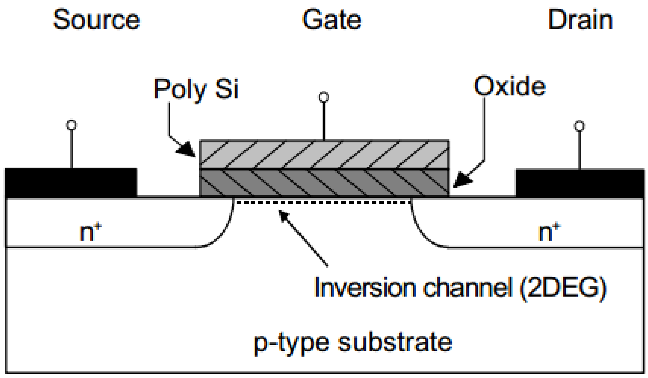

Fig. 1.16 Schematic of a MOSFET structure. (Reprinted with permission from *Solid-State Electronics,* 2003, **47**, 1881. Copyrigt 2003 Elsevier Ltd.)

1.3.1 Synthesis of CuNPs, GeNPs, and Cu/GeNPs

CuNPs. Chemical reduction methods involving precursor reduction are the most widely used synthetic approaches to prepare CuNCs. There are a variety of reducing agents, that are commonly employed including hydrazine,[134] ascorbic acid,[135] sodium borohydride ($NaBH_4$),[136] and polyol.[137] Kapoor *et al.* prepared CuNPs by the reduction of copper sulfate ($CuSO_4$) using $NaBH_4$ at room temperature.[138] This reaction yielded CuNPs with diameters of 8 – 10 nm. Wu *et al.* also reported reduction of cupric chloride ($CuCl_2$) with hydrazine in the aqueous hexadecyl-trimethyl-ammonium bromide (CTAB) solution.[139] The mean diameter could be tuned from 5 nm to 15 nm by tailoring the ratio of hydrazine to $CuCl_2$ (Fig. 1.16). Several other methods have been developed for CuNP synthesis including thermal reduction,[140] vacuum vapor deposition,[141] electronreduction,[142] and laser irradiation.[143]

GeNPs. Solution-based methods involving precursor reduction are widely used to prepare GeNPs, but size and shape control has yet to be fully realized.[123] Kornowski *et al.* reported the reduction of germanium chloride ($GeCl_4$) with lithium naphthalide and obtained particles of broad size distribution (6 – 60 nm) (Scheme 1.3A).[144] A metathesis reaction of $GeCl_4$ and Zintl salts (NaGe,[145-147] KGe,[146] and Mg_2Ge[146]) has also been reported for chloride terminated GeNPs. Further surface functionalization is needed to minimize surface oxidation (Scheme 1.3B). Thermal reduction of organogermanium precursors is another method for GeNPs synthesis. Henderson *et al.* reported the preparation of luminescent oxide-embedded germanium nanocrystals (Ge-NC/GeO_2) by the reductive thermal processing of polymers $(C_6H_5GeO_{1.5})_n$ derived from phenyl trichlorogermane (C_6H_5-$GeCl_3$) (Scheme 1.3C).[148]

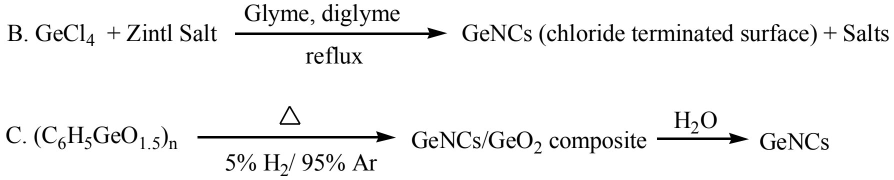

Scheme 1.3 Synthetic methods for the preparation of GeNCs.

Cu/Ge alloy films synthesis will be discussed in detail in Chapter 3. To date, no CuGe nanoparticles have been prepared, and the knowledge of existing methods for preparing the alloy films was applied to prepare the alloy particles.

1.4 Thesis outline

The present material in introduction chapter focuses on the history, properties, and application of nanoscale material. This thesis concentrates on the synthesis of SiNCs surface functionalization and their biological applications and the synthesis of Cu/Ge alloy nanoparticles. Chapter 2 focuses on the synthesis of water soluble Si-NCs functionalized with D-mannose sugar and L-alanine amino acid. In addition, cell studies were investigated to show mannose and alanine functionalized Si-NCs have strong binding affinity to MCF-7 cells. Chapter 3 presents a straightforward method for the synthesis of copper-germanium alloy (Cu_3Ge and $Cu_{0.85}Ge_{0.15}$) nanocrystals via the reductive thermal processing of Cu@GeO2 nanoparticles. Finally, Chapter 4 summaries the discoveries and challenges made in Chapter 2 and 3, and a brief outlook of future work is also provided.

1.5 References

---

1. M. A. Meyers, A. Mishra and D. J. Benson, *Prog. Mater Sci.*, 2006, **51**, 427.
2. A. H. Lu, E. L. Salabas and F. Schuth, *Angew. Chem. Int. Ed.*, 2007, **46**, 1222.
3. S. P. Gubin, Y. A. Koksharov, G. B. Khomutov and G. Y. Yurkov, *Usp. Khim.*, 2005, **74**, 539.
4. J. Gao, H. Gu and B. Xu, *Acc. Chem. Res.*, 2009, **42**, 1097.
5. A. Henglein, *Chem. Rev.* , 1989, **89**, 1861.
6. S. Link and M. A. El-Sayed, *Annu. Rev. Phys. Chem.*, 2003, **54**, 331.
7. D. Kovalev, H. Heckler, G. Polisski and F. Koch, *Phys. Stat. Sol.*, 1999, **215**, 871.
8. S. Eustis and M. A. El-Sayed, *Chem. Soc. Rev.*, 2005, **35**, 209.
9. I. L. Medintz, H. T. Uyeda, E. R. Goldman and H. Mattoussi, *Nat. Mater.*, 2005, **4**, 435.
10. F. Wang, W. B. Tan, Y. Zhang, X. Fan and M. Wang, *Nanotechnology*, 2006, **17**, R1.
11. M. Bruchez, M. Moronne, P. Gin, S. Weiss and A. P. Alivisatos, *Science*, 1998, **281**, 2013.
12. T. Jamieson, R. Bakhshi, D. Petrova, R. Pocock, M. Imani and A. M. Seifalian, *Biomaterials*, 2007, **28**, 4717.
13. X. Gao, Y. Cui, R. M. Levenson, L. W. Chung and S. Nie, *Nat. Biotechnol.*, 2004, **22**, 969.
14. J.-U. A. H. Junghanns and R. H. Muller, *Int. J. Nanomed.*, 2008, **3**, 295.
15. J. Kim, H. S. Kim, N. Lee, T. Kim, H. Kim, T. Yu, I. C. Song, W. K. Moon and T. Hyeon, *Angew. Chem. Int. Ed.*, 2008, **47**, 8438.
16. R. H. Muller and C. M. Keck, *J. Biotechnol.*, 2004, **113**, 150.
17. Z. Y. Zhou, N. Tian, J. T. Li, I. Broadwell and S. G. Sun, *Chem. Soc. Rev.*, 2011, **40**, 4167.
18. K. Zhou and Y. Li, *Angew. Chem. Int. Ed.*, 2012, **51**, 602.
19. B. Wu and N. Zheng, *Nano Today*, 2013, **8**, 168.
20. R. C. Somers, M. G. Bawendi and D. G. Nocera, *Chem. Soc. Rev.*, 2007, **36**, 579.
21. P. T. Snee, R. C. Somers, G. Nair, J. P. Zimmer, M. G. Bawendi and D. G. Nocera, *J. Am. Chem. Soc.*, 2006, **128**, 13320.
22. I. Freestone, N. Meeks, M. Sax and C. Higgitt, *Gold Bull*, 2007, **40**, 270.
23. L. M. Liz-Marzan, *Mater. Today*, 2004, **7**, 26.

24. B. Fahlman, *Materials Chemistry*, Springer: Dordretcht, Netherlands, 2007.

25. G. Binnig and H. Rohrer, *Helv. Phys. Acta.* , 1982, **55**, 726.

26. L. E. Brus, *J. Chem. Phys.*, 1983, **79**, 5566.

27. L. E. Brus, *J. Chem. Phys.*, 1984, **80**, 4403.

28. G. Binnig, C. F. Quate and C. Gerber, *Phys. Rev. Lett.*, 1986, **56**, 930.

29. R. D. Piner, J. Zhu, F. Xu, S. Hong and C. A. Mirkin, *Science*, 1999, **283**, 661.

30. S. Link and M. A. El-Sayed, *J. Phys. Chem. B*, 1999, **103**, 8410.

31. C. B. Murray, D. J. Norris and M. G. Bawendi, *J. Am. Chem. Soc.*, 1993, **115**, 8706.

32. A. P. Alivisatos, *Science*, 1993, **271**, 933.

33. J. A. Kelly, E. J. Henderson and J. G. Veinot, *Chem. Commun.*, 2010, **46**, 8704.

34. M. W. Dashiell, U. Denker, C. Müller, G. Costantini, C. Manzano, K. Kern and O. G. Schmidt, *Appl. Phys. Lett.*, 2002, **80**, 1279.

35. A. Kellersohn, E. Knözinger, W. Langel and M. Giersig, *Adv. Matter*, 1995, **7**, 652.

36. D. Dutta and D. Bahadur, *J. Mater. Chem.* , 2012, **22**, 24545.

37. A. P. Alivisatos, *J. Phys. Chem.*, 1996, **100**, 13226.

38. E. Roduner, *Chem. Soc. Rev.*, 2006, **35**, 583.

39. Y. M. Huh, Y. W. Jun, H. T. Song, S. Kim, J. S. Choi, J. H. Lee, S. Yoon, K. S. Kim, J. S. Shin, J. S. Suh and J. Cheon, *J. Am. Chem. Soc.*, 2005, **127**, 12387.

40. P. F. Trwoga, A. J. Kenyon and C. W. Pitt, *J. Appl. Phys.*, 1998, **83**, 3789.

41. A. I. Ekimov, F. Hache, M. C. Schanne-Klein, D. Ricard, C. Flytzanis, I. A. Kudryavtsev, T. V. Yazeva, A. V. Rodina and A. L. Efros, *J. Opt. Soc. Am. B*, 1993, **10**, 100.

42. A. L. Efros, M. Rosen, M. Kuno, M. Nirmal, D. J. Norris and M. Bawendi, *Phys. Rev. B*, 1996, **54**, 4843.

43. K. Leung, S. Pokrant and K. B. Whaley, *Phys. Rev. B*, 1998, **57**, 12291.

44. C. Delerue, G. Allan and M. Lannoo, *Phys. Rev. B*, 1993, **48**, 11024.

45. B. R. Cuenya, *Thin Solid Films*, 2010, **518**, 3127.

46. A. N. Goldstein, C. M. Echer and A. P. Alivisatos, *Science*, 1992, **256**, 1425.

47. F. M. Davidson, A. D. Schricker, R. J. Wiacek and B. A. Korgel, *Adv. Mater.*, 2004, **16**, 646.

48. Y. Xu, N. Al-Salim, C. W. Bumby and R. D. Tilley, *J. Am. Chem. Soc.*, 2009, **131**, 15990.

49. J. E. Murphy, M. C. Beard, A. G. Norman, S. P. Ahrenkiet, J. C. Johnson, P. Yu, O. I. Mićić, R. J. Ellingson and A. J. Nozik, *J. Am. Chem. Soc.*, 2006, **128**, 3241.
50. M. Benaissa, K. E. Gonsalves and S. P. Rangarajan, *Appl. Phys. Lett.*, 1997, **71**, 3685.
51. Q. Guo, H. W. Hillhouse and R. Agrawal, *J. Am. Chem. Soc.*, 2009, **131**, 11672.
52. M. Bruchez Jr, M. Moronne, P. Gin, S. Weiss and A. P. Alivisatos, *Science*, 1998, **281**, 2013.
53. P. V. Kamat, *J. Phys. Chem. C*, 2008, **112**, 18737.
54. E. J. Anglin, L. Cheng, W. R. Freeman and M. J. Sailor, *Adv. Drug Deliv. Rev.*, 2008, **60**, 1266.
55. N. Lewinski, V. Colvin and R. Drezek, *Small*, 2008, **4**, 26.
56. J. G. Veinot, *Chem. Commun.*, 2006, 4160.
57. S. O. Kasap, *Optoelectronics and Photonics: Principles and Practices 2nd edition*, **Prentice Hall, 2012**.
58. L. Brus, *J. Phys. Chem.*, 1994, **98**, 3575.
59. J. G. C. Veinot, *Chem. Commun.* , 2006, 4160.
60. J. R. Heath, *Science*, 1992, **258**, 1131.
61. N. A. Dhas, C. P. Raj and A. Gedanken, *Chem. Mater.*, 1998, **10**, 3278.
62. R. A. Bley and S. M. Kauzlarich, *J. Am. Chem. Soc.*, 1996, **118**, 12462.
63. C.-S. Yang, R. A. Bley, S. M. Kauzlarich, H. W. H. Lee and G. R. Delgado, *J. Am. Chem. Soc.*, 1999, **121**, 5191.
64. D. Mayeri, B. L. Phillips, M. P. Augustine and S. M. Kauzlarich, *Chem. Mater.*, 2001, **13**, 765.
65. J. Zou, R. K. Baldwin, K. A. Pettigrew and S. M. Kauzlarich, *Nano Lett.*, 2004, **4**, 1181.
66. A. S. Heintz, M. J. Fink and B. S. Mitchell, *Adv. Mater.*, 2007, **19**, 3984.
67. G. Belomoin, J. Therrien, A. Smith, S. Rao, R. Twesten, S. Chaieb, M. H. Nayfeh, L. Wagner and L. Mitas, *Appl. Phys. Lett.*, 2002, **80**, 841.
68. R. A. Bley, S. M. Kauzlarich, J. E. Davis and H. W. H. Lee, *Chem. Mater.*, 1996, **8**, 1881.
69. C. M. Hessel, E. J. Henderson and J. G. C. Veinot, *Chem. Mater.*, 2006, **18**, 6139.
70. M. Pauthe, E. Bernstein, J. Dumas, L. Saviot, A. Pradel and M. Ribes, *J. Mater. Chem.*, 1999, **9**, 187.
71. S.-M. Liu, S. Sato and K. Kimura, *Langmuir : the ACS journal of surfaces and*

colloids, 2005, 6324.
72. S.-M. Liu, Y. Yang, S. Sato and K. Kimura, *Chem. Mater.*, 2006, **18**, 637.
73. T. U. M. S. Murthy, N. Miyamoto, M. Shimbo and J. Nishizawa, *J. Cryst. Growth*, 1976, **33**, 1.
74. X. Li, Y. He and M. T. Swihart, *Langmuir : the ACS journal of surfaces and colloids*, 2004, **20**, 4720.
75. R. Anthony and U. Kortshagen, *Phys. Rev. B*, 2009, **80**, 115407.
76. A. G. Cullis and L. T. Canham, *Nature*, 1991, **353**, 335.
77. M. Rosso-Vasic, E. Spruijt, Z. Popović, K. Overgaag, B. van Lagen, B. Grandidier, D. Vanmaekelbergh, D. Domínguez-Gutiérrez, L. De Cola and H. Zuilhof, *J. Mater. Chem.*, 2009, **19**, 5926.
78. J. Fan and P. K. Chu, *Small*, 2010, **6**, 2080.
79. W. Tan, K. Wang, X. He, X. J. Zhao, T. Drake, L. Wang and R. P. Bagwe, *Med. Res. Rev.*, 2004, **24**, 621.
80. K. D. Hirschman, L. Tsybeskov, S. P. Duttagupta and P. M. Fauchet, *Nature*, 1996, **384**, 338.
81. K. Y. Cheng, R. Anthony, U. R. Kortshagen and R. J. Holmes, *Nano Lett.*, 2010, **10**, 1154.
82. M. V. Wolkin, J. Jorne and P. M. Fauchet, *Phys. Rev. Lett.*, 1999, **82**, 197.
83. L. E. Brus, P. F. Szajowski, W. L. Wilson, T. D. Harris, S. Schuppler and P. H. Citrin, *J. Am. Chem. Soc.*, 1995, **117**, 2915.
84. D. Kovalev, H. Heckler, M. Ben-Chorin, G. Polisski, M. Schwartzkopff and F. Koch, *Phys. Rev. Lett.*, 1998, **81**, 2803.
85. A. Puzder, A. J. Williamson, J. C. Grossman and G. Galli, *Phys. Rev. Lett.*, 2002, **88**, 097401.
86. Y. Kanemitsu, T. Ogawa, K. Shiraishi and K. Takeda, *Phys. Rev. B*, 1993, **48**, 4883.
87. M. Dasog, G. B. De los Reyes, L. V. Titova, F. a. Hegmann and J. G. C. Veinot, *ACS Nano*, 2014, doi: 10.1021/nn504109a.
88. O. Wolf, M. Dasog, Z. Yang, I. Balberg, J. G. C. Veinot and O. Millo, *Nano Lett.*, 2013, **13**, 2516.
89. J. O. Escobedo, O. Rusin, S. Lim and R. M. Strongin, *Curr. Opin. Chem. Biol.*, 2010, **14**, 64.
90. L. Yuan, W. Lin, K. Zheng, L. He and W. Huang, *Chem. Soc. Rev.*, 2013, **42**, 622.

91. U. Resch-Genger, M. Grabolle, S. Cavaliere-Jaricot, R. Nitschke and T. Nann, *Nat. Methods*, 2008, **5**, 763.

92. X. Michalet, F. F. Pinaud, L. A. Bentolila, J. M. Tsay, S. Doose, J. J. Li, G. Sundaresan, A. M. Wu, S. S. Gambhir and S. Weiss, *Science*, 2005, **307**, 538.

93. Y. He, C. Fan and S.-T. Lee, *Nano Today*, 2010, **5**, 282.

94. W. C. Chan, D. J. Maxwell, X. Gao, R. E. Bailey, M. Han and S. Neie, *Curr. Opin. Biotechnol.*, 2002, **13**, 40.

95. C. M. Niemeyer, *Angew. Chem. Int. Ed.*, 2001, **40**, 4128.

96. M. De, P. S. Ghosh and V. M. Rotello, *Adv. Mater.*, 2008, **20**, 4225.

97. R. Hardman, *Environ. Health Perspect.*, 2006, **114**, 165.

98. T. S. Hauck, R. E. Anderson, H. C. Fischer, S. Newbigging and W. C. Chan, *Small*, 2010, **6**, 138.

99. Y. Su, M. Hu, C. Fan, Y. He, Q. Li, W. Li, L. H. Wang, P. Shen and Q. Huang, *Biomaterials*, 2010, **31**, 4829.

100. A. M. Derfus, W. C. W. Chan and S. N. Bhatia, *Nano Lett.*, 2004, **4**, 11.

101. B. F. P. McVey and R. D. Tilley, *Acc. Chem. Res.*, 2014, **47**, 3045.

102. S. Bhattacharjee, I. M. Rietjens, M. P. Singh, T. M. Atkins, T. K. Purkait, Z. Xu, S. Regli, A. Shukaliak, R. J. Clark, B. S. Mitchell, G. M. Alink, A. T. Marcelis, M. J. Fink, J. G. Veinot, S. M. Kauzlarich and H. Zuilhof, *Nanoscale*, 2013, **5**, 4870.

103. A. Shiohara, S. Hanada, S. Prabakar, K. Fujioka, T. H. Lim, K. Yamamoto, P. T. Northcote and R. D. Tilley, *J. Am. Chem. Soc.*, 2010, **132**, 248.

104. Z. F. Li and E. Ruckenstein, *Nano Lett.*, 2004, **4**, 1463.

105. J. H. Park, L. Gu, G. von Maltzahn, E. Ruoslahti, S. N. Bhatia and M. J. Sailor, *Nat Mater.*, 2009, **8**, 331.

106. F. Erogbogbo, K. T. Yong, I. Roy, G. Xu, P. N. Prasad and M. T. Swihart, *ACS Nano*, 2008, **2**, 873.

107. Y. Zhong, F. Peng, X. Wei, Y. Zhou, J. Wang, X. Jiang, Y. Su, S. Su, S.-T. Lee and Y. He, *Angew. Chem. Int. Ed.*, 2012, **51**, 8485.

108. Y. Zhong, F. Peng, F. Bao, S. Wang, X. Ji, L. Yang, Y. Su, S. T. Lee and Y. He, *J. Am. Chem. Soc.*, 2013, **135**, 8350.

109. F. Chen and R. L. Johnston, *ACS Nano*, 2008, **2**, 165.

110. F. Chen and R. L. Johnston, *Acta Mater.*, 2008, **56**, 2374.

111. B. M. Muñoz-Flores, B. I. Kharisov, V. M. Jiménez-Pérez, M. P. Elizondo and S. T. López, *Ind. Eng. Chem. Res.*, 2011, **50**, 7705.

112. F. Ai, A. Yao, W. Huang, D. Wang and X. Zhang, *Physica E*, 2010, **42**, 1281.

113. F. Aguilera-Granja and A. Vega, *Phys. Rev. B*, 2009, **79**, 144423.

114. C. L. Bracey, P. R. Ellis and G. J. Hutchings, *Chem. Soc. Rev.*, 2009, **38**, 2231.

115. D. A. Slanac, W. G. Hardin, K. P. Johnston and K. J. Stevenson, *J. Am. Chem. Soc.*, 2012, **134**, 9812.

116. C. Zhu, S. Guo and S. Dong, *J. Mater. Chem.*, 2012, **22**, 14851.

117. R. Ferrando, J. Jellinek and R. L. Johnston, *Chem. Rev.*, 2008, **108**, 845.

118. A. K. Sra and R. E. Schaak, *J. Am. Chem. Soc.* , 2001, **126**, 6667.

119. N. H. Chou and R. E. Schaak, *J. Am. Chem. Soc.*, 2007, **129**, 7339.

120. N. Mikami, N. Hata, T. Kikkawa and H. Machida, *AppL. Phys. Lett.*, 2003, **83**, 5181.

121. R. Rosenberg, D. C. Edelstein, C.-K. Hu and K. P. Rodbell, *Annu. Rev. Mater. Sci.*, 2000, **30**, 229.

122. J. Li, Y. Shacham-Diamand and J. W. Mayer, *Mater. Sci. Rep.*, 1992, **9**, 1.

123. D. D. Vaughn, J. F. Bondi and R. E. Schaak, *Chem. Mater.*, 2010, **22**, 6103.

124. D. V. Talapin, J.-S. Lee, M. V. Kovalenko and E. V. Shevchenko, *Chem. Rev.*, 2010, **110**, 389.

125. L. Krusin-Elbaum and M. O. Aboelfotoh, *Appl. Phys. Lett.*, 1991, **58**, 1341.

126. M. A. Borek, S. Oktyabrsky, M. O. Aboelfotoh and J. Narayan, *Appl. Phys. Lett.*, 1996, **69**, 3560.

127. H. K. Liou, J. S. Huang and K. N. Tu, *J. Appl. Phys.*, 1995, **77**, 5443.

128. N. A. Tabet and M. A. Salim, *Appl. Surf. Sci.*, 1998, **134**, 275.

129. J. P. Doyle, B. G. Svensson and S. Johansson, *Appl. Phys. Lett.*, 1995, **67**, 2804.

130. T. Brchhart, A. Lugstein, Y. J. Hyun, G. Hochleitner and E. Bertagnolli, *Nano Lett.*, 2009, **9**, 3739.

131. J. J. Liou and F. Schwierz, *Solid-State Electronics*, 2003, **47**, 1881.

132. M. O. Aboelfotoh and L. Krusin-Elbaum, *J. Appl. Phys.*, 1991, **70**, 3382.

133. S. Wang, S. Suthar, C. Hoeflich and B. J. Burrow, *J. Appl. Phys.*, 1993, **73**, 2301.

134. A. Kumar, A. Saxena, A. De, R. Shankar and S. Mozumdar, *RSC Adv.*, 2013, **3**, 5015.

135. M. Blosi, S. Albonetti, M. Dondi, C. Martelli and G. Baldi, *J. Nanoparticle Res.*, 2011, **13**, 127.

136. X. Song, S. Sun, W. Zhang and Z. Yin, *J. Colloid Interface Sci.*, 2004, **273**, 463.

137. B. K. Park, S. Jeong, D. Kim, J. Moon, S. Lim and J. S. Kim, *J. Colloid Interface*

Sci., 2007, **311**, 417.

138. S. Kapoor, R. Joshi and T. Mukherjee, *Chem. Phys. Lett.*, 2002, **354**, 443.
139. S. H. Wu and D. H. Chen, *J. Colloid Interface Sci.*, 2004, **273**, 165.
140. N. A. Dhas, C. P. Raj and A. Gedanken, *Chem. Mater.*, 1998, **10**, 1446.
141. Z. Liu and Y. Bando, *Adv. Mater.*, 2003, **15**, 303.
142. M. Raja, J. Subha, F. B. Ali and S. H. Ryu, *Mater. Manuf. Processes*, 2008, **23**, 782.
143. M.-S. Yeh, Y.-S. Yang, Y.-P. Lee, H.-F. Lee, Y.-H. Yeh and C.-S. Yeh, *J. Phys. Chem. B*, 1999, **103**, 6851.
144. A. Kornowski, M. Giersig, R. Vogel, A. Chemseddine and H. Weller, *Adv. Mater.*, 1993, **5**, 634.
145. B. R. Taylor, S. M. Kauzlarich, H. W. H. Lee and G. R. Delgado, *Chem. Mater.*, 1998, **10**, 22.
146. B. R. Taylor, S. M. Kauzlarich, G. R. Delgado and H. W. H. Lee, *Chem. Mater.*, 1999, **11**, 2493.
147. X. Ma, F. Wu and S. M. Kauzlarich, *J. Solid State Chem.*, 2008, **181**, 1628.
148. E. J. Henderson, C. M. Hessel and J. G. C. veinot, *J. Am. Chem. Soc.*, 2008, **130**, 3624.

Chapter 2:

Water-soluble Photoluminescent D-Mannose and L-Alanine Functionalized Silicon Nanocrystals and Their Application to Cancer Cell Imaging

A version of this chapter has been published:

Y. Zhai, M. Dasog, R. B. Snitynsky, T. K. Purkait, M. Aghajamali, A. H. Hahn, C. B. Sturdy, T. L. Lowary and J. G. C. Veinot, *J. Mater. Chem. B*, 2014, **2**, 8427.

2.1 Introduction

Luminescent quantum dots (QDs) have been proposed as additional type of materials to fluorescent organic dyes for bio-imaging applications.[1-5] Photobleaching is among the most important challenges associated with organic dyes and limits long-term *in vitro* and *in vivo* bioimaging.[6] QDs do not photobleach, exhibit tunable optical properties,[1] and possess tailorable surface chemistry.[7] However, II-VI QDs (*e.g.*, CdSe/ZnS QDs) and III-V (*e.g.*, InAs/GaAs QDs) are cytotoxic unless a biocompatible coating is added to reduce the cytotoxicity.[8] This is the main reason that limits practical utility for applications involving biological systems.[9-12]

Silicon nanocrystals (SiNCs) have attracted considerable interest in recent years for biological applications[13-17] because of their established biocompatibility,[18] abundance, and tunability.[19] The Veinot research group has reported the preparation of free standing hydride-terminated Si NCs through a reductive thermal annealing of hydrogen silsesquioxane (HSQ) (Scheme 2.1).[20] Briefly, HSQ was thermally processed under slightly reducing conditions (5% H_2/95%Ar) at 1100 ^{o}C for 1 h. Then, a 1:1:1 hydrofluoric acid (HF)/ethanol/water etching was performed to obtain hydride-terminated Si NCs. The resulting free standing Si NCs were purified by centrifugation and redispersed in toluene.

Because oxidation can change and even quench SiNC photoluminescence (PL), it is crucial that their surfaces be passivated. Unfortunately, protocols typically used to modify II-VI QDs are not readily compatible with SiNCs and alternative methods must be devised. To date, most approaches used to modify SiNC surfaces have aimed to introduce long chain alkyl groups rendering NCs hydrophobic and soluble in common organic solvents. Materials modified in this way are typically insoluble in water and their compatibility with biological systems is limited unless further modification is performed (*e.g.,* polymer coating).[21]

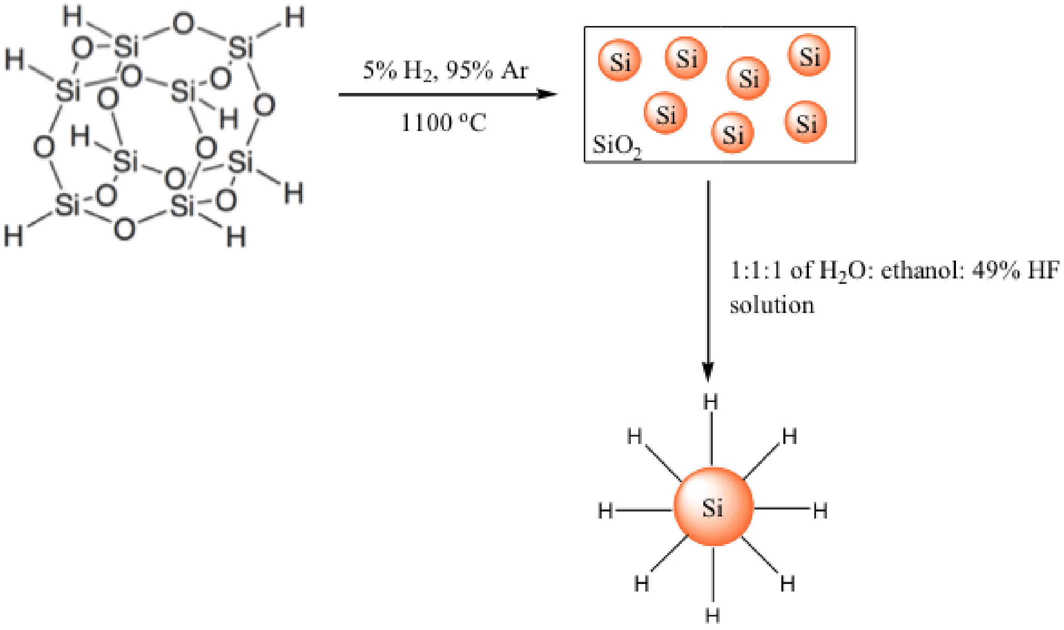

Scheme 2.1 Schematic representation of the synthesis of hydride-terminated SiNCs from thermal decomposition of HSQ.

Drawing on established approaches for rendering other QDs water-soluble, polar functionalities (e.g., $–NH_2$ and –COOH) have been tethered to SiNC surfaces.[7, 21-24] Unfortunately, amine terminated SiNCs are cytotoxic[25] and carboxylic acid terminated particles can be challenging to prepare and often show weak PL.[26] In this context, it is useful to explore alternative surface functionalities. Among potential candidates, carbohydrates and amino acids are particularly attractive due to the following reasons. First, carbohydrate functionalized NCs surfaces play a critical role in cell imaging, drug delivery and cancer detection, due to the rich structural variations of carbohydrates[27] and protein-carbohydrate interactions.[28] Mannose is chosen for its strong binding affinity to MCF 7 cancer cells.[29] Second, amino acid monomers could be linked by peptide bonds to form peptides. Biomolecules such as peptides and DNA functionalized NCs have become increasingly important for medicine, biotechnology and surgery.[30, 31] Alanine is chosen due to the structural simplicity. Third, carbohydrates and amino acids could provide high water solubility for biological applications. While reports describing carbohydrate functionalized SiNCs have appeared,[32, 33] these methods typically involve laborious multi-step procedures, as well as the use of costly and potentially toxic noble metal catalysts[34] that can compromise SiNC optical response.[35] To our knowledge, there are no reports of amino acid terminated SiNCs. In this chapter, we report a straightforward synthetic protocol for preparing water-soluble SiNCs functionalized with D-mannose and L-alanine and demonstrate a prototype application of these particles as luminescent imaging agents for the visualization of MCF-7 human breast cancer cells. MCF-7 human breast cancer cells were chosen as the targeting cells because they are an epithelial human cell line that grows quickly and easily and offer a convenient test imaging system.

2.2 Experimental

2.2.1 Reagents and Materials

A methyl isobutyl ketone solution of hydrogen silsesquioxane (HSQ) (*i.e.*, FOx® 17) was obtained from Dow Corning. The solvent was removed *in vacuo* to obtain a white solid that was used without further purification. Electronics grade hydrofluoric acid (HF, 49%) was purchased from J.T. Baker. Phosphorus pentachloride (PCl_5, 95%), toluene (reagent grade and anhydrous), methanol (reagent grade), ethylene glycol (99.8%), boron trifluoride diethyl etherate ($BF_3{\cdot}O(C_2H_5)_2$, 46.5% BF_3), azobisisobutyronitrile, and L-alanine methyl ester hydrochloride (99%) were purchased from Sigma-Aldrich. Sodium methoxide ($NaOCH_3$, 95%, Fisher), D-mannose (99%, Alfa Aesar), acetic anhydride (97%, Caledon Laboratories), pyridine (99%, Caledon Laboratories), dimethylaminopyridine (DMAP, 98%, Fluka), 4-pentenoic acid (98%, Alfa Aesar), and sodium hydroxide (NaOH, reagent grade, EMD Chemicals) were used as received. DMEM/High glucose medium and gold antifade reagent were purchased from HyClone and Prolong Pharmaceuticals, respectively.

2.2.2 Preparation of functionalized SiNCs

2.2.2.1 Synthesis of 1,2,3,4,6-penta-*O*-acetyl-α-D-mannopyranose

D-Mannose (2.0 g, 11.1 mmol) was dissolved in acetic anhydride (30 mL) at 0 °C. A catalytic quantity of DMAP was added, followed by pyridine (40 mL). The solution stirred overnight (16 h) while warming to room temperature. After co-evaporation with toluene (3 × 50 mL), the residue was dissolved in ethyl acetate and washed with 1 M HCl (2 × 50 mL), water (1 × 50 mL), saturated aqueous $NaHCO_3$ (2 × 50 mL), and brine (1 × 50 mL). The solution was dried over Na_2SO_4, filtered, and concentrated giving a clear, slightly yellow oil. The crude material was purified by column chromatography (silica, 3:1 → 1:1 hexane:ethyl acetate) to yield 4.4 g (10.7 mmol, 96%) of the α-anomer of the desired compound as a white solid. The NMR spectrum obtained for the product was consistent with previously published data.[36] ^1H NMR (500 MHz, $CDCl_3$) δ 6.09 (d, *J* = 2.0 Hz, 1H, H-1), 5.36–5.34 (m, 2H, H-3, H-4), 5.26 (dd, *J* = 3.0, 2.0 Hz, 1H, H-2), 4.28 (dd, *J* = 12.5, 5.0 Hz, 1H, H-6), 4.11 (dd, *J* = 12.5, 2.5 Hz, 1H, H-6′), 4.05 (ddd, *J* = 9.5, 5.0, 2.5 Hz, 1H, H-5), 2.18 (s, 3H, $COCH_3$), 2.17 (s, 3H, $COCH_3$), 2.10 (s, 3H, $COCH_3$), 2.05 (s, 3H, $COCH_3$), 2.01 (s, 3H, $COCH_3$); ^{13}C NMR (125 MHz, $CDCl_3$) δ 170.7, 170.0, 169.8, 169.6, 168.1 (5 x *CO*CH3), 90.7 (C-1), 70.7 (C-5), 68.8 (C-3), 68.4 (C-2), 65.6 (C-4), 62.2 (C-6), 20.9, 20.8, 20.8, 20.7, 20.7 (5 x COCH_3).

2.2.2.2 Synthesis of 2′-hydroxyethyl 2,3,4,6-tetra-*O*-acetyl-α-D-mannopyranoside (1)

1,2,3,4,6-Penta-*O*-acetyl-α-D-mannopyranose (4.4 g, 10.7 mmol) and anhydrous ethylene glycol (3.0 mL, 53.5 mmol) stirring in dry CH_2Cl_2 (40 mL) under an argon atmosphere were cooled to 0°C. BF_3•OEt_2 (6.7 mL, 53.5 mmol) was added, and the solution gradually warmed to room temperature. After 16 hours, $NaHCO_3$ saturated solution (40 mL) was added and stirred until gas evolution ceased. The organic layer was separated and washed with $NaHCO_3$ saturated solution (40 mL) and brine (30 mL), then dried over Na_2SO_4, filtered, and concentrated to a yellow oil. The crude material was purified by column chromatography (silica, 1:1 hexane:ethyl acetate) to yield 1.14 g of pure material as a colorless oil (2.91 mmol, 27%). The NMR spectrum obtained on the product was consistent with previously published data.[37] $[\alpha]_D$ = +40 (*c* = 0.73, CH_2Cl_2); FTIR (thin film): 3492, 2941, 2882, 1747, 1232 cm^{-1}; ^1H NMR (400 MHz, $CDCl_3$) δ 5.36 (dd, *J* = 10.4, 3.6 Hz, 1H, H-3), 5.31-5.24 (m, 2H, H-2, H-4), 4.87 (d, *J* = 1.6 Hz, 1H, H-1), 4.26 (dd, *J* = 12.0, 5.6 Hz, 1H, H-6), 4.13 (dd, *J* = 12.0, 2.4 Hz, 1H, H-6′), 4.07 (ddd, *J* = 10.0, 5.6, 2.4 Hz, 1H, H-5), 3.83-3.65 (m, 4H, OCH_2CH_2OH), 2.16 (s, 3H, COCH_3), 2.10 (s, 3H, COCH_3), 2.05 (s, 3H, COCH_3), 2.00 (s, 3H, CO*CH_3*); ^{13}C NMR (100 MHz, $CDCl_3$) δ 170.7, 170.1, 170.0, 170.0 (4 x *CO*CH_3), 98.1 (C-1), 70.6 (CH_2*CH_2*OH), 69.6 (C-2), 69.0 (C-3), 68.8 (C-5), 66.3 (C-4), 62.6 (C-6), 61.8 (*CH_2*CH_2OH), 20.9, 20.8, 20.7, 20.7 (4 x CO*CH_3*); HRMS (ESI) m/z Calcd for $C_{16}H_{24}NaO_{11}$ [M+Na]+: 415.1211. Found: 415.1206.

2.2.2.3 Synthesis of hydride-terminated SiNCs

HSQ (3.0 g) was transferred to a quartz boat and thermally processed under slightly reducing conditions (*i.e.*, flowing 5% H_2/95% Ar) at 1100 °C for 1 h in a tube furnace. After the resulting product was cooled to room temperatures the amber solid consisting of oxide-embedded SiNCs was ground using an agate mortar and pestle. To obtain freestanding hydride-terminated SiNCs, the ground SiNC/SiO_2 composite (0.30 g) was etched using 9 mL of a 1:1:1/v:v:v mixture of H_2O: ethanol: 49% HF solution. The mixture was stirred for an hour under ambient conditions to remove the SiO_2 matrix. The resulting hydride terminated SiNCs were extracted using three 10 mL portions of toluene. The product was centrifuged at 3000 rpm for 10 min and the supernatant was discarded.

2.2.2.4 Synthesis of chloride-terminated SiNCs

PCl_5 （0.30 g, 1.4 mmol） was added to a dry Schlenk flask containing hydride-terminated SiNCs (ca. 60 mg) dispersed in toluene (10 mL) to form a cloudy orange suspension. The resulting mixture was stirred for 1.5 h under argon atmosphere. Following the reaction the product mixture appeared as a light yellow clear solution. The solvent and reaction by products were then removed *in vacuo* to yield chloride terminated SiNCs (Cl-SiNCs) as an orange solid.

2.2.2.5 Synthesis of D-mannose functionalized SiNCs

1 (0.10 g, 0.4 mmol) was transferred to a Schlenk flask containing Cl-SiNCs (*vide supra*). 12 mL of anhydrous toluene were added to the reaction flask. The resulting mixture was stirred for 16 h at 40 °C under inert Ar atmosphere. Subsequently, the toluene was removed from the crude product mixture under vacuum and the resulting particles were dispersed in 10 mL methanol. Solid sodium methoxide was added to the methanol solution until the pH ~ 9. The resulting solution was stirred in air at ambient temperature for 12 h and then neutralized using Amberlite IR-120 ion exchange resin (acid form). The neutralization was monitored using pH paper. The resulting neutral solution was concentrated to yield a solid using a rotary evaporator and then functionalized SiNCs were redispersed in water and the exchange resin was removed via gravity filtration.

2.2.2.6 Synthesis of L-alanine functionalized SiNCs

L-alanine methyl ester (0.08 g, 0.6 mmol) was added to a dry Schlenk flask containing Cl-SiNCs (*vide supra*). 12 mL dry toluene were added to the reaction flask and the resulting mixture was stirred for 16 h at 40 °C under inert Ar atmosphere. Following the reaction the solvent was removed using a rotary evaporator. The resulting solid residue was redispersed in 5 mL of methanol. 2.5 mL of 1 M aqueous NaOH were added to the alanine methyl ester functionalized SiNCs. The solution was then heated to reflux and stirred for 1 hour followed by cooling to room temperature. The resulting solution was neutralized using Amberlite IR-120 ion exchange resin (acid form), and the neutralization process was monitored using pH paper. The solution was concentrated to yield a solid using rotary evaporator. The SiNCs were redispersed in water and the exchange resin was removed via gravity filtration.

2.2.2.7 Synthesis of pentanoic acid functionalized SiNCs

Immediately after etching 0.2 g of SiNC/SiO_2 composite, the resulting hydride-terminated SiNCs were isolated and redispersed in 15 mL dry toluene in a Schlenk flask equipped with a stir bar. Azobisisobutyronitrile (AIBN, 10 mg) and 4-pentenoic acid (4 mL) were added to the flask and the mixture degassed by performing three freeze/pump/thaw cycles using an Ar charged Schlenk line. The solution was stirred at 65 °C for 15 h after which time the reaction mixture was transferred into test tubes and centrifuged at 3000 rpm. The supernatant was discarded and the solid product was purified by three successive dispersion/precipitation cycles by the addition of ethanol/pentane mixture as the solvent/antisolvent and centrifugation.

2.2.2.8 Cell Studies

10 μL of the solution of mannose functionalized SiNCs (620 μg/mL) was added to 300 μL medium containing MCF-7 cells (6000 cells/well). The same concentration of solutions of alanine and pentanoic acid functionalized SiNCs were prepared and added to MCF-7 cells respectively. The cells were incubated at 37 °C for 24 hours. Subsequently, the medium was removed upon washing with phosphate buffered saline (PBS). Cells were "fixed" upon incubation with paraformaldehyde for 30 minutes. Fixed cells were washed with PBS three times and a small drop of anti-fade solution was added to each slide. A coverslip was placed over the specimen and the edges were sealed with clear nail polish.

2.2.3 Material Characterization

2.2.3.1 Fourier Transform Infrared Spectroscopy (FTIR)

FTIR was performed on powder samples using a Nicolet Magna 750 IR spectrometer. Samples were prepared as films drop-cast from solution onto KBr pellets, the films were measured as prepared in reflectance mode.

2.2.3.2 Quantum Yield

The relative fluorescence quantum yields were determined using methods adapted from the work of Williams *et al.* 9,10-biphenylanthracene in cyclohexane and coumarin 1 in absolute ethanol were used as the reference organic dyes.[38] The functionalized Si-NCs were dissolved in methanol. All the organic solvents were passed through a column of anhydrous magnesium sulfate to remove any adhering moisture prior to making the solutions. The stock solutions were prepared by dissolving 10 mg of the organic dye in the appropriate solvent mentioned above and was stirred until the entire solid was dissolved. The solutions were subsequently filtered through a membrane filter (2 μm) to remove suspended impurities and series of diluted solution were made with absorbances ranging from 0.1 and 0.01. PL spectra were acquired for the exact same solutions at the excitation wavelength of 300 nm. The slopes of integrated fluorescence intensity versus UV-Vis absorbance curves were plotted and compared to confirm the quality of the reference curves. In all cases, the experimentally determined quantum yields were in good agreement with literature values: 9, 10-biphenylanthracene, 0.9 and coumarin 1, 0.73. The Si-NC samples and the reference samples were excited at the same wavelength and PL was recorded with the same slit width. The quantum yields were determined using the following equation:

$$\varphi_{x=}\,\varphi_{st}\,\left(\frac{m_x}{m_{st}}\right)\left(\frac{\eta_x^2}{\eta_{st}^2}\right)$$

where ‘ɸ’ is the quantum yield, ‘m’ is the slope of the integrated PL versus absorbance curve and ‘η’ is the refractive index of the solvent. The subscript ‘st’ refers to the standard organic dye while ‘x’ indicates the unknown species to be calculated.

2.2.3.3 Photoluminescence (PL) spectroscopy

PL spectra of solution samples were acquired using a Varian Cary Eclipse Fluorescence Spectrometer.

2.2.3.4 Transmission Electron Microscopy (TEM) and high resolution TEM

TEM analysis was performed using a JOEL-2010 (LaB_6 filament) with an accelerating voltage of 200 kV. High resolution (HR) TEM images were obtained from Hitachi-9500 electron microscope with an accelerating voltage of 300 kV. TEM and high resolution TEM samples were prepared by dropcoating freestanding SiNC suspensions onto a carbon coated copper grid and the solvent was removed under vacuum. The NC size was averaged for 200 particles using Image J software (version 1.45).

2.2.3.5 X-Ray Photoelectron Spectroscopy (XPS)

XPS analyses were performed using a Kratos Axis Ultra instrument operating in energy spectrum mode at 210 W. Samples were prepared as films drop-cast from solution onto a copper foil substrate. The base and operating chamber pressure were maintained at 10^{-7} Pa. A monochromatic Al K_α source ($\lambda = 8.34$ Å) was used to irradiate the samples, and the spectra were obtained with an electron take-off angle of 90°. To minimize sample charging, the charge neutralizer filament was used when required. Survey spectra were collected using an elliptical spot with major and minor axis lengths of 2 and 1 mm, respectively, and 160 eV pass energy with a step of 0.33 eV. CasaXPS software (VAMAS) was used to interpret high-resolution (HR) spectra. All spectra were internally calibrated to the C 1s emission (284.8 eV). After calibration, a Shirley-type background was applied to remove most of the extrinsic loss structure. The FWHM for all the fitted peaks was maintained below 1.2 eV.

2.2.3.6 Dynamic Light Scattering (DLS)

DLS samples consisted of SiNCs in ethanol (refractive index 1.361). All samples were filtered using a 0.45 μm PTFE syringe filter and equilibrated to 25 °C before measurements were acquired. All measurements were made using a Malvern Zetasizer Nano S series dynamic light scatterer with 633 nm laser. A refractive index of 1.460 for

SiO_2 was used for all measurements since it was assumed that the remaining unfunctionalized SiNC surface would be oxidized in water.

2.2.3.7 Cell imaging

Cell imaging was performed using a Leica microscope (DM5500B; Wetzlar, Germany) with a 20× objective and a Retiga Exi camera (Qimaging, Surrey, BC, Canada) using Openlab 5.1 (Perkin Elmer Inc., Waltham, MA, USA).

2.3 Results and discussion

2.3.1 SiNCs synthesis and surface functionalization

Our group previously reported the preparation of oxide-embedded and freestanding SiNCs from the reductive thermal processing of HSQ.[26] This procedure affords well-defined, comprehensively characterized materials with dimensions that depend upon the processing conditions.[20, 39] Chloride terminated SiNCs (Cl-SiNCs) are obtained upon reaction of hydride terminated SiNCs with phosphorus pentachloride (PCl_5).[40] Reaction byproducts and toluene are readily removed from the Cl-SiNCs *in vacuo*. It is these Cl-terminated NCs that were used as the functionalization platform for the present study. Further derivatization of Cl-SiNCs (Scheme 2.2) was achieved upon direct addition of acetate-protected D-mannose or L-alanine methyl ester hydrochloride followed by neutralization and appropriate deprotection. The resulting functionalized SiNCs were dispersed in water.

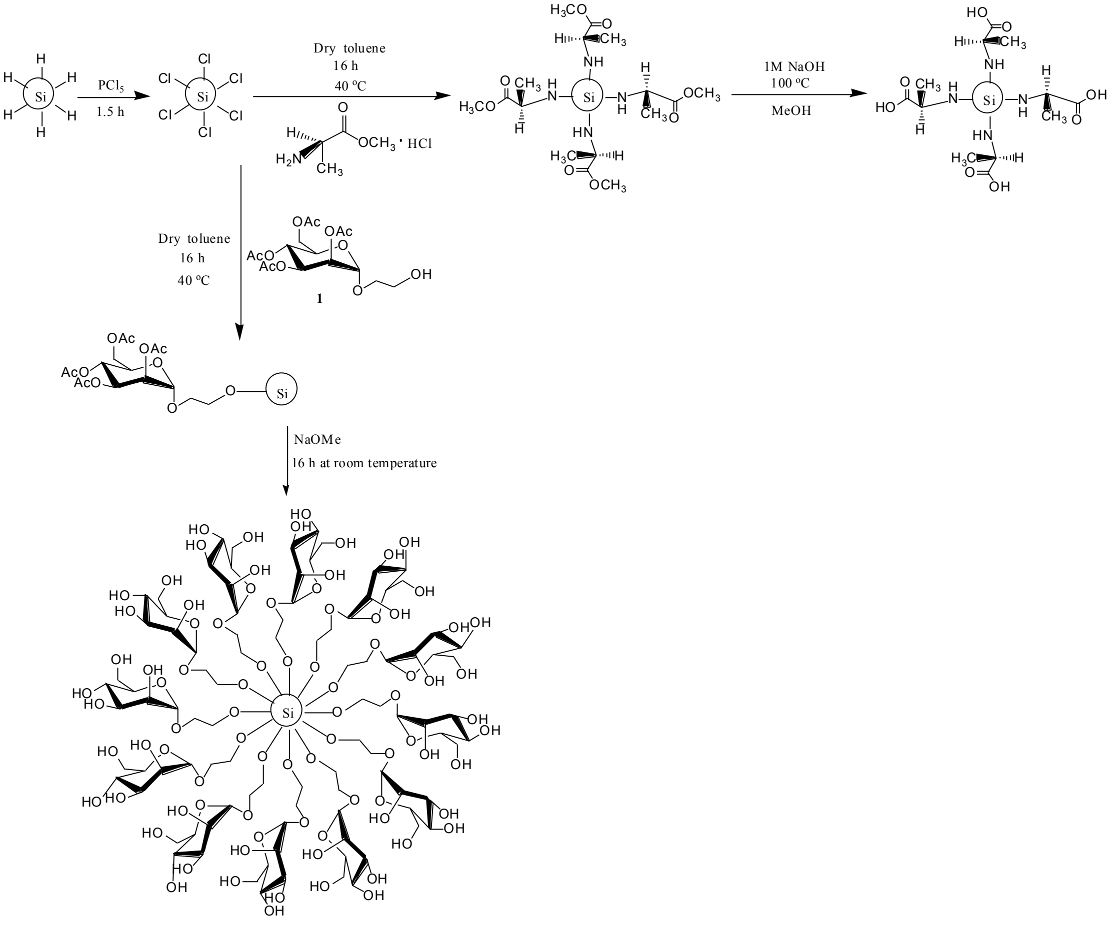

Scheme 2.2 Chlorination of hydride-terminated SiNCs and the synthesis of mannose and alanine functionalized SiNCs.

2.3.2 Nanocrystal characterization

FTIR spectroscopy provides valuable insight into the nature of the SiNC surface chemistry (Fig. 2.1 and 2.2). As expected, the FTIR spectrum of hydride terminated SiNCs (not shown) reveals a characteristic Si–H stretching feature at 2100 cm^{-1}.[20] The reactivity of Cl-SiNCs precluded isolation and direct characterization; however, comprehensive characterization (*vide infra*) of the products isolated from subsequent derivatization procedures confirm the NC integrity was not compromised by exposure to PCl_5.

Functionalization with an acetate-protected D-mannose-derived glycoside, L-alanine methyl ester, and pentanoic acid yielded SiNCs displaying FTIR spectra with features characteristic of the target surface groups (See Fig. 2.1). Among the most dominant features in both spectra is an absorption at ca. 1735 cm^{-1} that is readily attributed to C=O stretching arising from the ester functionalities. Following deprotection of the D-mannose SiNCs the C=O feature was replaced by a broad absorption centred at 3350 cm^{-1} consistent with the presence of –OH moieties. A comparison of the spectra obtained before and after deprotection of the alanine methyl ester functionalized SiNCs revealed similar changes.

Among the attractive properties of the present SiNCs that can be applied to biological imaging is their PL response. SiNC PL can be influenced by surface chemistry although the exact origin of the luminescence remains the subject of much investigation.[40-43] Aqueous solutions of the presented mannose and alanine functionalized SiNCs show blue photoluminescence (PL) with maximum ca. 415 nm and 400 nm upon excitation at 350 nm (Fig. 2.3). Blue emission may not be as ideal as red emission for cell imaging, but still remains useful. The PL spectrum of an aqueous solution of pentanoic acid functionalized SiNCs shows a maximum at ~ 640 nm upon excitation at 350 nm. Quantum yields of mannose and alanine functionalized SiNCs have been investigated. The quantum yield of mannose functionalized SiNCs is 13% and of alanine functionalized SiNCs is 17%. The quantum yield is relatively low compare to organic dyes (0.5-1.0 in visible light range) and other quantum dots (0.65-0.85 for CdSe, ≤0.6 for CdS and 0.1-0.4 for InP).[6]

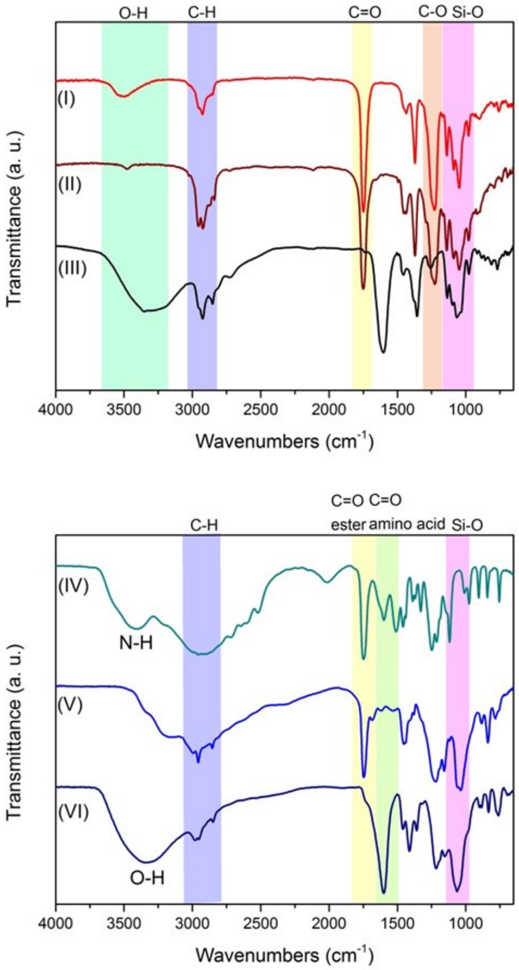

Fig. 2.1 FTIR spectra of (I) **1**, (II) **1** functionalized SiNCs, (III) mannose functionalized SiNCs, (IV) L-alanine methyl ester hydrochloride, (V) alanine methyl ester functionalized SiNCs and (VI) alanine functionalized SiNCs.

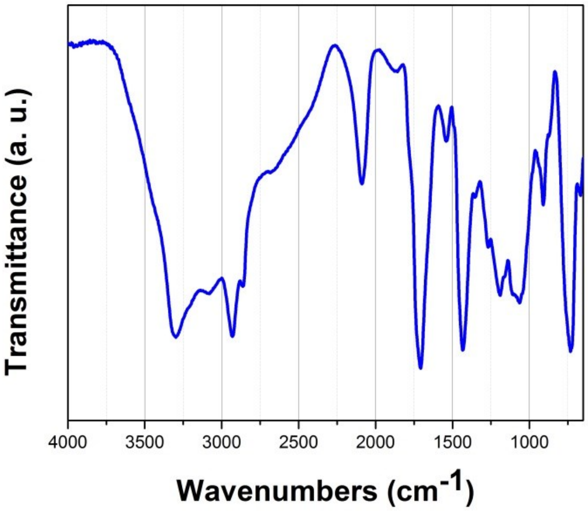

Fig. 2.2 FTIR spectra of pentanoic acid functionalized SiNCs.

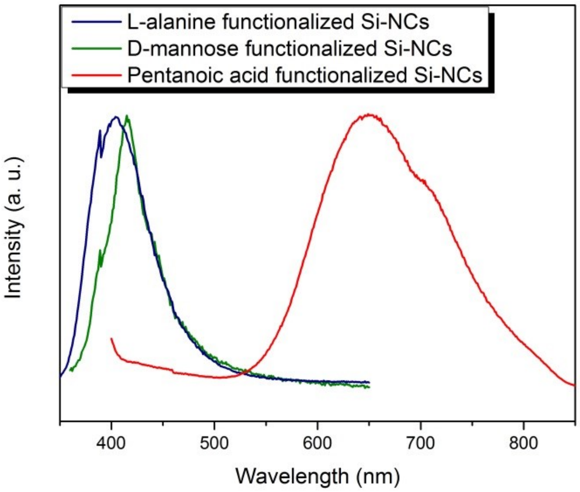

Fig 2.3 PL spectra of mannose functionalized SiNCs excited at 350 nm, alanine functionalized SiNCs excited at 335 nm, and pentanoic acid functionalized SiNCs excited at 350 nm.

XPS provides information regarding the elemental composition of the functionalized SiNCs, insight into the degree of surface oxidation, and confirmation that the SiNC core remains intact. Survey XP spectra of the presented NCs (Fig. 2.4) showed expected elemental emission features. The emissions at 102.2 eV (Fig. 2.5A), 102.1 eV (Fig. 2.5B), and 100.3 eV (Fig. 2.5C) can be attributed to Si–O, Si–N and Si–C functionalities, respectively.[41] The emission feature at lower binding energy (i.e., ca. 99.3 eV) confirms the presence of a Si (0) core in each sample. The N 1s peak (Fig. 2.5D) is consistent with the presence of alanine on the particle surface.

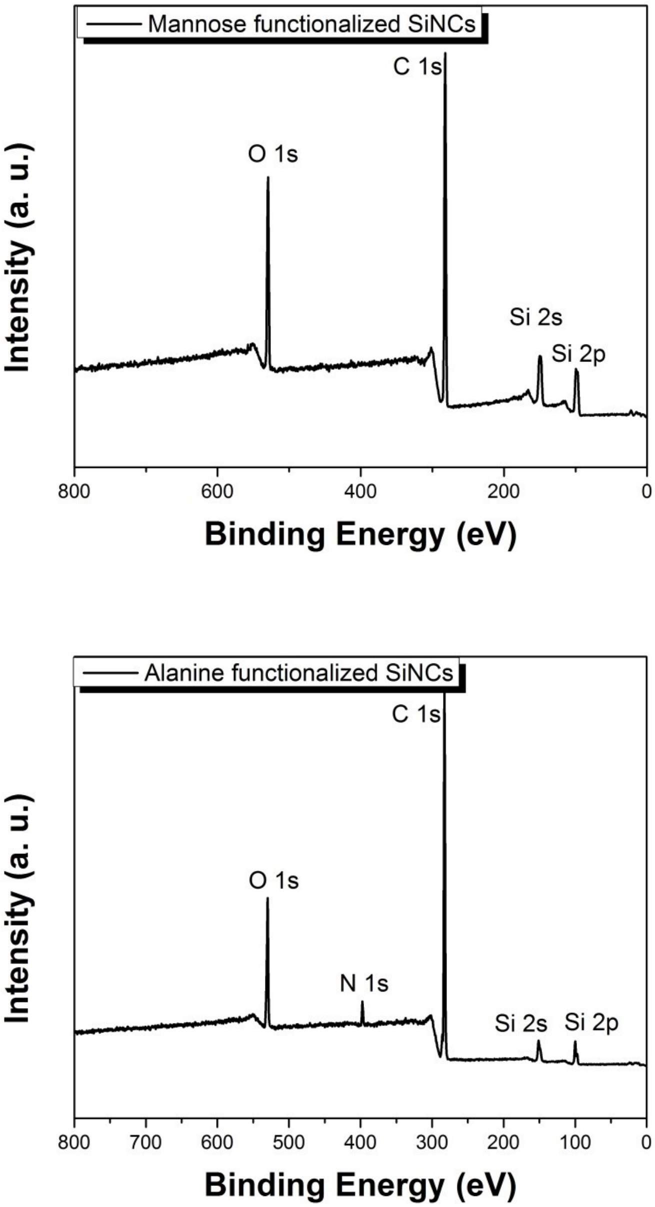

Fig. 2.4 XPS survey spectrum of mannose surface functionalized SiNCs and alanine surface functionalized SiNCs.

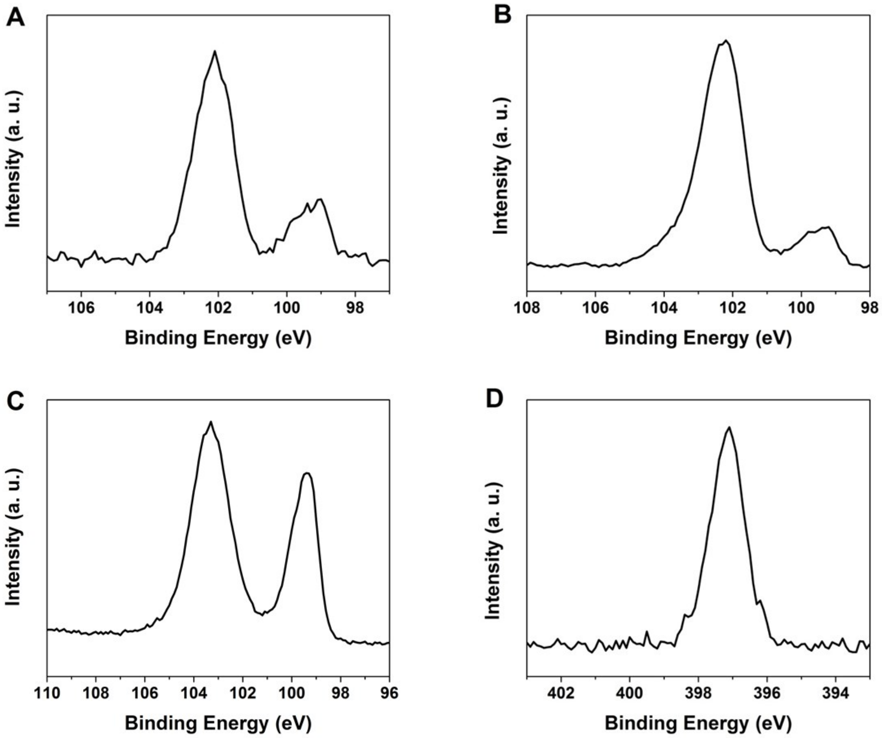

Fig. 2.5 X-ray photoelectron spectra (XPS) of the (A) Si 2p spectral region of mannose functionalized SiNCs, (B) Si 2p spectral region of alanine functionalized SiNCs, (C) Si 2p spectral region of pentanoic acid functionalized SiNCs, and (D) N 1s spectral region of alanine functionalized SiNCs.

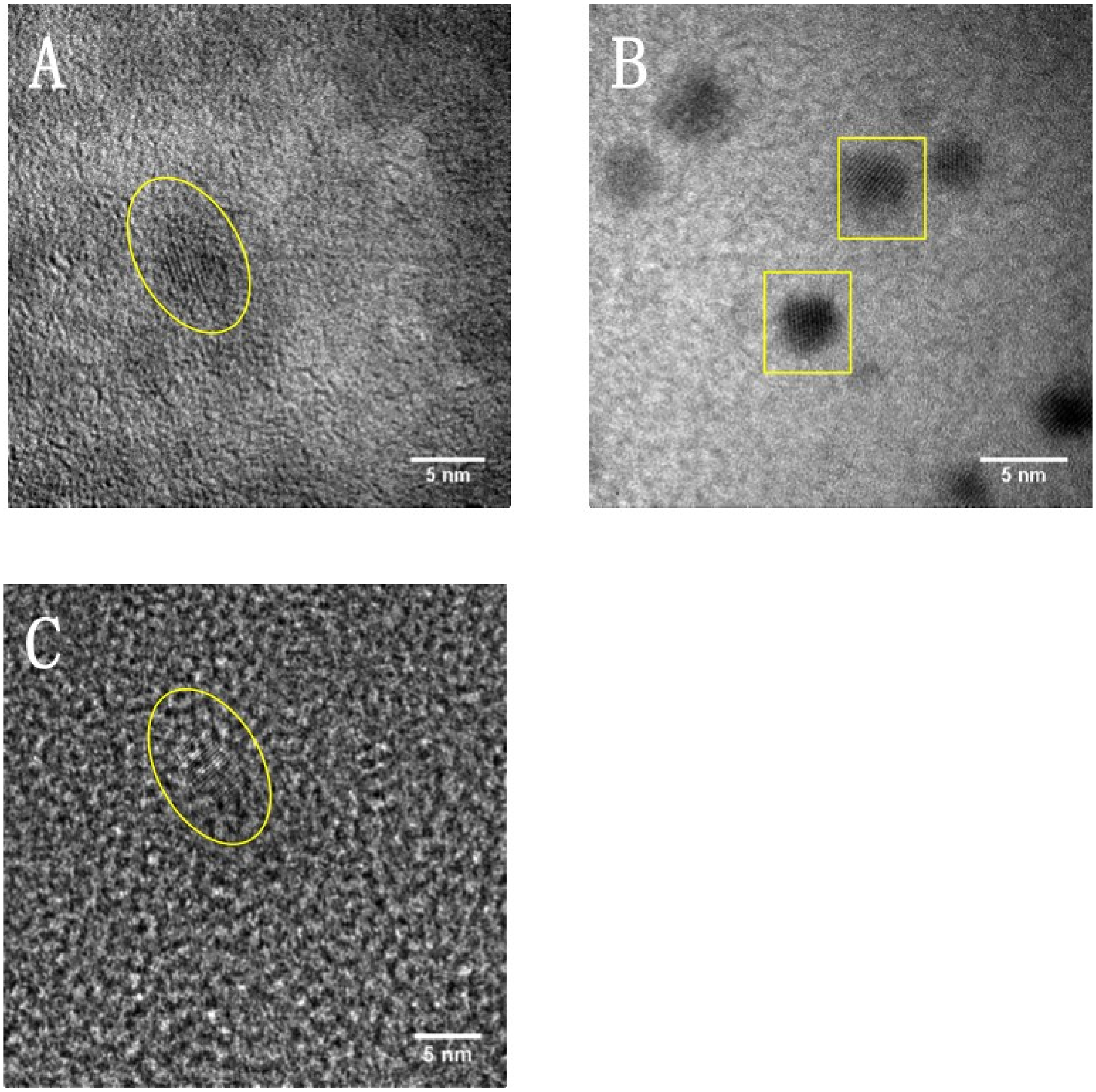

Fig. 2.6 HRTEM images of (A) mannose functionalized SiNCs, (B) alanine functionalized SiNCs, and (C) pentanoic acid functionalized SiNCs.

HRTEM imaging (Fig. 2.6) further confirms the SiNCs crystalline core remains intact. Lattice fringes spaced by 0.33 nm, characteristic of (111) separation,[44] are noted for D-mannose, L-alanine and pentanoic acid particles. TEM images (Fig. 2.7) also show mannose functionalized SiNCs with diameters of 2.6 ±

0.6 nm and alanine functionalized SiNCs with diameters of 2.7 ± 0.5 nm. Size distributions of these particles are shown in Fig.2.8 and DLS measurements are shown in Fig. 2.9. In all cases, the particle diameters measured by DLS are greater than the diameters measures by HRTEM. This observation is due to the formation of a water solvation sphere that increases the hydrodynamic diameters.

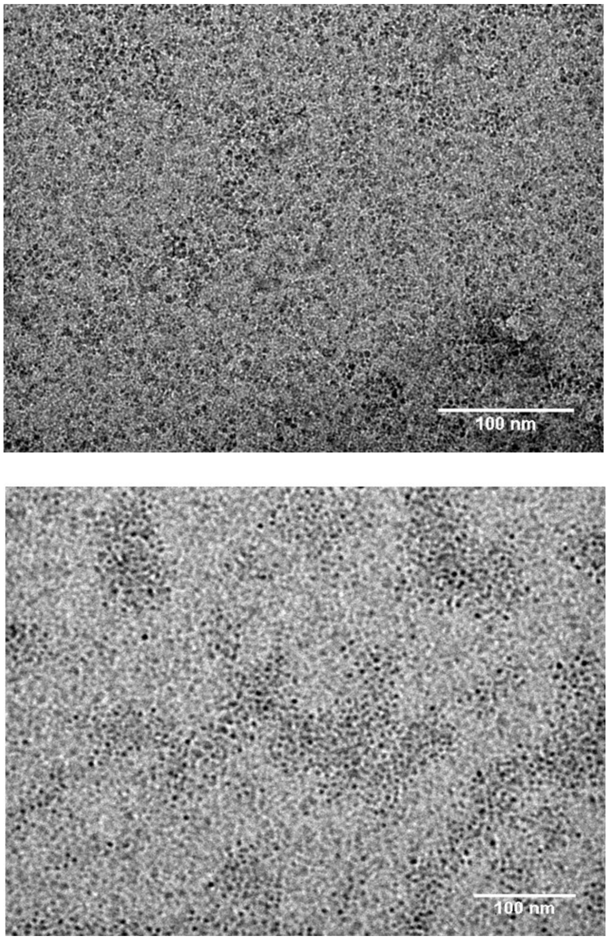

Fig. 2.7 TEM images of mannose functionalized Si NCs (top), and alanine functionalized SiNCs (bottom).

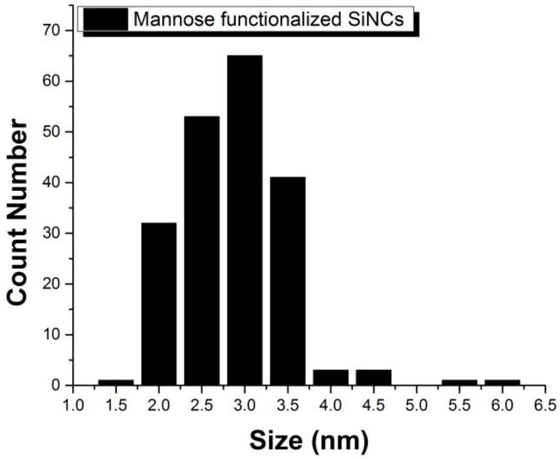

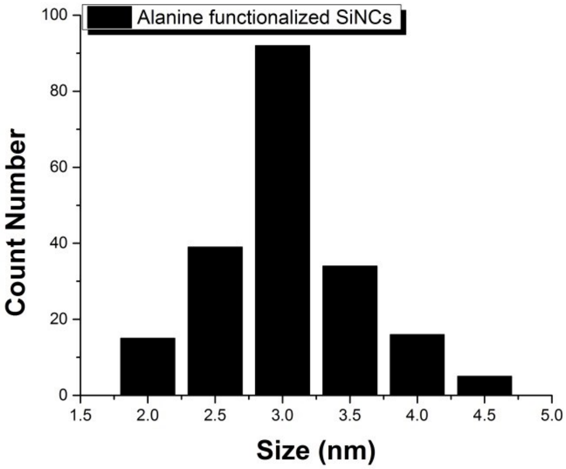

Fig. 2.8 Size distribution of mannose functionalized Si NCs with diameters of 2.6 ± 0.6 nm and alanine functionalized Si NCs with diameters of 2.7 ± 0.5 nm.

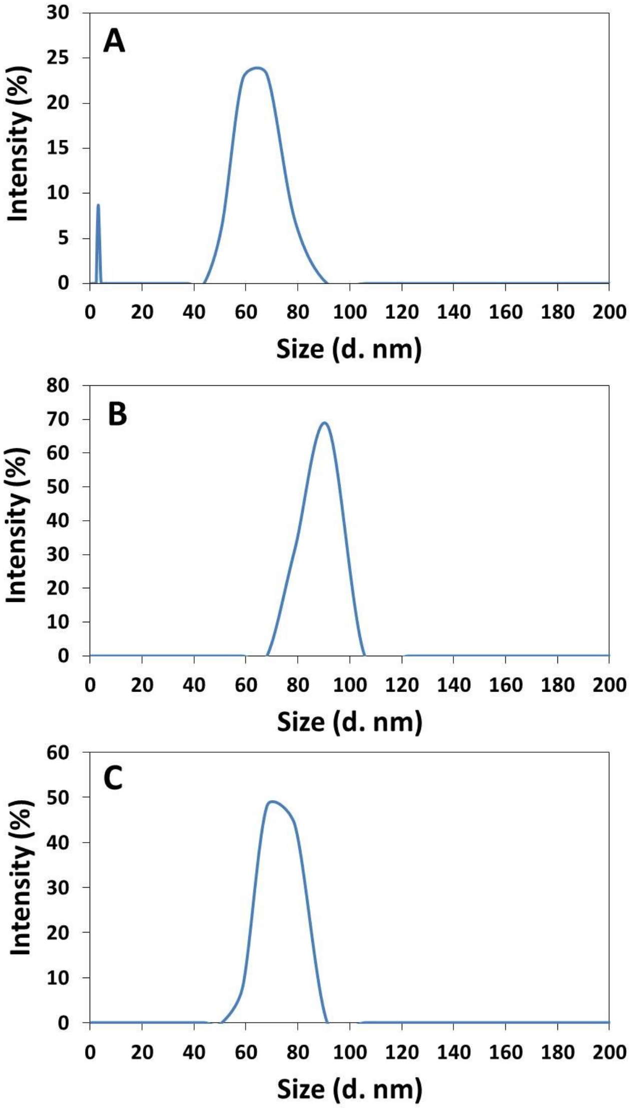

Fig. 2.9 DLS measurement of (A) mannose functionalized SiNCs, (B) alanine functionalized SiNCs, and (C) pentanoic acid functionalized SiNCs.

2.3.3 Cell study

It was shown in previous study that mannose has strong binding affinity to lectin (especially Concanavalin A lectin), which exist on the surface of the cells.[29] In addition, a detailed study of binding mannose with Escherichia coli was reported.[45] The present surface modifications were chosen for their known strong binding affinity (i.e., mannose), structural simplicity (i.e., alanine), and water solubility (i.e., pentanoic acid) the particles were exposed to MCF-7 human breast cancer cells. MCF-7 cells are an epithelial human cell line that grows quickly and easily. As well, they are an endogenous cell line, which means that they were actual cancer cells taken from a living human, and were not ordinary cells that were made to be cancerous through the action of a virus or other means at a later time. The uptake of mannose (Fig. 2.10A) and alanine (Fig. 2.10B) functionalized SiNCs by MCF-7 breast cancer cells was observed. To show that particle uptake resulted from the mannose or alanine functionalization, and not straightforward water solubility, cells were exposed to water-soluble red photoluminescent pentanoic acid functionalized SiNCs. No uptake of pentanoic acid functionalized SiNCs by the MCF-7 breast cancer cell was observed. These observations support the conclusion that mannose and alanine functionalization promoted cell uptake.

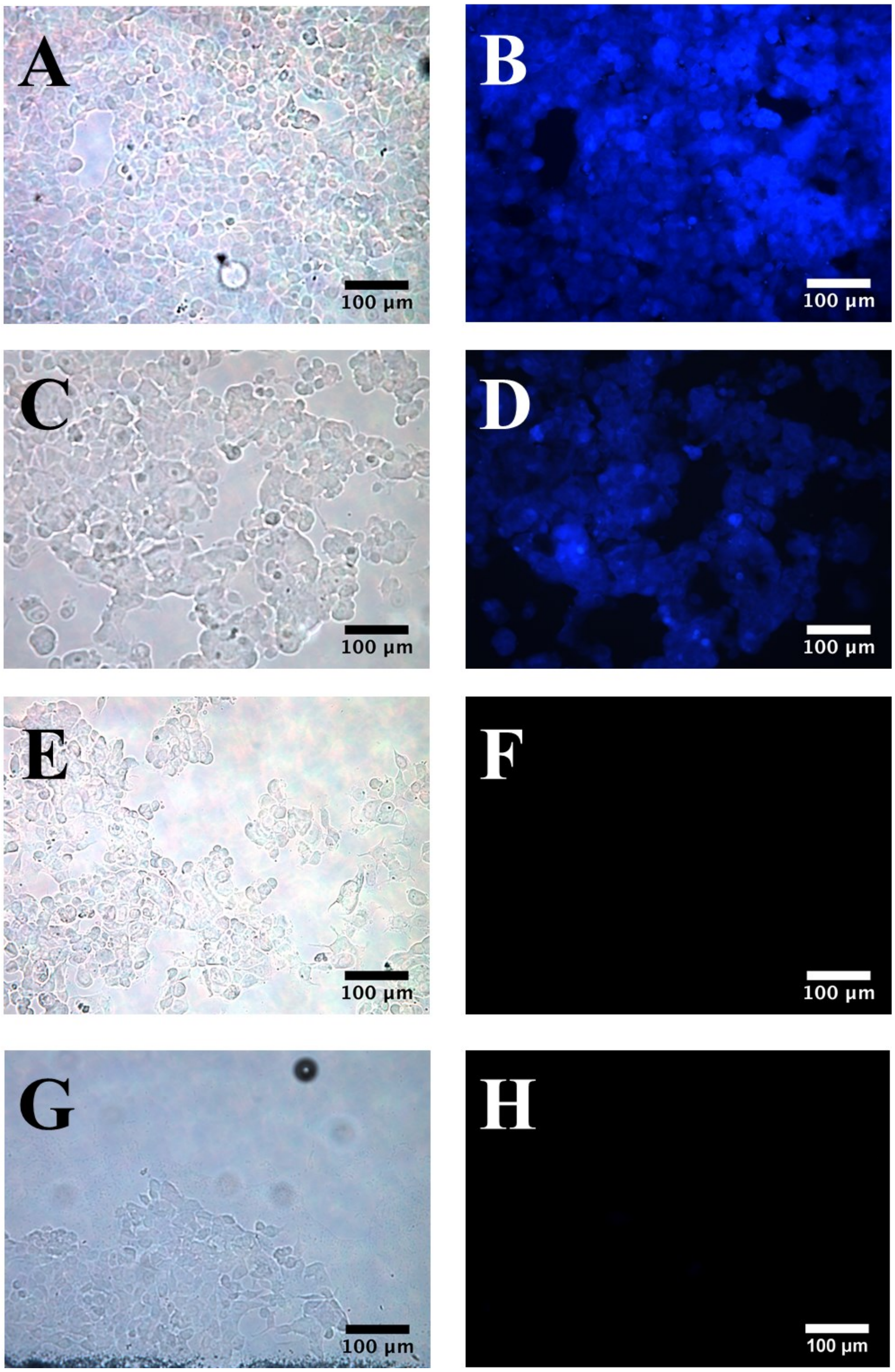

Fig. 2.10 Fluorescence images of MCF-7 cancer cells: (A) fluorescence from mannose functionalized SiNCs; (B) fluorescence from alanine functionalized SiNCs; (C) Control (without SiNCs), and (D) Control (pentanoic acid functionalized SiNCs).

2.4 Conclusions

In this chapter, we have demonstrated the synthesis and characterization of water-soluble, photoluminescent functionalized SiNCs bearing D-mannose, L-alanine, or pentanoic acid. These particles were subsequently visualized in MCF-7 human breast cancer cells. Mannose and alanine functionalized SiNCs were found to be taken up by MCF-7 cells allowing imaging; however, the pentanoic acid terminated SiNC did not. This observation indicates SiNCs can be effective luminescent imaging agents and that appropriate surface chemistry is crucial to their effectiveness in this application.

2.5 References

1. X. Michalet, F. F. Pinaud, L. A. Bentolila, J. M. Tsay, S. Doose, J. J. Li, G. Sundaresan, A. M. Wu, S. S. Gambhir and S. Weiss, *Science*, 2005, **307**, 538.
2. Y. He, C. Fan and S.-T. Lee, *Nano Today*, 2010, **5**, 282.
3. M. Bruchez Jr, M. Moronne, P. Gin, S. Weiss and A. P. Alivisatos, *Science*, 1998, **281**, 2013.
4. W. C. Chan, D. J. Maxwell, X. Gao, R. E. Bailey, M. Han and S. Neie, *Curr. Opin. Biotechnol.*, 2002, **13**, 40.
5. C. M. Niemeyer, *Angew. Chem. Int. Ed.*, 2001, **40**, 4128.
6. U. Resch-Genger, M. Grabolle, S. Cavaliere-Jaricot, R. Nitschke and T. Nann, *Nat. Methods*, 2008, **5**, 763.
7. M. De, P. S. Ghosh and V. M. Rotello, *Adv. Mater.*, 2008, **20**, 4225.
8. N. Lewinski, V. Colvin and R. Drezek, *Small*, 2008, **4**, 26.
9. R. Hardman, *Environ. Health Perspect.*, 2006, **114**, 165.
10. T. S. Hauck, R. E. Anderson, H. C. Fischer, S. Newbigging and W. C. Chan, *Small*, 2010, **6**, 138.
11. Y. Su, M. Hu, C. Fan, Y. He, Q. Li, W. Li, L. H. Wang, P. Shen and Q. Huang, *Biomaterials*, 2010, **31**, 4829.
12. A. M. Derfus, W. C. W. Chan and S. N. Bhatia, *Nano Lett.*, 2004, **4**, 11.
13. Z. Kang, Y. Liu and S. T. Lee, *Nanoscale*, 2011, **3**, 777.
14. F. Erogbogbo, K. T. Yong, I. Roy, R. Hu, W. C. Law, W. Zhao, H. Ding, F. Wu, R. Kumar, M. T. Swihart and P. N. Prasad, *ACS Nano*, 2011, **5**, 413.
15. J. Liu, F. Erogbogbo, K. T. Yong, L. Ye, J. Liu, R. Hu, H. Chen, Y. Hu, Y. Yang, J. Yang, I. Roy, N. A. Karker, M. T. Swihart and P. N. Prasad, *ACS Nano*, 2013, **7**, 7303.
16. F. Erogbogbo, C. W. Chang, J. L. May, L. Liu, R. Kumar, W. C. Law, H. Ding, K. T. Yong, I. Roy, M. Sheshadri, M. T. Swihart and P. N. Prasad, *Nanoscale*, 2012, **4**, 5483.
17. E. Borsella, R. D'Amato, M. Falconieri, E. Trave, A. Panariti and I. Rivolta, *J. Mater. Res.*, 2013, **28**, 193.
18. J. H. Park, L. Gu, G. von Maltzahn, E. Ruoslahti, S. N. Bhatia and M. J. Sailor, *Nat Mater.*, 2009, **8**, 331.
19. J. A. Kelly, A. M. Shukaliak, M. D. Fleischauer and J. G. Veinot, *J. Am. Chem.*

Soc., 2011, **133**, 9564.

20. C. M. Hessel, E. J. Henderson and J. G. C. Veinot, *Chem. Mater.*, 2006, **18**, 6139.
21. C. M. Hessel, M. R. Rasch, J. L. Hueso, B. W. Goodfellow, V. A. Akhavan, P. Puvanakrishnan, J. W. Tunnel and B. A. Korgel, *Small*, 2010, **6**, 2026.
22. Y. He, Y. Zhong, F. Peng, X. Wei, Y. Su, Y. Lu, S. Su, W. Gu, L. Liao and S. T. Lee, *J. Am. Chem. Soc.*, 2011, **133**, 14192.
23. F. Erogbogbo, C. A. Tien, C. W. Chang, K. T. Yong, W. C. Law, H. Ding, I. Roy, M. T. Swihart and P. N. Prasad, *Bioconjug Chem.*, 2011, **22**, 1081.
24. N. Prtljaga, E. D'Amato, A. Pitanti, R. Guider, E. Froner, S. Larcheri, M. Scarpa and L. Pavesi, *Nanotechnology*, 2011, **22**, 215704.
25. L. Ruizendaal, S. Bhattacharjee, K. Pournazari, M. Rosso-Vasic, L. H. J. de Haan, G. M. Alink, A. T. M. Marcelis and H. Zuilhof, *Nanotoxicology*, 2009, **3**, 339.
26. R. J. Clark, M. K. Dang and J. G. Veinot, *Langmuir : the ACS journal of surfaces and colloids*, 2010, **26**, 15657.
27. K. El-Boubbou, D. C. Zhu, C. Vasileiou, B. Borhan, D. Prosperi, W. Li and X. Huang, *J. Am. Chem. Soc.*, 2010, **132**, 4490.
28. C. Earhart, N. R. Jana, N. Erathodiyil and J. K. Ying, *Langmuir : the ACS journal of surfaces and colloids*, 2008, **24**, 6215.
29. X. Jiang, A. Housni, G. Gody, P. Boullanger, M.-T. Charreyre, T. Delair and R. Narain, *Bioconjugate Chem.*, 2010, **21**, 521.
30. L. Gentilucci, A. Tolomelli and F. Squassabia, *Curr. Med. Chem.* , 2006, **13**, 2449.
31. R. Kikkeri, B. Lepenies, A. Adibekian, P. Laurino and P. H. Seeberger, *J. Am. Chem. Soc.*, 2011, **131**, 2110.
32. J. H. Ahire, I. Chambrier, A. Mueller, Y. Bao and Y. Chao, *ACS Appl. Mater. Interfaces*, 2013, **5**, 7384.
33. Y. Nakahara, K. Machiya, T. Sato, N. T. Nwe, T. Furuike, H. Tamura and K. Kimura, *Chem. Lett.*, 2013, **42**, 498.
34. J. M. Lambert, *J. Biomed. Mater. Res. B*, 2006, **78B**, 167.
35. Z. Yang, M. H. Wahl and J. G. C. Veinot, *Can. J. Chem.*, 2014, **92**, 1 dio: 10.1139/cjc-2014-0048.
36. M. Dowlut, D. G. Hall and O. Hindsgaul, *J. Org. Chem.*, 2005, **70**, 9809.
37. W. Hayes, H. M. I. Osborn, S. D. Osborne, R. A. Rastall and B. Romagnoli, *Tetrahedron*, 2003, **59**, 7983.
38. A. T. R. Williams, S. A. Winfield and J. N. Miller, *Analyst*, 1983, **108**, 1067.

39. Z. Yang, A. R. Dobbie, K. Cui and J. G. Veinot, *J. Am. Chem. Soc.*, 2012, **134**, 13958.
40. M. Dasog and J. G. C. Veinot, *phys. Status Solidi A*, 2012, **209**, 1844.
41. M. Dasog, Z. Yang, S. Regli, T. M. Atkins, A. Faramus, M. P. Singh, E. Muthuswamy, S. M. Kauzlarich, R. D. Tilley and J. G. C. Veinot, *ACS Nano*, 2013, **7**, 2676.
42. S. S. Nekrashevich and V. A. Gritsenko, *J. Appl. Phys.*, 2011, **110**, 114103.
43. M. Dasog, G. B. De los Reyes, L. V. Titova, F. A. Hegmann and J. G. C. Veinot, *ACS Nano*, **doi: 10.1021/nn504109a**.
44. S. M. Liu, M. Kobayashi, S. Sato and K. Kimura, *Chem. Commun.*, 2005, 4690.
45. K. El-Boubbou, C. Gruden and X. Huang, *J. Am. Chem. Soc.*, 2007, **129**, 13392.

Chapter 3:

Synthesis of Copper-Germanium Alloy Nanoparticles from Copper@Germania Core/Shell Nanostructures

3.1 Introduction

In silicon-based semiconductor device technology, researchers are continually pursuing smaller, faster, and more efficient devices. In 1965, Moore observed and postulated that the number of transistors on an integrated circuit doubles every year; this has come to be known as Moore's law.[1, 2] As the number of devices increase and dimensions decrease, their speed is primarily determined by non-scaling effects, such as resistor-capacitor (RC) delays in the interconnect lines.[3] The realization and application of these smaller devices, and by extension the development of more efficient and rapid electronics is limited by existing metallization materials for integrated circuit interconnects and Ohmic contacts.[4] In this context, development of new materials of tailored resistivity is a key research target.

3.1.1 Metallization Materials

Copper. Historically copper has been the metallization material of choice for Si-based devices because of its low resistivity (~ 2 $\mu\Omega$ cm at 300 K), high reliability, and low cost,[5-7] but it is far from perfect. Cu oxidizes forming CuO and Cu_2O when exposed to elevated temperatures (i.e., ca. 250 °C) in air,[8, 9] which have much higher resistivities (ca. 25 Ω cm) and result in degraded device performance.[10] Furthermore, Cu defuses rapidly in Si – in fact, Cu can defuse through a standard 4 inch p-type Si wafer in 15 hours;[11] this diffusion leads to the formation of highly resistive Cu_3Si. Finally, Cu does not adhere well to SiO_2[8] making an adhesion layer necessary. While many of these challenges have been addressed by creative solutions appropriate for larger devices, when device dimensions are decreased the issues resurface.

Metal silicides. Metal silicides are attractive Cu alternatives.[12-14] They are generally prepared by depositing metal onto a Si substrate followed by annealing.[15] Metal silicides have attracted much attention because of their thermal stability and comparatively low resistivity (e.g., $TiSi_2$, 13–16 μΩ cm; $CoSi_2$, 18–20 μΩ cm).[4] Unfortunately, the high annealing temperature (i.e., 800 °C) of $TiSi_2$ required to achieve the desired electronic properties exceeds the thermal budget of a standard complementary metal oxide semiconductor (CMOS) chips.[4] Copper silicides are impractical. The resistivity of Cu_3Si films (~ 60 μΩ cm at 300 K),[16, 17] is about 30 times higher than Cu, and high susceptibility of Cu_3Si surface to oxidize at room temperature.

Copper Germanide. Copper germanide appears to be an appealing material and has been considered as an alternative to Cu and metal silicide due to the low resistivity (5.5 μΩ cm).[3] Copper germanide is oxidatively stable up to 520 °C,[4] and also shows less diffusion than Cu metal (see above).[18, 19] Copper germanide also adheres well to SiO_2.[4] The potential application of copper germanide as a metallization material in Si-based devices has been well documented in several reports.[4, 20-22]

3.1.2 Copper Germanide Synthetic Methods

A variety of procedures have been developed to prepare copper germanide. In this section, key examples are briefly summarized.

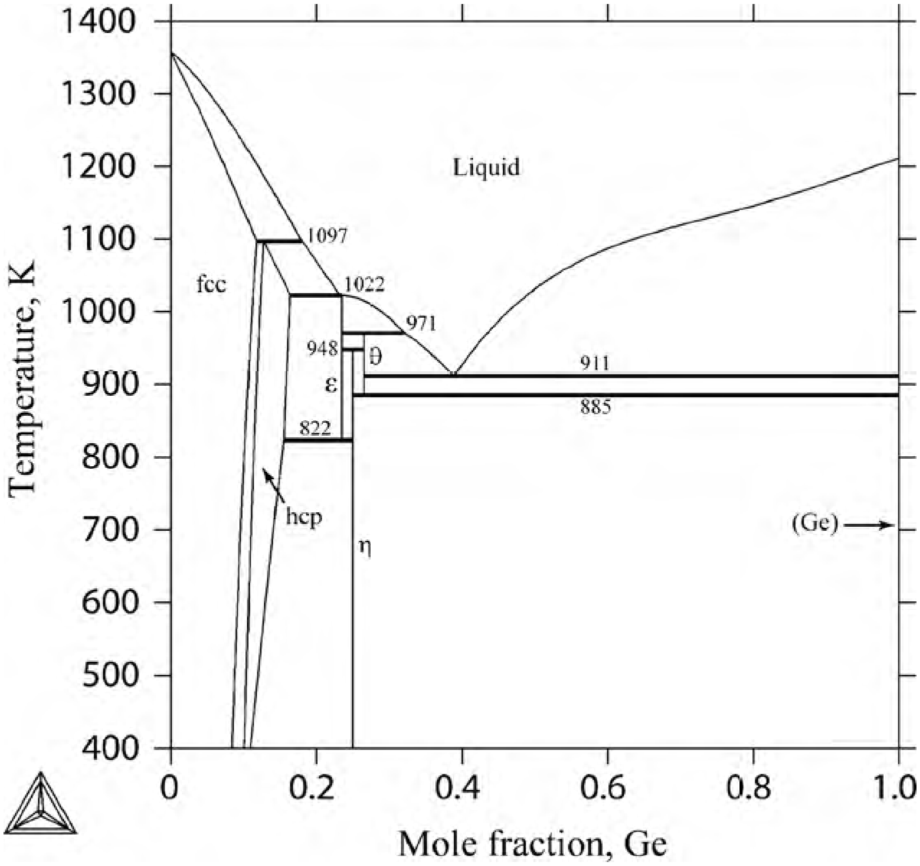

Fig. 3.1 Calculated phase diagram of the Cu/Ge binary system with experimental data. (Reprinted with permission from *J. Alloys Compd.,* 2010, **504**, 159. Copyrigt 2010 Elsevier B.V.)

In order to prepare Cu/Ge alloy, it is crucial to understand the phase diagram of the binary system. The solution phases, including liquid, face-centered cubic (fcc), hexagonal close-packed (hcp) and diamond (Ge) were investigated by Wang *et al.* (Fig. 3.1). According to the phase diagram of Cu/Ge binary system they published, the eutectic temperature for Cu/Ge is *ca.* 910 K with Ge composition of 38.9%.[23] Nanocrystalline materials process unique physical properties compared to bulk materials,[24] so there is the possibility that the eutectic temperature for nano-scale Cu/Ge is below 910 K. Moreover, the size of nanoparticles plays critical role in melting temperature.[25, 26] In nanoparticles, surface atoms make up a large portion of the total atoms compared bulk materials.[24] Surface atoms make significant contribution to surface energy; the overall energy becomes higher with decreasing particle size.[24] The decreasing of solid to liquid transition temperature with decreasing particle size has been reported.[26-29] The main reason for this phenomenon is the surface energy in liquid state is always lower than that in solid state.[24] Surface atoms move to minimize the surface energy to form a dynamic favourable state (liquid state).

Physical vapor deposition (PVD). PVD techniques including sputtering, electron beam and thermal evaporation[30, 31] have been used to prepare well-defined copper germanide thin films. Cu-Ge mixtures are commonly obtained by melting Cu and Ge components in alumina crucibles and subsequently the alloys are thermally evaporated to provide thin films.[30] A schematic of a thermal evaporation apparatus is shown in Fig. 3.2. In 1979, Nath *et al.* reported the preparation of Cu/Ge films using thermal evaporation for the first time.[30] Cu/Ge films were obtained by melting the constituents at 300 K and in a vacuum of about 10^{-6} Torr in an alumina crucible for 1 h. Of late thermal evaporation has been supplanted by more advanced physical vapor deposition methods (e.g., sputtering,[32] electron beam evaporation[33]) to yield more stable and uniform thin films. Various reports have shown the formation of copper germanide films by ion beam mixing. Dhar *et al.* reported room-temperature synthesis by ion beam mixing of the Cu3Ge phase In 2013, Das *et al.* reported the preparation of copper germanide thin films upon room temperature co-sputtering high purity Cu and Ge onto p-type Si wafers followed by microwave annealing.[34] Copper germanide thin films exhibiting a resistivity of 14 μΩ cm were obtained after 60 s microwave annealing at *ca.* 80 °C.

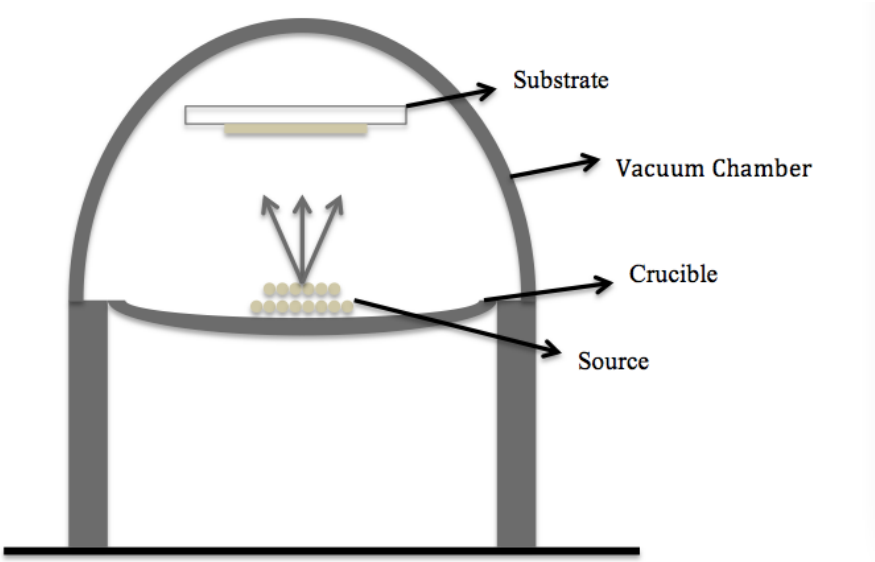

Fig. 3.2 Schematic of a thermal evaporation experiment.

Vapor-solid reactions. The synthesis of copper germanide through vapor-solid reaction has been reported by Elshocht group.[18] Cu was deposited on a substrate by PVD to obtain the Cu film. The Cu film was exposed to germane (GeH_4) in a mixture of N_2 at a pressure of 4.2 Torr. Different Cu film thicknesses, temperature and time were evalauted. 60 nm Cu film, 400 °C exposure-temperature and 30 s exposure-time were found to yield high quality copper germanide.

In this chapter an investigation into the synthesis and properties of Cu/Ge alloy nanoparticles is described. The general approach used here involves the synthesis of

Cu@GeO_2 core@shell nanoparticles using solution methods that are subsequently annealed in a reducing environment to yield Cu/Ge alloy nanoparticles (Scheme 3.1).

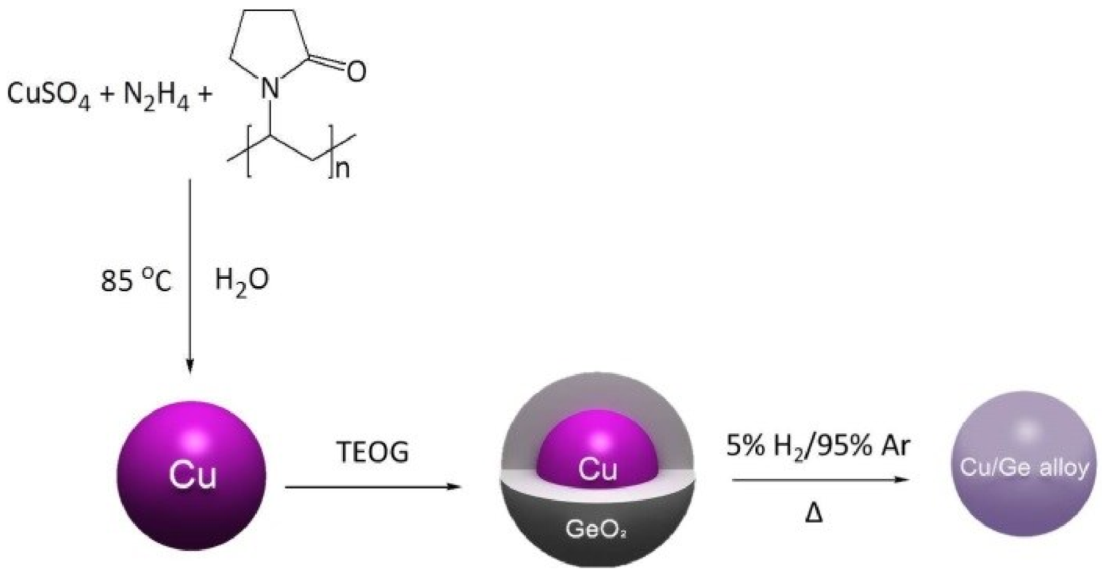

Scheme. 3.1 A schematic summary of the synthesis of Cu/Ge alloy.

3.2 Experimental

3.2.1 Reagents and materials

Polyvinylpyrrolidone (Sigma-Aldrich), hydrazine monohydrate (98%, Alfa Aesar), sodium hydroxide (NaOH, reagent grade, EMD Chemicals), and anhydrous copper sulphate ($CuSO_4$, Fisher) were used as received. Tetraethoxygermane (TEOG, 99.99%) was purchased from Gelest, stored in an argon-filled glovebox and used as received.

3.2.2 Preparation of Cu/Ge nanoparticles

3.2.2.1 Synthesis of Cu nanoparticles

Synthesis of CuNPs was achieved using a modification of the procedures described by Kumar, A[35] and Blosi, M[36] and their coworkers. Polyvinylpyrrolidone (2 g) was dissolved in deionized water (100 mL) in a 250 ml flask at ambient conditions. The reaction mixture was heated to 80 °C after which 4 mL of 1 M hydrazine hydrate solution and 1.6 ml of 0.1 M copper sulphate solution were added sequentially. The resulting solution was stirred for 5 min at 80 °C. The crude product solution was a dark purple. It was transferred to centrifuge tubes at ambient conditions. The crude product was isolated by centrifugation at 14000 rpm for 15 min as a purple/black solid. The clear colourless supernatant was decanted and discarded. The solid was subsequently sonicated using a bath sonicator in 100% ethanol. The resulting suspension was subjected to three sonication/centrifugation cycles and the purified particles were stored as an ethanol suspension. Products were characterized by X-Ray powder diffraction (XRD), X-ray photoelectron spectroscopy (XPS), transmission electron microscopy (TEM), and auger electron spectroscopy (AES).

3.2.2.2 Synthesis of Cu@GeO$_2$ core-shell nanoparticles

The as prepared Cu NPs were dispersed in 16 ml of absolute ethanol and 30 μL tetraethoxygermane (TEOG) were added to a Schlenk flask under argon atmosphere and the mixture was stirred at room temperature for 16 h. The crude product suspension was dark purple. It was transferred into centrifuge tubes at ambient conditions. The crude product was isolated by centrifugation at 14000 rpm for 15 min as a purple/black solid. The clear colourless supernatant was decanted and discarded. The solid was subsequently sonicated using a bath sonicator in 100% ethanol. The resulting suspension was subjected to three sonication/centrifugation cycles and the purified particles were stored as an ethanol suspension. Products were characterized by XRD, XPS, TEM, and AES.

3.2.2.3 Synthesis of copper germanide nanoparticles

The Cu@GeO$_2$ nanoparticle suspension was deposited onto Si wafers and subsequently placed in a quartz boat, transferred to a Lindberg Blue tube furnace, and heated from ambient to a peak processing temperature (600 °C, 700 °C, and 800 °C) at 18 °C min^{-1} in a slightly reducing atmosphere (5% H$_2$/95% Ar). The samples were maintained at the peak processing temperature for 15 h. Upon cooling to room temperature, the products were characterized by XRD, XPS, SEM, and AES.

3.2.3 Material Characterization

3.2.3.1 Transmission Electron Microscopy (TEM)

TEM analysis was performed using a JOEL-2010 equipped with a LaB_6 source at an accelerating voltage of 200 kV. TEM samples of CuNCs and Cu/Ge NPs were drop-coated onto a carbon coated nickel grid and the solvent was removed under vacuum. NC dimensions were determined for 200 particles using Image J software (version 1.45).

3.2.3.2 X-Ray Photoelectron Spectroscopy (XPS)

XPS analyses were performed using a Kratos Axis Ultra instrument operating in energy spectrum mode at 210 W. Samples were prepared as films drop-cast from solution onto a Si wafer substrate. The base and operating chamber pressure were maintained at 10^{-7} Pa. Samples were irradiated using a monochromatic Al K_α source (λ = 8.34 Å). To minimize sample charging, the charge neutralizer filament was used when required. Survey spectra were collected using an elliptical spot with major and minor axis lengths of 2 and 1 mm, respectively 160 eV pass energy with a step of 0.33 eV and take-off angle of 90°. CasaXPS software (VAMAS) was used to interpret high-resolution (HR) spectra. All spectra were internally calibrated to the C 1s emission (284.8 eV).[37] After calibration, a Shirley-type background was applied to remove most of the extrinsic loss structure.

3.2.3.3 X-Ray powder diffraction (XRD)

XRD patterns were collected using an INEL XRG 3000 X-Ray diffractometer equipped with Cu-Kα radiation (λ = 1.54 Å). Crystallinity of samples was evaluated for powders mounted on a low-intensity background Si (100) holder.

3.2.3.4 Scanning electron microscopy (SEM)

SEM images were obtained by using a JEOL 6301F field-emission scanning electron microscope with an acceleration voltage of 5 kV. A Si wafer was cleaned by ethanol. Samples were prepared as films drop-cast from solution onto a clean Si (100) wafer.

3.3 Results and discussion

3.3.1 Cu/Ge nanoparticles synthesis

3.3.1.1 CuNPs synthesis

A number of methods for preparing copper nanoparticles (CuNPs) were explored with varying degrees of success.[38-41] Our initial attempts to obtain CuNPs was through a modification of the published work of Panigrahi, S and co-workers (Scheme 3.3).[42] Briefly, 6 g glucose was dissolved in 25 mL 2×10^{-2} M NaOH after which 90 mL H_2O was added and the solution was heated up to 80 °C using a hot plate. 1.6 mL of 10^{-1} M $CuSO_4$ was added to the hot solution and the solution was left stirring for 20 min at 80 °C. The crude product was isolated by centrifugation at 14000 rpm for 15 min as a yellow solid. The clear supernatant was removed using pasteur pipette. The solid was subsequently sonicated using a bath sonicator in 100% ethanol. The remaining solution was subjected to three centrifugation cycles as described above and the purified particles were stored as an ethanol suspension. The products were characterized by XRD (Fig. 3.3). The resulting pattern shows five characteristic reflections at 30.3°, 37.2°, 43.2°, 62.6° and 75.0° attributable to the (110), (111), (200), (220) and (311) planes of Cu_2O.[43] Under the basic conditions, α-glucose transforms into β-glucose through the open chain structure (Scheme 3.2). In open chain form, the free –CHO group is reactive and causes the reduction of the Cu (II). Based on the XRD pattern, two possible reasons of the production of Cu_2O NPs instead of CuNPs could be addressed. First, -CHO group is not strong enough to reduce Cu (II) to Cu (0), only Cu (II) to Cu (I) happened in the reaction. Second, the as prepared CuNPs are unstable and prone to oxidation to yield Cu_2O eventually. In this context, it was necessary to explore alternative methods for preparing CuNPs.

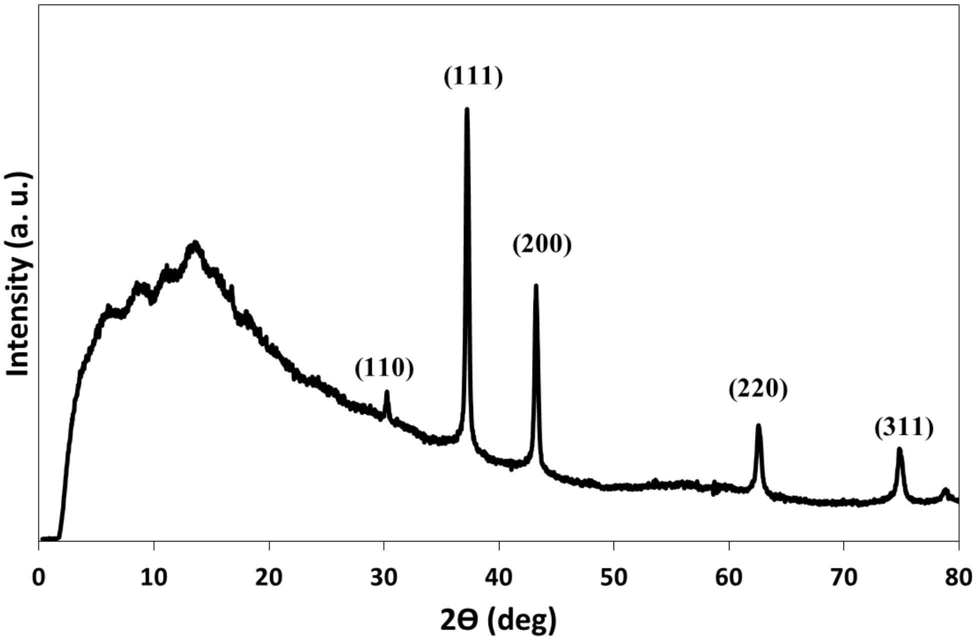

Fig. 3.3 X-ray powder diffraction of as prepared Cu_2O NPs.

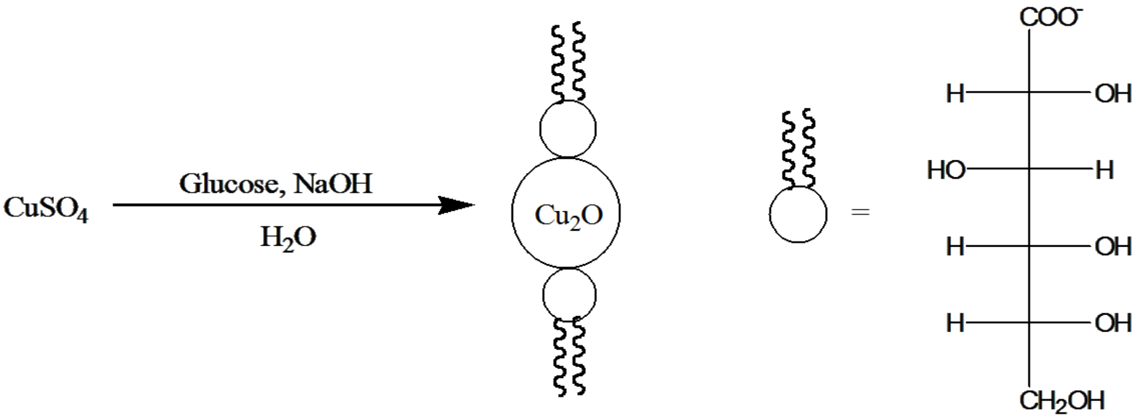

Scheme 3.2 Schematic summary of the synthesis of Cu_2O NPs.

Effective synthesis of CuNPs was achieved using a modification of the work of Kumar[35] and Blosi[36] as described in the Experimental section (Scheme 3.3). Transmission electron microscopy (TEM) images (Fig. 3.4 A) indicate the Cu nanoparticles have diameter of 39.8 ± 18.1 nm and is consistent with Scherrer analysis of XRD signal broadening.

$$2Cu^{2+} + N_2H_4 + 4OH^- \xrightarrow{\hspace{6em}} 2Cu + N_2 + 4H_2O$$

Scheme 3.3 The synthesis of CuNPs. (Scheme from Reference 24)

3.3.1.2 Cu@GeO$_2$ NPs synthesis

To our knowledge, there are no reports of GeO$_2$ coated CuNPs. Here we applied sol-gel reaction using tetraethoxygermane (TEOG) as precursor for Germania. GeO$_2$ nanoshells can be obtained under either acid,[44] base[45] or neutral[46] conditions. In this study, we applied neutral reaction conditions. TEOG was added to a suspension of CuNPs in ethanol and stirred for 16 h at room temperature at ambient conditions. The crude product was isolated by centrifugation as a purple/black solid， and redispersed in 100% ethanol. TEM images (Fig. 3.4 B) indicate the formation of a GeO$_2$ shell with diameter of 4.9 ± 1.3 nm.

3.3.1.3 Cu/Ge Nanoparticle synthesis

According to the Cu/Ge phase diagram the eutectic temperature is 644 °C with Cu composition of *ca.* 64%,[47] and the lowest temperature of liquid state of the most common composition Cu_3Ge is ca. 730 °C.[23] A size dependent decrease of solid to liquid transition temperature has been reported.[27-29] As a result, temperatures of 600 °C, 700 °C, and 800 °C were evaluated to investigate the formation of the copper germanide.

3.3.2 Nanoparticle characterization

The products were subsequently characterized using TEM, SEM, X-ray powder diffraction (XRD), X-ray photoelectron spectroscopy (XPS), and Auger electron spectroscopy.

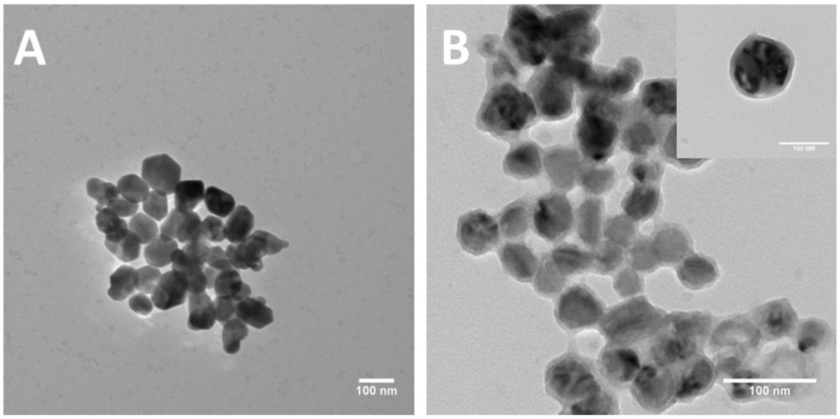

Fig. 3.4 TEM images of (A) Cu nanoparticles and (B) Cu@GeO_2 nanoparticles. Inset: high magnification TEM image showing the core@shell structure. Scale bars are 100 nm.

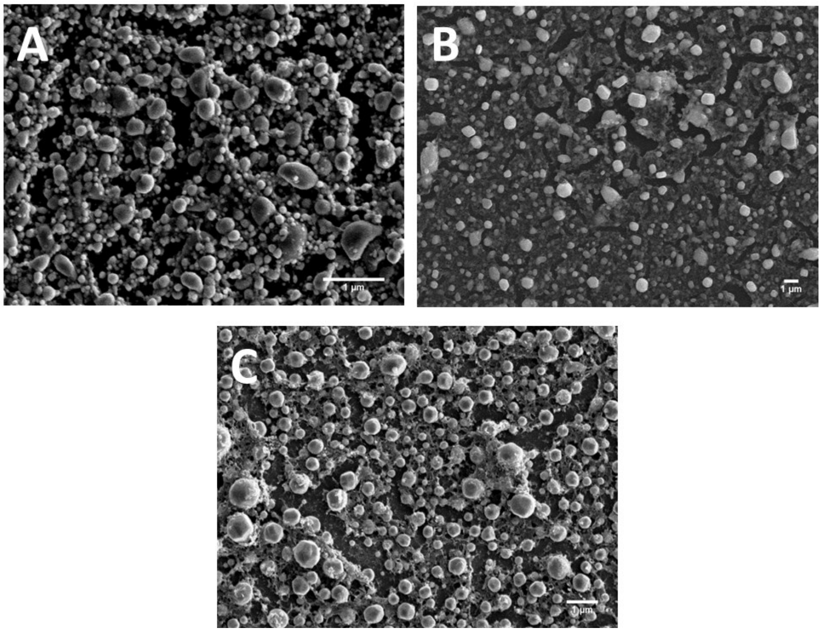

Fig 3.5 Scanning electron microscope (SEM) images of annealed Cu@GeO_2 NPs at (A) 600 °C/15 h, (B) 700 °C/15 h and (C) 800 °C/15 h. Scale bars are 1 μm.

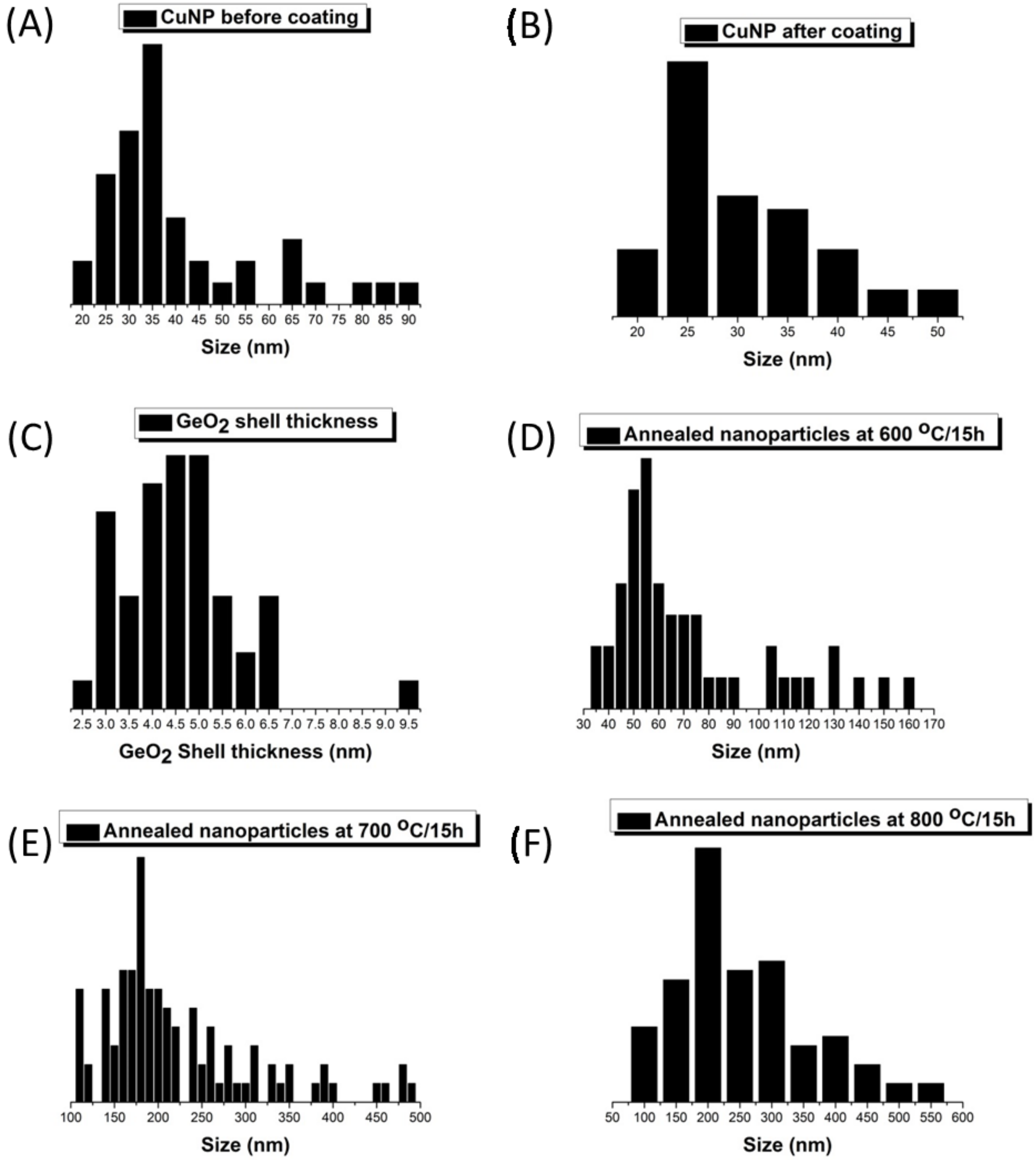

Fig. 3.6 Size distribution of (A) CuNP before GeO_2 coating, (B) CuNP after GeO_2 coating, (C) GeO_2 shell thickness, annealed Cu@GeO_2 NPs at (D) 600 °C/15 h, (E) 700 °C/15 h and (F) 800 °C/15 h.

The TEM (Fig. 3.4) and SEM (Fig. 3.5) images of Cu@GeO_2 and copper germanide nanoparticles show an increased particle size (Fig. 3.6) with increasing annealing temperature. At higher annealling temperatures, surface atoms move to minimize surface energy to form energetically favoured larger particles. This is because surface atoms are less stable than the atoms in interior.

The X-ray photoelectron spectroscopy (XPS) spectra of the Cu 2p region (Fig. 3.7) confirm there is a significant amount of Cu (0). In addition, XPS indicates there is Cu_2O in samples prepared at 600 °C/ 15 h (Fig. 3.7 B) and 800 °C/ 15 h (Fig. 3.7 D), consistent with XRD results. One of the possible reasons is 600 °C is not efficient enough to convert all Cu to Cu/Ge alloy; excess Cu is subsequently oxidized and formed Cu_2O. More GeO_2 evaporated at 800 °C compare to 600 °C and 700 °C, leaving excess Cu left in the system and got oxidized later during the characterization. A comparison of the Ge 3d region of the XP spectrum for samples prepared at different temperatures (Fig. 3.8) indicates there is a slight increase of the ratio of Ge (0)/Ge (IV) with increasing annealing temperature. This may be due to more of the GeO_2 coating being reduced to Ge as the result of increasing temperature in a reducing atmosphere. The presence of Cu and Ge is further shown using auger electron spectroscopy, which is shown in Fig. 3.9.

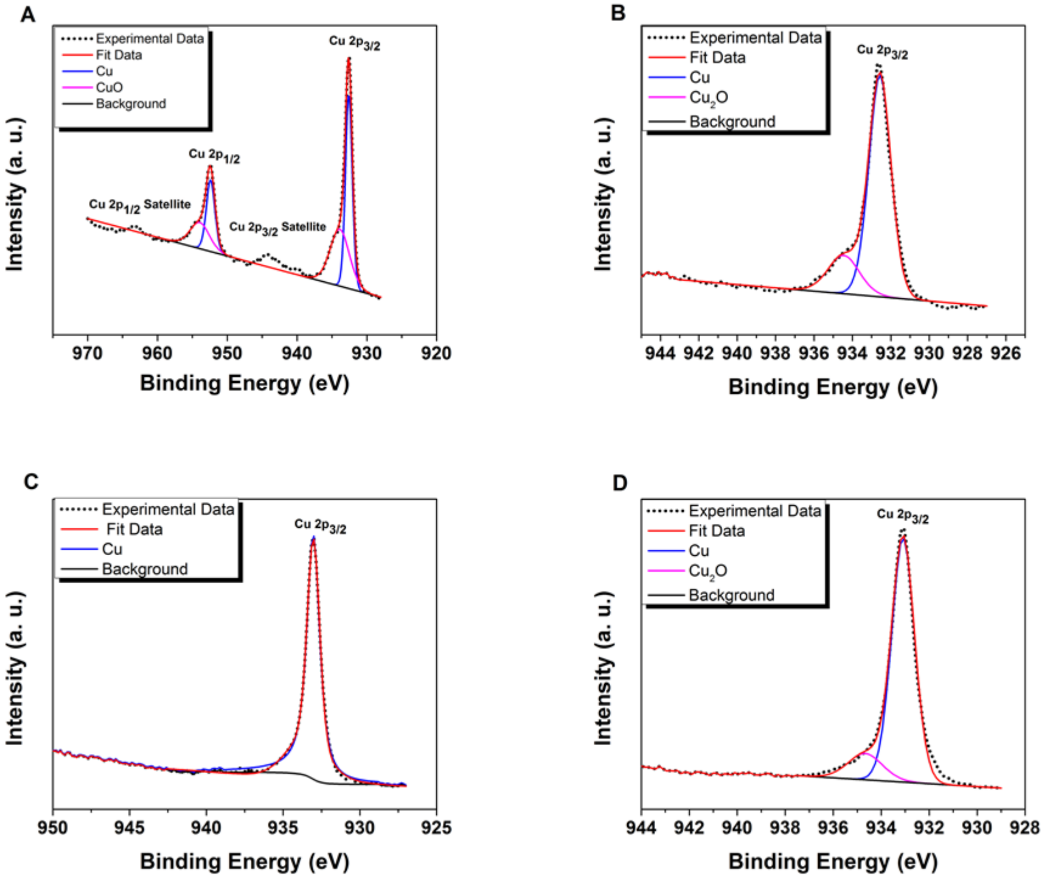

Fig. 3.7 XPS spectra of Cu 2p region of (A) CuNPs, annealed Cu@GeO$_2$ NPs at (B) 600 °C /15 h, (C) 700 °C /15 h and (D) 800 °C /15 h. Only Cu 2p$_{3/2}$ fitting peaks are shown. Cu 2p$_{1/2}$ components have been omitted for clarity.

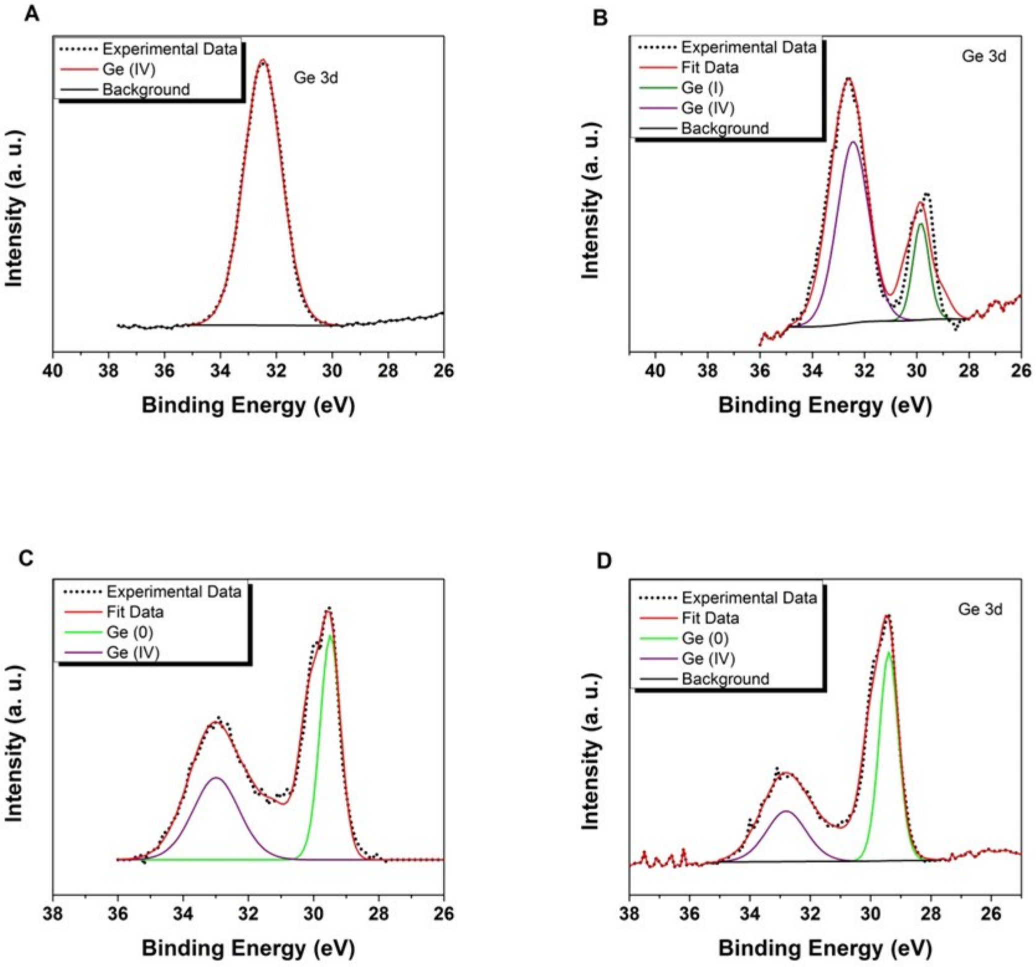

Fig. 3.8 XPS spectra of Ge 3d region of (A) Cu@GeO$_2$ NPS, annealed Cu@GeO$_2$ NPs at (B) 600 °C /15 h, (C) 700 °C /15 h and (D) 800 °C /15 h. Only Ge 3d$_{5/2}$ fitting peaks are shown. Ge 3d$_{3/2}$ components have been omitted for clarity.

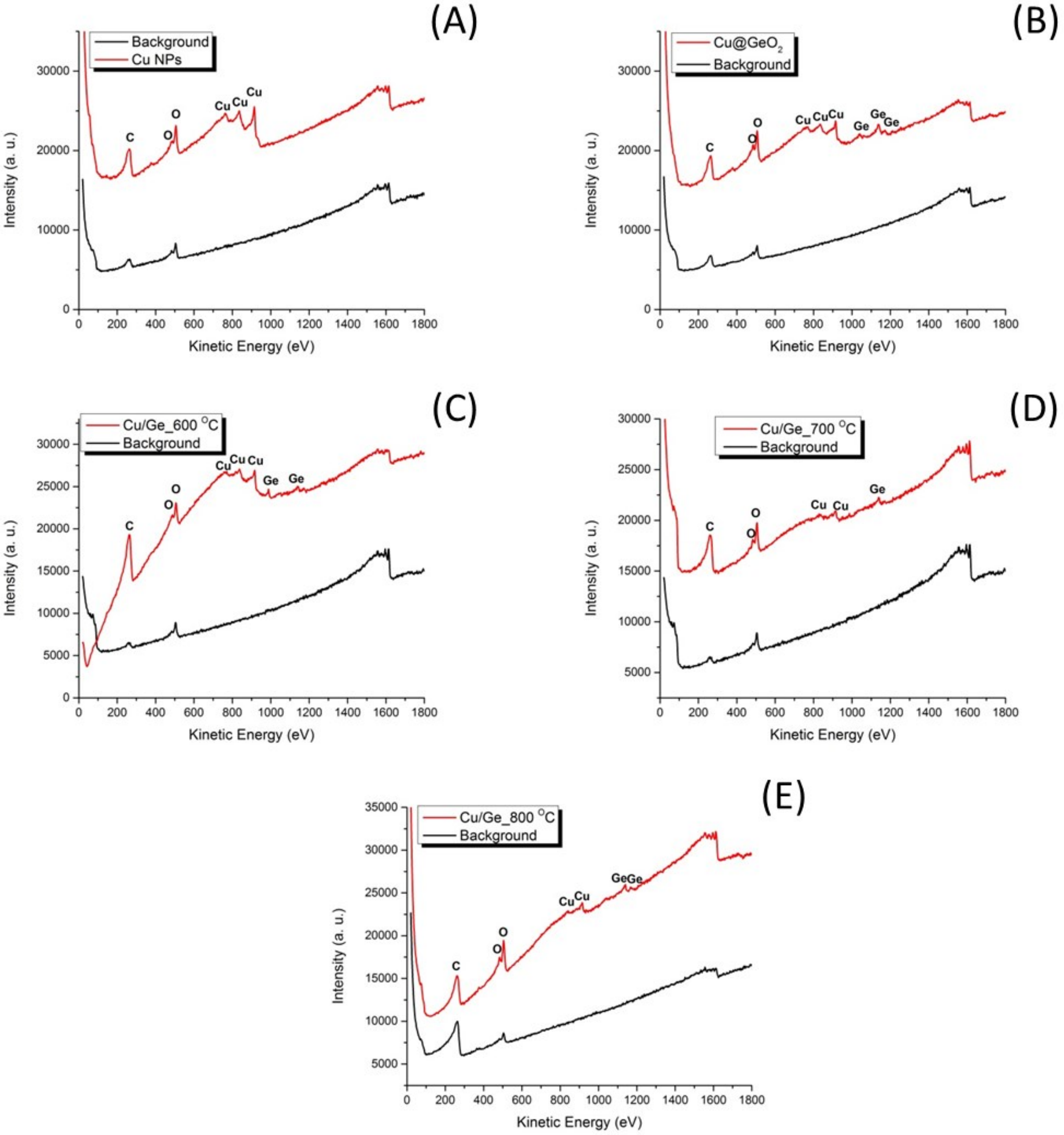

Fig. 3.9 Auger electron spectroscopy of (A) CuNP, (B) Cu@GeO$_2$ NP, annealed Cu@GeO$_2$ NPs at (C) 600 °C/15 h, (D) 700 °C/15h and (E) 800 °C/15h.

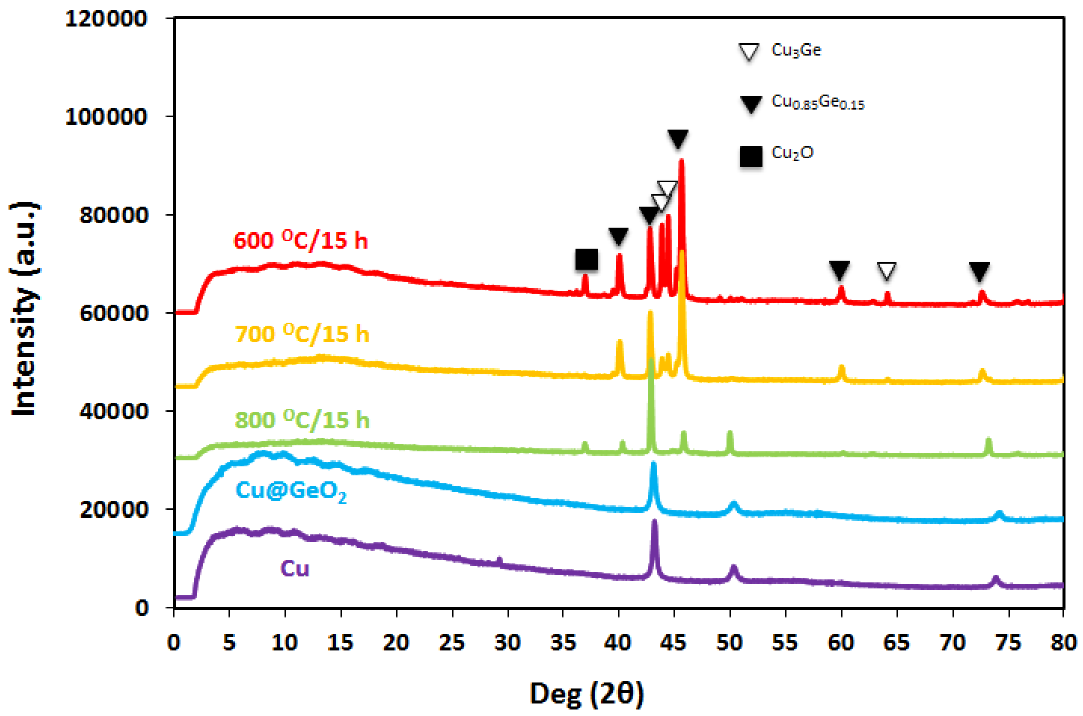

Fig. 3.10 X-ray powder diffraction of CuNPs (purple line), Cu@GeO$_2$ NPs (blue line), annealed Cu@GeO$_2$ NPs at 800 ^{0}C/15 h (green line), 700 ^{0}C/15 h (yellow line) and 600 ^{0}C/15 h (red line).

CuNPs, Cu@GeO$_2$ NPs, annealed Cu@GeO$_2$ NPs at 600 ^{O}C, 700 ^{O}C, and 800 ^{O}C were evaluated for the presence crystalline Ge and Cu using XRD. The XRD pattern of the CuNPs is depicted in Fig. 3.10 (purple line) and shows three characteristic peaks at 43.2°, 50.3° and 73.9° representing the (111), (200) and (220) planes, respectively.[25] The XRD pattern of the Cu@GeO$_2$ shows the same characteristic peaks as Cu, which indicates that there is no crystalline GeO$_2$ at the sensitivity of XRD. At 600 °C/ 15 h annealing temperature/ time, we obtained two

Cu/ Ge alloy components, $Cu_{0.85}Ge_{0.15}$ and Cu_3Ge. When the annealing temperature increased to 700 °C, more $Cu_{0.85}Ge_{0.15}$ was obtained, which means we have less Ge in the alloy system. This may due to the evaporation of GeO_2 above 510 °C.[8] This hypothesis is also confirmed by the XRD pattern of the annealed particles at 800 °C/ 15 h. At 800 °C, no more Cu_3Ge component exists in the system, while Cu peaks begin to appear, which further shows more Ge has evaporated out from the system.

3.4 Conclusion

In conclusion, we have reported a straightforward method for preparing Cu/Ge alloy nanoparticles via the reductive thermal processing of Cu@GeO_2 nanoparticles. The synthesis of Cu nanoparticles is difficult; the choice of reducing agent may affect the formation of the final product (CuNPs or Cu_2O NPs). Different Cu/Ge alloy compositions were obtained by varying the annealing temperature. Ongoing investigations are aimed at the applications of the alloy nanoparticles and the mechanism of the annealing process.

3.5 References

1. G. E. Moore, *Proc. IEEE*, 1998, **86**, 82-85 (Reprinted from Electronics, pp. 114-117, 1965).
2. P. K. Bondyopadhyay, *Proc. IEEE*, 1998, **86**, 78.
3. L. Krusin-Elbaum and M. O. Aboelfotoh, *Appl. Phys. Lett.*, 1991, **58**, 1341.
4. M. A. Borek, S. Oktyabrsky, M. O. Aboelfotoh and J. Narayan, *Appl. Phys. Lett.*, 1996, **69**, 3560.
5. N. Mikami, N. Hata, T. Kikkawa and H. Machida, *AppL. Phys. Lett.*, 2003, **83**, 5181.
6. R. Rosenberg, D. C. Edelstein, C.-K. Hu and K. P. Rodbell, *Annu. Rev. Mater. Sci.*, 2000, **30**, 229.
7. J. Li, Y. Shacham-Diamand and J. W. Mayer, *Mater. Sci. Rep.*, 1992, **9**, 1.
8. H. K. Liou, J. S. Huang and K. N. Tu, *J. Appl. Phys.*, 1995, **77**, 5443.
9. J.-W. Lim, J. Iijima, Y. Zhu, J. H. Yoo, G.-S. Choi, K. Mimura and M. Isshiki, *Thin Solid Films*, 2008, **516**, 4040.
10. V. F. Drobny and D. L. Pulfrey, *Thin Solid Films*, 1979, **61**, 89.
11. A. A. Istratov and E. R. Weber, *J. Electrochem. Soc.*, 2002, **149**, G21.
12. I. P. Nikitina, K. V. Vassilevski, N. G. Wright, A. B. Horsfall, A. G. O'Neill and C. M. Johnson, *J. Appl. Phys.*, 2005, **97**, 083709.
13. J. M. Gallego, J. M. García, J. Alvarez and R. Miranda, *Phys. Rev. B*, 1992, **46**, 13339.
14. J. P. Gambino and E. G. Colgan, *Mater. Chem. Phys.*, 1998, **52**, 99.
15. S.-L. Zhang and M. Östling, *Crit. Rev. Solid State Mater. Sci.*, 2003, **28**, 1.
16. M. O. Aboelfotoh and L. Krusin-Elbaum, *J. Appl. Phys.*, 1991, **70**, 3382.
17. S. Wang, S. Suthar, C. Hoeflich and B. J. Burrow, *J. Appl. Phys.*, 1993, **73**, 2301.
18. A. P. Peter, L. Carbonell, M. Schaekers, C. Adelmann, J. Meersschaut, A. Franquet, O. Richard, H. Bender, T. Zsolt and S. van Elshocht, *Intermetallics*, 2013, **34**, 35.
19. Y.-L. Chao, Y. Xu, R. Scholz and J. C. S. Woo, *IEEE Electron Device Lett.*, 2006, **27**, 549.
20. J. P. Doyle, B. G. Svensson and M. O. Aboelfotoh, *J. Appl. Phys.*, 1996, **80**, 2530.
21. S. Oktyabrsky, M. O. Aboelfotoh, J. Narayan and J. M. Woodall, *J. Electron. Mater.*, 1996, **25**, 1662.

22. M. O. Aboelfotoh, M. A. Borek and J. Narayan, *Appl. Phys. Lett.*, 1999, **75**, 3953.
23. J. Wang, S. Jin, C. Leinenbach and A. Jacot, *J. Alloys Compd.*, 2010, **504**, 159.
24. A. P. Alivisatos, *J. Phys. Chem.*, 1996, **100**, 13226.
25. S. C. Tjong and H. Chen, *Mater. Sci. Eng., R*, 2004, **45**, 1.
26. T. Castro, R. Reifenberger, E. Choi and R. Andres, *Phys. Rev. B*, 1990, **42**, 8548.
27. P. Buffat and J.-P. Borel, *Phys. Rev. A*, 1976, **13**, 2287.
28. R. D. Beck, P. St. John, M. L. Homer and R. L. Whetten, *Science*, 1991, **253**, 879.
29. T. P. Martin, U. Näher, H. Schaber and U. Zimmermann, *J. Chem. Phys.*, 1994, **100**, 2322.
30. P. Nath and K. L. Chopra, *Thin Solid Films*, 1979, **58**, 339.
31. P. Nath, V. Dutta and K. L. Chopra, *Thin Solid Films*, 1979, **64**, 65.
32. S. Gaudet, C. Detavernier, A. J. Kellock, P. Desjardins and C. Lavoie, *J. Vac. Sci. Technol. A*, 2006, **24**, 474.
33. S. Dhar and V. N. Kulkarni, *Thin Solid Films*, 1998, **333**, 20.
34. S. Das and T. L. Alford, *Appl. Phys. Lett.*, 2013, **103**, 094104.
35. A. Kumar, A. Saxena, A. De, R. Shankar and S. Mozumdar, *RSC Adv.*, 2013, **3**, 5015.
36. M. Blosi, S. Albonetti, M. Dondi, C. Martelli and G. Baldi, *J. Nanoparticle Res.*, 2011, **13**, 127.
37. F. Petraki, V. Papaefthimiou and S. Kennou, *Org. Electron.*, 2007, **8**, 522.
38. D. Deng, Y. Jin, Y. Cheng, T. Qi and F. Xiao, *ACS Appl. Mater. Interfaces*, 2013, **5**, 3839.
39. J. Zhang, Y. Yuan, X. Xu, X. Wang and X. Yang, *ACS Appl. Mater. Interfaces*, 2011, **3**, 4092.
40. M. Grouchko, A. Kamyshny and S. Magdassi, *J. Mater. Chem.*, 2009, **19**, 3057.
41. N. A. Dhas, C. P. Raj and A. Gedanken, *Chem. Mater.*, 1998, **10**, 1446.
42. S. Panigrahi, S. Kundu, S. K. Ghosh, S. Nath, S. Praharaj, S. Basu and T. Pal, *Polyhedron*, 2006, **25**, 1263.
43. L. Guan, H. Pang, J. Wang, Q. Lu, J. Yin and F. Gao, *Chem. Commun.*, 2010, **46**, 7022.
44. A. Martucci, G. Brusatin and M. Guglielmi, *J. Sol-Gel Sci. Technol.*, 1998, **13**, 535.
45. U. Schubert and N. Hüsing, *Synthesis of Inorganic Materials*, Wiley, Weinheim, 3rd edn, 2012.

46. Y. Son, M. Park, Y. Son, J. S. Lee, J. H. Jang, Y. Kim and J. Cho, *Nano Lett.*, 2014, **14**, 1005.
47. J. Wirringa, R. Wartchow and M. Binnewies, *Z. Anorg. Allg. Chem.*, 2000, **626**, 1473.

Chapter 4:

Conclusions and Future Work

In this thesis, we presented an investigation on the synthesis of water-soluble silicon nanocrystals (SiNCs) and their biological applications. Cu/Ge alloy nanoparticles were studied for their potential use as metallization material in Si-based semiconductor devices. Current work and results and future directions are summarized in this Chapter.

4.1 Water-soluble functionalized Silicon nanocrystals and their application to cancer cell imaging (Chapter 2)

4.1.1 Conclusions

In Chapter 2, D-Mannose, L-Alanine, and pentanoic acid functionalized SiNCs with diameters of *ca.* 3 nm were synthesized. Among the attractive properties of the present SiNCs that can be applied to biological imaging is their photoluminescence (PL) response. Aqueous solutions of the presented mannose and alanine functionalized SiNCs show blue PL with maximum ca. 415 nm and 400 nm upon excitation at 350 nm. The PL spectrum of an aqueous solution of pentanoic acid functionalized SiNCs shows a maximum at ~ 640 nm upon excitation at 350 nm. The quantum yield of mannose functionalized SiNCs is 13% and of alanine functionalized SiNCs is 17%. Though the quantum yield is relatively low compare to organic dyes (0.5-1.0 in visible light range) and other quantum dots (0.65-0.85 for CdSe, $\leq$0.6 for CdS and 0.1-0.4 for InP),[1] the advantage of investigating SiNCs for bioimaging lies in the nontoxicity and photostability of Si.[2-4] To evaluate the application of mannose and alanine terminated SiNCs in fluorescent imaging, the particles were exposed to MCF-7 human breast cancer cells. Mannose and alanine functionalized SiNCs were found to be taken up by MCF-7 cells allowing imaging. Cells were exposed to water-soluble red photoluminescent pentanoic acid functionalized SiNCs to investigate if particle uptake resulted from the species on the surface (mannose or alanine). No uptake of pentanoic acid functionalized SiNCs by the MCF-7 breast cancer cell was observed.

4.1.2 Future work

These observations support the conclusion that mannose and alanine functionalization promoted cell uptake. Laser scanning confocal microscopy is a necessary characterization equipment to show the position of the particles after uptake (in nucleus or cytosol or endosome, *etc.*).[5]

To investigate if particle uptake resulted from the species on the surface (mannose or alanine), cells were exposed to water-soluble red photoluminescent pentanoic acid functionalized SiNCs in Chapter 2. No uptake of pentanoic acid functionalized SiNCs by the MCF-7 breast cancer cell was observed. Additional evidence is an asset to prove that the uptake is mediated by mannose and alanine, and not from water-solubility. The second evidence could be performed by adding mannose and alanine to the cells, and investigate if the uptake is inhibited.

The PL wavelength of the as prepared SiNCs is around 400 nm, which limits their application in bioimging due to autofluorescence to biological specimens.[6] SiNCs PL can be influenced by surface chemistry, but the exact mechanism is still under investigation. In 2014, Dasog et al. exploited surface-emitting species and reported the PL of SiNCs can be effectively tuned across the entire visible spectral region through variation of surface functionalization without changing particle size.[7] Fluorescence imaging of cancer cells using other color (*e.g.* red) photoluminescence SiNCs is another area of study.

4.2 Synthesis of copper-germanium alloy nanoparticles from copper@germania core/shell nanostructures (Chapter 3)

4.2.1 Conclusions

Chapter 3 presented a method for preparing Cu/Ge alloy (Cu_3Ge and $Cu_{0.85}Ge_{0.15}$) nanoparticles via the reductive thermal processing of Cu/GeO_2 core shell nanocrystals ($Cu@GeO_2$). Products were characterized by X-ray diffraction (XRD), X-ray photoelectron spectroscopy (XPS), transmission electron microscope (TEM), scanning electron microscope (SEM), and auger electron spectroscopy (AES). Different Cu/Ge alloy compositions were obtained by varying the annealing temperature and the TEM and SEM images show an increased particle size with increasing annealing temperature (i.e., 600 °C: 71.3 ± 31.5 nm, 700 °C: 172.3 ± 28.2 nm, 800 °C: 282.9 ± 109.7 nm). The XPS spectra of Ge 3d region indicate that there is a slight increase of the ratio of Ge (0)/Ge (IV) with increasing annealing temperature. This result may due to more of the GeO_2 coating being reduced to Ge as the result of increasing temperature. According to the XRD data, we obtained two Cu/ Ge alloy components, $Cu_{0.85}Ge_{0.15}$ and Cu_3Ge at 600 °C/ 15 h annealing temperature/ time. When the annealing temperature increased to 700 °C, more $Cu_{0.85}Ge_{0.15}$ was obtained, which indicates we have less Ge in the alloy system. At 800 °C, no more Cu_3Ge component exists in the system, while Cu peaks begin to appear. These observations support the conclusion that GeO_2 evaporates during the annealing process.

4.2.2 Future work

Copper germanide is an appealing metallization material and has been considered as an alternative to Cu and metal silicides due to its low resistivity, and oxidative stability in air up to 520 °C.[8] In order to fully understand the potential use of copper germanide as metallization material, the measurement of resistivity of the as prepared alloy nanoparticles should be assessed. Krusin-Elbaum *et al.* reported the resistivity of copper germanide could be as low as 5.5 μΩ cm.[9] The measurements of resistivity can be carried out by Van der Pauw method.[10]

Narrowing the size distribution of the alloy nanoparticles is another area of study for these materials. One method of reducing the size polydispersity is the surface functionalization (e.g., alkanethiols) of the as prepared alloy nanoparticles to make them toluene soluble, after which density gradient ultracentrifugation can be used to separate different size of particles. Upon further functionalization and filtration, narrower size distribution may be obtained.

4.3 References

1. U. Resch-Genger, M. Grabolle, S. Cavaliere-Jaricot, R. Nitschke and T. Nann, *Nat. Methods*, 2008, **5**, 763.
2. R. Hardman, *Environ. Health Perspect.*, 2006, **114**, 165.
3. L. Ruizendaal, S. Bhattacharjee, K. Pournazari, M. Rosso-Vasic, L. H. J. de Haan, G. M. Alink, A. T. M. Marcelis and H. Zuilhof, *Nanotoxicology*, 2009, **3**, 339.
4. N. H. Alsharif, C. E. Berger, S. S. Varanasi, Y. Chao, B. R. Horrocks and H. K. Datta, *Small*, 2009, **5**, 221.
5. D. J. Bharali, D. W. Lucey, H. Jayakumar, H. E. Pudavar and P. N. Prasad, *J. Am. Chem. Soc.*, 2005, **127**, 11364.
6. F. Wang and X. Liu, *J. Am. Chem. Soc.*, 2008, **130**, 5642.
7. M. Dasog, G. B. De los Reyes, L. V. Titova, F. a. Hegmann and J. G. C. Veinot, *ACS Nano*, 2014, doi: 10.1021/nn504109a.
8. M. A. Borek, S. Oktyabrsky, M. O. Aboelfotoh and J. Narayan, *Appl. Phys. Lett.*, 1996, **69**, 3560.
9. L. Krusin-Elbaum and M. O. Aboelfotoh, *Appl. Phys. Lett.*, 1991, **58**, 1341.
10. L. J. V. d. Pauw, *Philips Res. Rep. B*, 1958, **13**, 1.

Appendices

Appendix A: Cu_2O nanoparticles synthesis.

6 g glucose was dissolved in 2×10^{-2} M NaOH (25 mL) in a 250 ml flask at ambient conditions, after which 90 mL of deionized water was added and the solution was heated up to 80 °C using a hot plate. 1.6 mL of 10^{-1} M $CuSO_4$ was added to the hot solution and the solution was left stirring for 20 min at 80 °C to yield orange solution. The crude product was isolated by centrifugation at 14000 rpm for 15 min as a yellow solid. The clear supernatant was removed using pasteur pipette. The solid was subsequently sonicated using a bath sonicator in 100% ethanol. The remaining solution was subjected to three centrifugation cycles as described above and the purified particles were stored as an ethanol suspension.

Appendix B: Scherrer analysis of X-ray diffraction signal.

Scherrer Equation is a useful method to determine approximate average crystallite size based on the analysis of the broadening of X-ray diffraction (XRD) peaks. The measurement of broadening thus gives a mean of the crystallite size through the formula:

$$\varepsilon = \frac{K\lambda}{\beta \cos\theta}$$

where ε is the average crystallite size, K is the dimensionless shape factor (usually set as K = 0.9), λ is the wavelength of the radiation, β is the line broadening at half the maximum intensity (in radians), and θ is the Bragg angle.

In Chapter 3, we obtained XRD data for copper nanoparticles, Cu@GeO_2 nanoparticles, and annealed Cu@GeO_2 nanoparticles at different temperatures. Sample calculation of how to estimate the nanoparticle size based on XRD broadening will be shown in the following.

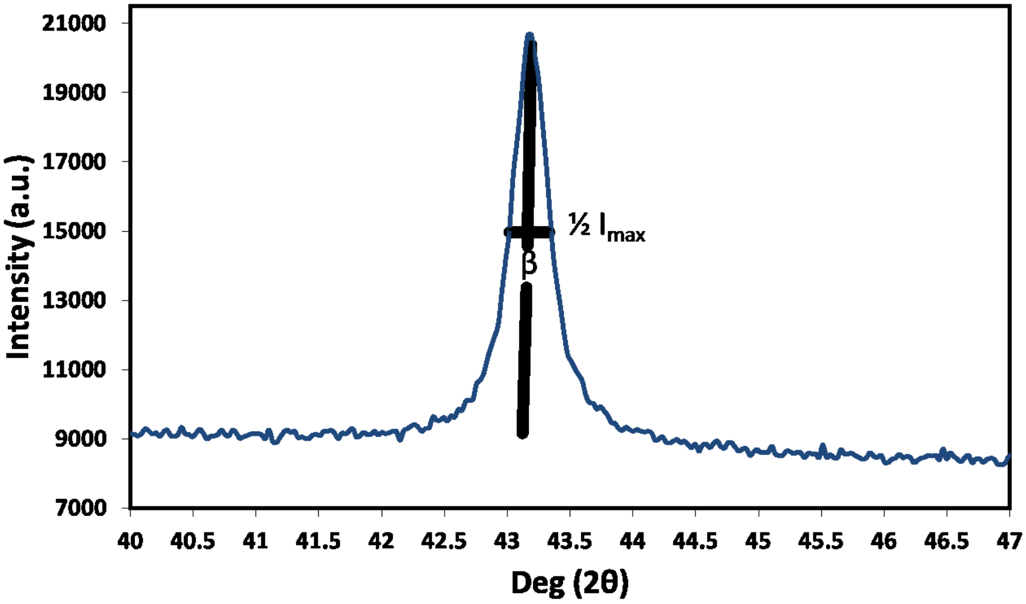

Fig. A.1 Schematic representation of one of the Cu nanoparticle XRD peak centered at 2θ with the maximum intensity I_{max}.

Peak at 43.2 ° in the Cu nanoparticle XRD was picked for the sample calculation. Sample calculation can be written as:

$$\varepsilon = \frac{0.9 \times 0.154\,nm}{0.0061 \times \cos 43.1} = 31.1\,nm$$

31.1 nm is comparable with the value obtained based on transmission electron microscopy (TEM) image (39.7 nm). It shows particle size from TEM analysis is greater than crystallite size from XRD. Scherrer analysis is a method for estimating the crystal size; however, a particle is made up of several crystals.

Bibliography

Chapter 1:

1. M. A. Meyers, A. Mishra and D. J. Benson, *Prog. Mater Sci.*, 2006, **51**, 427.
2. A. H. Lu, E. L. Salabas and F. Schuth, *Angew. Chem. Int. Ed.*, 2007, **46**, 1222.
3. S. P. Gubin, Y. A. Koksharov, G. B. Khomutov and G. Y. Yurkov, *Usp. Khim.*, 2005, **74**, 539.
4. J. Gao, H. Gu and B. Xu, *Acc. Chem. Res.*, 2009, **42**, 1097.
5. A. Henglein, *Chem. Rev.* , 1989, **89**, 1861.
6. S. Link and M. A. El-Sayed, *Annu. Rev. Phys. Chem.*, 2003, **54**, 331.
7. D. Kovalev, H. Heckler, G. Polisski and F. Koch, *Phys. Stat. Sol.*, 1999, **215**, 871.
8. S. Eustis and M. A. El-Sayed, *Chem. Soc. Rev.*, 2005, **35**, 209.
9. I. L. Medintz, H. T. Uyeda, E. R. Goldman and H. Mattoussi, *Nat. Mater.*, 2005, **4**, 435.
10. F. Wang, W. B. Tan, Y. Zhang, X. Fan and M. Wang, *Nanotechnology*, 2006, **17**, R1.
11. M. Bruchez, M. Moronne, P. Gin, S. Weiss and A. P. Alivisatos, *Science*, 1998, **281**, 2013.
12. T. Jamieson, R. Bakhshi, D. Petrova, R. Pocock, M. Imani and A. M. Seifalian, *Biomaterials*, 2007, **28**, 4717.
13. X. Gao, Y. Cui, R. M. Levenson, L. W. Chung and S. Nie, *Nat. Biotechnol.*, 2004, **22**, 969.
14. J.-U. A. H. Junghanns and R. H. Muller, *Int. J. Nanomed.*, 2008, **3**, 295.
15. J. Kim, H. S. Kim, N. Lee, T. Kim, H. Kim, T. Yu, I. C. Song, W. K. Moon and T. Hyeon, *Angew. Chem. Int. Ed.*, 2008, **47**, 8438.
16. R. H. Muller and C. M. Keck, *J. Biotechnol.*, 2004, **113**, 150.
17. Z. Y. Zhou, N. Tian, J. T. Li, I. Broadwell and S. G. Sun, *Chem. Soc. Rev.*, 2011, **40**, 4167.
18. K. Zhou and Y. Li, *Angew. Chem. Int. Ed.*, 2012, **51**, 602.
19. B. Wu and N. Zheng, *Nano Today*, 2013, **8**, 168.
20. R. C. Somers, M. G. Bawendi and D. G. Nocera, *Chem. Soc. Rev.*, 2007, **36**, 579.
21. P. T. Snee, R. C. Somers, G. Nair, J. P. Zimmer, M. G. Bawendi and D. G. Nocera, *J. Am. Chem. Soc.*, 2006, **128**, 13320.
22. I. Freestone, N. Meeks, M. Sax and C. Higgitt, *Gold Bull*, 2007, **40**, 270.
23. L. M. Liz-Marzan, *Mater. Today*, 2004, **7**, 26.
24. B. Fahlman, *Materials Chemistry*, Springer: Dordretcht, Netherlands, 2007.
25. G. Binnig and H. Rohrer, *Helv. Phys. Acta.* , 1982, **55**, 726.
26. L. E. Brus, *J. Chem. Phys.*, 1983, **79**, 5566.
27. L. E. Brus, *J. Chem. Phys.*, 1984, **80**, 4403.
28. G. Binnig, C. F. Quate and C. Gerber, *Phys. Rev. Lett.*, 1986, **56**, 930.
29. R. D. Piner, J. Zhu, F. Xu, S. Hong and C. A. Mirkin, *Science*, 1999, **283**, 661.

30. S. Link and M. A. El-Sayed, *J. Phys. Chem. B*, 1999, **103**, 8410.
31. C. B. Murray, D. J. Norris and M. G. Bawendi, *J. Am. Chem. Soc.*, 1993, **115**, 8706.
32. A. P. Alivisatos, *Science*, 1993, **271**, 933.
33. J. A. Kelly, E. J. Henderson and J. G. Veinot, *Chem. Commun.*, 2010, **46**, 8704.
34. M. W. Dashiell, U. Denker, C. Müller, G. Costantini, C. Manzano, K. Kern and O. G. Schmidt, *Appl. Phys. Lett.*, 2002, **80**, 1279.
35. A. Kellersohn, E. Knözinger, W. Langel and M. Giersig, *Adv. Matter*, 1995, **7**, 652.
36. D. Dutta and D. Bahadur, *J. Mater. Chem.* , 2012, **22**, 24545.
37. A. P. Alivisatos, *J. Phys. Chem.*, 1996, **100**, 13226.
38. E. Roduner, *Chem. Soc. Rev.*, 2006, **35**, 583.
39. Y. M. Huh, Y. W. Jun, H. T. Song, S. Kim, J. S. Choi, J. H. Lee, S. Yoon, K. S. Kim, J. S. Shin, J. S. Suh and J. Cheon, *J. Am. Chem. Soc.*, 2005, **127**, 12387.
40. P. F. Trwoga, A. J. Kenyon and C. W. Pitt, *J. Appl. Phys.*, 1998, **83**, 3789.
41. A. I. Ekimov, F. Hache, M. C. Schanne-Klein, D. Ricard, C. Flytzanis, I. A. Kudryavtsev, T. V. Yazeva, A. V. Rodina and A. L. Efros, *J. Opt. Soc. Am. B*, 1993, **10**, 100.
42. A. L. Efros, M. Rosen, M. Kuno, M. Nirmal, D. J. Norris and M. Bawendi, *Phys. Rev. B*, 1996, **54**, 4843.
43. K. Leung, S. Pokrant and K. B. Whaley, *Phys. Rev. B*, 1998, **57**, 12291.
44. C. Delerue, G. Allan and M. Lannoo, *Phys. Rev. B*, 1993, **48**, 11024.
45. B. R. Cuenya, *Thin Solid Films*, 2010, **518**, 3127.
46. A. N. Goldstein, C. M. Echer and A. P. Alivisatos, *Science*, 1992, **256**, 1425.
47. F. M. Davidson, A. D. Schricker, R. J. Wiacek and B. A. Korgel, *Adv. Mater.*, 2004, **16**, 646.
48. Y. Xu, N. Al-Salim, C. W. Bumby and R. D. Tilley, *J. Am. Chem. Soc.*, 2009, **131**, 15990.
49. J. E. Murphy, M. C. Beard, A. G. Norman, S. P. Ahrenkiet, J. C. Johnson, P. Yu, O. I. Mićić, R. J. Ellingson and A. J. Nozik, *J. Am. Chem. Soc.*, 2006, **128**, 3241.
50. M. Benaissa, K. E. Gonsalves and S. P. Rangarajan, *Appl. Phys. Lett.*, 1997, **71**, 3685.
51. Q. Guo, H. W. Hillhouse and R. Agrawal, *J. Am. Chem. Soc.*, 2009, **131**, 11672.
52. M. Bruchez Jr, M. Moronne, P. Gin, S. Weiss and A. P. Alivisatos, *Science*, 1998, **281**, 2013.
53. P. V. Kamat, *J. Phys. Chem. C*, 2008, **112**, 18737.
54. E. J. Anglin, L. Cheng, W. R. Freeman and M. J. Sailor, *Adv. Drug Deliv. Rev.*, 2008, **60**, 1266.
55. N. Lewinski, V. Colvin and R. Drezek, *Small*, 2008, **4**, 26.
56. J. G. Veinot, *Chem. Commun.*, 2006, 4160.

57. S. O. Kasap, *Optoelectronics and Photonics: Principles and Practices 2nd edition*, **Prentice Hall, 2012**.
58. L. Brus, *J. Phys. Chem.*, 1994, **98**, 3575.
59. J. G. C. Veinot, *Chem. Commun.* , 2006, 4160.
60. J. R. Heath, *Science*, 1992, **258**, 1131.
61. N. A. Dhas, C. P. Raj and A. Gedanken, *Chem. Mater.*, 1998, **10**, 3278.
62. R. A. Bley and S. M. Kauzlarich, *J. Am. Chem. Soc.*, 1996, **118**, 12462.
63. C.-S. Yang, R. A. Bley, S. M. Kauzlarich, H. W. H. Lee and G. R. Delgado, *J. Am. Chem. Soc.*, 1999, **121**, 5191.
64. D. Mayeri, B. L. Phillips, M. P. Augustine and S. M. Kauzlarich, *Chem. Mater.*, 2001, **13**, 765.
65. J. Zou, R. K. Baldwin, K. A. Pettigrew and S. M. Kauzlarich, *Nano Lett.*, 2004, **4**, 1181.
66. A. S. Heintz, M. J. Fink and B. S. Mitchell, *Adv. Mater.*, 2007, **19**, 3984.
67. G. Belomoin, J. Therrien, A. Smith, S. Rao, R. Twesten, S. Chaieb, M. H. Nayfeh, L. Wagner and L. Mitas, *Appl. Phys. Lett.*, 2002, **80**, 841.
68. R. A. Bley, S. M. Kauzlarich, J. E. Davis and H. W. H. Lee, *Chem. Mater.*, 1996, **8**, 1881.
69. C. M. Hessel, E. J. Henderson and J. G. C. Veinot, *Chem. Mater.*, 2006, **18**, 6139.
70. M. Pauthe, E. Bernstein, J. Dumas, L. Saviot, A. Pradel and M. Ribes, *J. Mater. Chem.*, 1999, **9**, 187.
71. S.-M. Liu, S. Sato and K. Kimura, *Langmuir : the ACS journal of surfaces and colloids*, 2005, 6324.
72. S.-M. Liu, Y. Yang, S. Sato and K. Kimura, *Chem. Mater.*, 2006, **18**, 637.
73. T. U. M. S. Murthy, N. Miyamoto, M. Shimbo and J. Nishizawa, *J. Cryst. Growth*, 1976, **33**, 1.
74. X. Li, Y. He and M. T. Swihart, *Langmuir : the ACS journal of surfaces and colloids*, 2004, **20**, 4720.
75. R. Anthony and U. Kortshagen, *Phys. Rev. B*, 2009, **80**, 115407.
76. A. G. Cullis and L. T. Canham, *Nature*, 1991, **353**, 335.
77. M. Rosso-Vasic, E. Spruijt, Z. Popović, K. Overgaag, B. van Lagen, B. Grandidier, D. Vanmaekelbergh, D. Domínguez-Gutiérrez, L. De Cola and H. Zuilhof, *J. Mater. Chem.*, 2009, **19**, 5926.
78. J. Fan and P. K. Chu, *Small*, 2010, **6**, 2080.
79. W. Tan, K. Wang, X. He, X. J. Zhao, T. Drake, L. Wang and R. P. Bagwe, *Med. Res. Rev.*, 2004, **24**, 621.
80. K. D. Hirschman, L. Tsybeskov, S. P. Duttagupta and P. M. Fauchet, *Nature*, 1996, **384**, 338.
81. K. Y. Cheng, R. Anthony, U. R. Kortshagen and R. J. Holmes, *Nano Lett.*, 2010, **10**, 1154.

82. M. V. Wolkin, J. Jorne and P. M. Fauchet, *Phys. Rev. Lett.*, 1999, **82**, 197.
83. L. E. Brus, P. F. Szajowski, W. L. Wilson, T. D. Harris, S. Schuppler and P. H. Citrin, *J. Am. Chem. Soc.*, 1995, **117**, 2915.
84. D. Kovalev, H. Heckler, M. Ben-Chorin, G. Polisski, M. Schwartzkopff and F. Koch, *Phys. Rev. Lett.*, 1998, **81**, 2803.
85. A. Puzder, A. J. Williamson, J. C. Grossman and G. Galli, *Phys. Rev. Lett.*, 2002, **88**, 097401.
86. Y. Kanemitsu, T. Ogawa, K. Shiraishi and K. Takeda, *Phys. Rev. B*, 1993, **48**, 4883.
87. M. Dasog, G. B. De los Reyes, L. V. Titova, F. a. Hegmann and J. G. C. Veinot, *ACS Nano*, 2014, doi: 10.1021/nn504109a.
88. O. Wolf, M. Dasog, Z. Yang, I. Balberg, J. G. C. Veinot and O. Millo, *Nano Lett.*, 2013, **13**, 2516.
89. J. O. Escobedo, O. Rusin, S. Lim and R. M. Strongin, *Curr. Opin. Chem. Biol.*, 2010, **14**, 64.
90. L. Yuan, W. Lin, K. Zheng, L. He and W. Huang, *Chem. Soc. Rev.*, 2013, **42**, 622.
91. U. Resch-Genger, M. Grabolle, S. Cavaliere-Jaricot, R. Nitschke and T. Nann, *Nat. Methods*, 2008, **5**, 763.
92. X. Michalet, F. F. Pinaud, L. A. Bentolila, J. M. Tsay, S. Doose, J. J. Li, G. Sundaresan, A. M. Wu, S. S. Gambhir and S. Weiss, *Science*, 2005, **307**, 538.
93. Y. He, C. Fan and S.-T. Lee, *Nano Today*, 2010, **5**, 282.
94. W. C. Chan, D. J. Maxwell, X. Gao, R. E. Bailey, M. Han and S. Neie, *Curr. Opin. Biotechnol.*, 2002, **13**, 40.
95. C. M. Niemeyer, *Angew. Chem. Int. Ed.*, 2001, **40**, 4128.
96. M. De, P. S. Ghosh and V. M. Rotello, *Adv. Mater.*, 2008, **20**, 4225.
97. R. Hardman, *Environ. Health Perspect.*, 2006, **114**, 165.
98. T. S. Hauck, R. E. Anderson, H. C. Fischer, S. Newbigging and W. C. Chan, *Small*, 2010, **6**, 138.
99. Y. Su, M. Hu, C. Fan, Y. He, Q. Li, W. Li, L. H. Wang, P. Shen and Q. Huang, *Biomaterials*, 2010, **31**, 4829.
100. A. M. Derfus, W. C. W. Chan and S. N. Bhatia, *Nano Lett.*, 2004, **4**, 11.
101. B. F. P. McVey and R. D. Tilley, *Acc. Chem. Res.*, 2014, **47**, 3045.
102. S. Bhattacharjee, I. M. Rietjens, M. P. Singh, T. M. Atkins, T. K. Purkait, Z. Xu, S. Regli, A. Shukaliak, R. J. Clark, B. S. Mitchell, G. M. Alink, A. T. Marcelis, M. J. Fink, J. G. Veinot, S. M. Kauzlarich and H. Zuilhof, *Nanoscale*, 2013, **5**, 4870.
103. A. Shiohara, S. Hanada, S. Prabakar, K. Fujioka, T. H. Lim, K. Yamamoto, P. T. Northcote and R. D. Tilley, *J. Am. Chem. Soc.*, 2010, **132**, 248.
104. Z. F. Li and E. Ruckenstein, *Nano Lett.*, 2004, **4**, 1463.
105. J. H. Park, L. Gu, G. von Maltzahn, E. Ruoslahti, S. N. Bhatia and M. J. Sailor, *Nat Mater.*, 2009, **8**, 331.

106. F. Erogbogbo, K. T. Yong, I. Roy, G. Xu, P. N. Prasad and M. T. Swihart, *ACS Nano*, 2008, **2**, 873.
107. Y. Zhong, F. Peng, X. Wei, Y. Zhou, J. Wang, X. Jiang, Y. Su, S. Su, S.-T. Lee and Y. He, *Angew. Chem. Int. Ed.*, 2012, **51**, 8485.
108. Y. Zhong, F. Peng, F. Bao, S. Wang, X. Ji, L. Yang, Y. Su, S. T. Lee and Y. He, *J. Am. Chem. Soc.*, 2013, **135**, 8350.
109. F. Chen and R. L. Johnston, *ACS Nano*, 2008, **2**, 165.
110. F. Chen and R. L. Johnston, *Acta Mater.*, 2008, **56**, 2374.
111. B. M. Muñoz-Flores, B. I. Kharisov, V. M. Jiménez-Pérez, M. P. Elizondo and S. T. López, *Ind. Eng. Chem. Res.*, 2011, **50**, 7705.
112. F. Ai, A. Yao, W. Huang, D. Wang and X. Zhang, *Physica E*, 2010, **42**, 1281.
113. F. Aguilera-Granja and A. Vega, *Phys. Rev. B*, 2009, **79**, 144423.
114. C. L. Bracey, P. R. Ellis and G. J. Hutchings, *Chem. Soc. Rev.*, 2009, **38**, 2231.
115. D. A. Slanac, W. G. Hardin, K. P. Johnston and K. J. Stevenson, *J. Am. Chem. Soc.*, 2012, **134**, 9812.
116. C. Zhu, S. Guo and S. Dong, *J. Mater. Chem.*, 2012, **22**, 14851.
117. R. Ferrando, J. Jellinek and R. L. Johnston, *Chem. Rev.*, 2008, **108**, 845.
118. A. K. Sra and R. E. Schaak, *J. Am. Chem. Soc.* , 2001, **126**, 6667.
119. N. H. Chou and R. E. Schaak, *J. Am. Chem. Soc.*, 2007, **129**, 7339.
120. N. Mikami, N. Hata, T. Kikkawa and H. Machida, *AppL. Phys. Lett.*, 2003, **83**, 5181.
121. R. Rosenberg, D. C. Edelstein, C.-K. Hu and K. P. Rodbell, *Annu. Rev. Mater. Sci.*, 2000, **30**, 229.
122. J. Li, Y. Shacham-Diamand and J. W. Mayer, *Mater. Sci. Rep.*, 1992, **9**, 1.
123. D. D. Vaughn, J. F. Bondi and R. E. Schaak, *Chem. Mater.*, 2010, **22**, 6103.
124. D. V. Talapin, J.-S. Lee, M. V. Kovalenko and E. V. Shevchenko, *Chem. Rev.*, 2010, **110**, 389.
125. L. Krusin-Elbaum and M. O. Aboelfotoh, *Appl. Phys. Lett.*, 1991, **58**, 1341.
126. M. A. Borek, S. Oktyabrsky, M. O. Aboelfotoh and J. Narayan, *Appl. Phys. Lett.*, 1996, **69**, 3560.
127. H. K. Liou, J. S. Huang and K. N. Tu, *J. Appl. Phys.*, 1995, **77**, 5443.
128. N. A. Tabet and M. A. Salim, *Appl. Surf. Sci.*, 1998, **134**, 275.
129. J. P. Doyle, B. G. Svensson and S. Johansson, *Appl. Phys. Lett.*, 1995, **67**, 2804.
130. T. Brchhart, A. Lugstein, Y. J. Hyun, G. Hochleitner and E. Bertagnolli, *Nano Lett.*, 2009, **9**, 3739.
131. J. J. Liou and F. Schwierz, *Solid-State Electronics*, 2003, **47**, 1881.
132. M. O. Aboelfotoh and L. Krusin-Elbaum, *J. Appl. Phys.*, 1991, **70**, 3382.
133. S. Wang, S. Suthar, C. Hoeflich and B. J. Burrow, *J. Appl. Phys.*, 1993, **73**, 2301.
134. A. Kumar, A. Saxena, A. De, R. Shankar and S. Mozumdar, *RSC Adv.*, 2013, **3**, 5015.

135. M. Blosi, S. Albonetti, M. Dondi, C. Martelli and G. Baldi, *J. Nanoparticle Res.*, 2011, **13**, 127.
136. X. Song, S. Sun, W. Zhang and Z. Yin, *J. Colloid Interface Sci.*, 2004, **273**, 463.
137. B. K. Park, S. Jeong, D. Kim, J. Moon, S. Lim and J. S. Kim, *J. Colloid Interface Sci.*, 2007, **311**, 417.
138. S. Kapoor, R. Joshi and T. Mukherjee, *Chem. Phys. Lett.*, 2002, **354**, 443.
139. S. H. Wu and D. H. Chen, *J. Colloid Interface Sci.*, 2004, **273**, 165.
140. N. A. Dhas, C. P. Raj and A. Gedanken, *Chem. Mater.*, 1998, **10**, 1446.
141. Z. Liu and Y. Bando, *Adv. Mater.*, 2003, **15**, 303.
142. M. Raja, J. Subha, F. B. Ali and S. H. Ryu, *Mater. Manuf. Processes*, 2008, **23**, 782.
143. M.-S. Yeh, Y.-S. Yang, Y.-P. Lee, H.-F. Lee, Y.-H. Yeh and C.-S. Yeh, *J. Phys. Chem. B*, 1999, **103**, 6851.
144. A. Kornowski, M. Giersig, R. Vogel, A. Chemseddine and H. Weller, *Adv. Mater.*, 1993, **5**, 634.
145. B. R. Taylor, S. M. Kauzlarich, H. W. H. Lee and G. R. Delgado, *Chem. Mater.*, 1998, **10**, 22.
146. B. R. Taylor, S. M. Kauzlarich, G. R. Delgado and H. W. H. Lee, *Chem. Mater.*, 1999, **11**, 2493.
147. X. Ma, F. Wu and S. M. Kauzlarich, *J. Solid State Chem.*, 2008, **181**, 1628.
148. E. J. Henderson, C. M. Hessel and J. G. C. veinot, *J. Am. Chem. Soc.*, 2008, **130**, 3624.

Chapter 2:

1. X. Michalet, F. F. Pinaud, L. A. Bentolila, J. M. Tsay, S. Doose, J. J. Li, G. Sundaresan, A. M. Wu, S. S. Gambhir and S. Weiss, *Science*, 2005, **307**, 538.
2. Y. He, C. Fan and S.-T. Lee, *Nano Today*, 2010, **5**, 282.
3. M. Bruchez Jr, M. Moronne, P. Gin, S. Weiss and A. P. Alivisatos, *Science*, 1998, **281**, 2013.
4. W. C. Chan, D. J. Maxwell, X. Gao, R. E. Bailey, M. Han and S. Neie, *Curr. Opin. Biotechnol.*, 2002, **13**, 40.
5. C. M. Niemeyer, *Angew. Chem. Int. Ed.*, 2001, **40**, 4128.
6. U. Resch-Genger, M. Grabolle, S. Cavaliere-Jaricot, R. Nitschke and T. Nann, *Nat. Methods*, 2008, **5**, 763.
7. M. De, P. S. Ghosh and V. M. Rotello, *Adv. Mater.*, 2008, **20**, 4225.
8. N. Lewinski, V. Colvin and R. Drezek, *Small*, 2008, **4**, 26.
9. R. Hardman, *Environ. Health Perspect.*, 2006, **114**, 165.
10. T. S. Hauck, R. E. Anderson, H. C. Fischer, S. Newbigging and W. C. Chan,

Small, 2010, **6**, 138.

11. Y. Su, M. Hu, C. Fan, Y. He, Q. Li, W. Li, L. H. Wang, P. Shen and Q. Huang, *Biomaterials*, 2010, **31**, 4829.
12. A. M. Derfus, W. C. W. Chan and S. N. Bhatia, *Nano Lett.*, 2004, **4**, 11.
13. Z. Kang, Y. Liu and S. T. Lee, *Nanoscale*, 2011, **3**, 777.
14. F. Erogbogbo, K. T. Yong, I. Roy, R. Hu, W. C. Law, W. Zhao, H. Ding, F. Wu, R. Kumar, M. T. Swihart and P. N. Prasad, *ACS Nano*, 2011, **5**, 413.
15. J. Liu, F. Erogbogbo, K. T. Yong, L. Ye, J. Liu, R. Hu, H. Chen, Y. Hu, Y. Yang, J. Yang, I. Roy, N. A. Karker, M. T. Swihart and P. N. Prasad, *ACS Nano*, 2013, **7**, 7303.
16. F. Erogbogbo, C. W. Chang, J. L. May, L. Liu, R. Kumar, W. C. Law, H. Ding, K. T. Yong, I. Roy, M. Sheshadri, M. T. Swihart and P. N. Prasad, *Nanoscale*, 2012, **4**, 5483.
17. E. Borsella, R. D’Amato, M. Falconieri, E. Trave, A. Panariti and I. Rivolta, *J. Mater. Res.*, 2013, **28**, 193.
18. J. H. Park, L. Gu, G. von Maltzahn, E. Ruoslahti, S. N. Bhatia and M. J. Sailor, *Nat Mater.*, 2009, **8**, 331.
19. J. A. Kelly, A. M. Shukaliak, M. D. Fleischauer and J. G. Veinot, *J. Am. Chem. Soc.*, 2011, **133**, 9564.
20. C. M. Hessel, E. J. Henderson and J. G. C. Veinot, *Chem. Mater.*, 2006, **18**, 6139.
21. C. M. Hessel, M. R. Rasch, J. L. Hueso, B. W. Goodfellow, V. A. Akhavan, P. Puvanakrishnan, J. W. Tunnel and B. A. Korgel, *Small*, 2010, **6**, 2026.
22. Y. He, Y. Zhong, F. Peng, X. Wei, Y. Su, Y. Lu, S. Su, W. Gu, L. Liao and S. T. Lee, *J. Am. Chem. Soc.*, 2011, **133**, 14192.
23. F. Erogbogbo, C. A. Tien, C. W. Chang, K. T. Yong, W. C. Law, H. Ding, I. Roy, M. T. Swihart and P. N. Prasad, *Bioconjug Chem.*, 2011, **22**, 1081.
24. N. Prtljaga, E. D'Amato, A. Pitanti, R. Guider, E. Froner, S. Larcheri, M. Scarpa and L. Pavesi, *Nanotechnology*, 2011, **22**, 215704.
25. L. Ruizendaal, S. Bhattacharjee, K. Pournazari, M. Rosso-Vasic, L. H. J. de Haan, G. M. Alink, A. T. M. Marcelis and H. Zuilhof, *Nanotoxicology*, 2009, **3**, 339.
26. R. J. Clark, M. K. Dang and J. G. Veinot, *Langmuir : the ACS journal of surfaces and colloids*, 2010, **26**, 15657.
27. K. El-Boubbou, D. C. Zhu, C. Vasileiou, B. Borhan, D. Prosperi, W. Li and X. Huang, *J. Am. Chem. Soc.*, 2010, **132**, 4490.
28. C. Earhart, N. R. Jana, N. Erathodiyil and J. K. Ying, *Langmuir : the ACS journal of surfaces and colloids*, 2008, **24**, 6215.
29. X. Jiang, A. Housni, G. Gody, P. Boullanger, M.-T. Charreyre, T. Delair and R. Narain, *Bioconjugate Chem.*, 2010, **21**, 521.
30. L. Gentilucci, A. Tolomelli and F. Squassabia, *Curr. Med. Chem.* , 2006, **13**, 2449.
31. R. Kikkeri, B. Lepenies, A. Adibekian, P. Laurino and P. H. Seeberger, *J. Am.*

Chem. Soc., 2011, **131**, 2110.

32. J. H. Ahire, I. Chambrier, A. Mueller, Y. Bao and Y. Chao, *ACS Appl. Mater. Interfaces*, 2013, **5**, 7384.
33. Y. Nakahara, K. Machiya, T. Sato, N. T. Nwe, T. Furuike, H. Tamura and K. Kimura, *Chem. Lett.*, 2013, **42**, 498.
34. J. M. Lambert, *J. Biomed. Mater. Res. B*, 2006, **78B**, 167.
35. Z. Yang, M. H. Wahl and J. G. C. Veinot, *Can. J. Chem.*, 2014, **92**, 1 dio: 10.1139/cjc-2014-0048.
36. M. Dowlut, D. G. Hall and O. Hindsgaul, *J. Org. Chem.*, 2005, **70**, 9809.
37. W. Hayes, H. M. I. Osborn, S. D. Osborne, R. A. Rastall and B. Romagnoli, *Tetrahedron*, 2003, **59**, 7983.
38. A. T. R. Williams, S. A. Winfield and J. N. Miller, *Analyst*, 1983, **108**, 1067.
39. Z. Yang, A. R. Dobbie, K. Cui and J. G. Veinot, *J. Am. Chem. Soc.*, 2012, **134**, 13958.
40. M. Dasog and J. G. C. Veinot, *phys. Status Solidi A*, 2012, **209**, 1844.
41. M. Dasog, Z. Yang, S. Regli, T. M. Atkins, A. Faramus, M. P. Singh, E. Muthuswamy, S. M. Kauzlarich, R. D. Tilley and J. G. C. Veinot, *ACS Nano*, 2013, **7**, 2676.
42. S. S. Nekrashevich and V. A. Gritsenko, *J. Appl. Phys.*, 2011, **110**, 114103.
43. M. Dasog, G. B. De los Reyes, L. V. Titova, F. A. Hegmann and J. G. C. Veinot, *ACS Nano*, **doi: 10.1021/nn504109a**.
44. S. M. Liu, M. Kobayashi, S. Sato and K. Kimura, *Chem. Commun.*, 2005, 4690.
45. K. El-Boubbou, C. Gruden and X. Huang, *J. Am. Chem. Soc.*, 2007, **129**, 13392.

Chapter 3:

1. G. E. Moore, *Proc. IEEE*, 1998, **86**, 82-85 (Reprinted from Electronics, pp. 114-117, 1965).
2. P. K. Bondyopadhyay, *Proc. IEEE*, 1998, **86**, 78.
3. L. Krusin-Elbaum and M. O. Aboelfotoh, *Appl. Phys. Lett.*, 1991, **58**, 1341.
4. M. A. Borek, S. Oktyabrsky, M. O. Aboelfotoh and J. Narayan, *Appl. Phys. Lett.*, 1996, **69**, 3560.
5. N. Mikami, N. Hata, T. Kikkawa and H. Machida, *AppL. Phys. Lett.*, 2003, **83**, 5181.
6. R. Rosenberg, D. C. Edelstein, C.-K. Hu and K. P. Rodbell, *Annu. Rev. Mater. Sci.*, 2000, **30**, 229.
7. J. Li, Y. Shacham-Diamand and J. W. Mayer, *Mater. Sci. Rep.*, 1992, **9**, 1.
8. H. K. Liou, J. S. Huang and K. N. Tu, *J. Appl. Phys.*, 1995, **77**, 5443.
9. J.-W. Lim, J. Iijima, Y. Zhu, J. H. Yoo, G.-S. Choi, K. Mimura and M. Isshiki, *Thin Solid Films*, 2008, **516**, 4040.

10. V. F. Drobny and D. L. Pulfrey, *Thin Solid Films*, 1979, **61**, 89.
11. A. A. Istratov and E. R. Weber, *J. Electrochem. Soc.*, 2002, **149**, G21.
12. I. P. Nikitina, K. V. Vassilevski, N. G. Wright, A. B. Horsfall, A. G. O'Neill and C. M. Johnson, *J. Appl. Phys.*, 2005, **97**, 083709.
13. J. M. Gallego, J. M. García, J. Alvarez and R. Miranda, *Phys. Rev. B*, 1992, **46**, 13339.
14. J. P. Gambino and E. G. Colgan, *Mater. Chem. Phys.*, 1998, **52**, 99.
15. S.-L. Zhang and M. Östling, *Crit. Rev. Solid State Mater. Sci.*, 2003, **28**, 1.
16. M. O. Aboelfotoh and L. Krusin-Elbaum, *J. Appl. Phys.*, 1991, **70**, 3382.
17. S. Wang, S. Suthar, C. Hoeflich and B. J. Burrow, *J. Appl. Phys.*, 1993, **73**, 2301.
18. A. P. Peter, L. Carbonell, M. Schaekers, C. Adelmann, J. Meersschaut, A. Franquet, O. Richard, H. Bender, T. Zsolt and S. van Elshocht, *Intermetallics*, 2013, **34**, 35.
19. Y.-L. Chao, Y. Xu, R. Scholz and J. C. S. Woo, *IEEE Electron Device Lett.*, 2006, **27**, 549.
20. J. P. Doyle, B. G. Svensson and M. O. Aboelfotoh, *J. Appl. Phys.*, 1996, **80**, 2530.
21. S. Oktyabrsky, M. O. Aboelfotoh, J. Narayan and J. M. Woodall, *J. Electron. Mater.*, 1996, **25**, 1662.
22. M. O. Aboelfotoh, M. A. Borek and J. Narayan, *Appl. Phys. Lett.*, 1999, **75**, 3953.
23. J. Wang, S. Jin, C. Leinenbach and A. Jacot, *J. Alloys Compd.*, 2010, **504**, 159.
24. A. P. Alivisatos, *J. Phys. Chem.*, 1996, **100**, 13226.
25. S. C. Tjong and H. Chen, *Mater. Sci. Eng., R*, 2004, **45**, 1.
26. T. Castro, R. Reifenberger, E. Choi and R. Andres, *Phys. Rev. B*, 1990, **42**, 8548.
27. P. Buffat and J.-P. Borel, *Phys. Rev. A*, 1976, **13**, 2287.
28. R. D. Beck, P. St. John, M. L. Homer and R. L. Whetten, *Science*, 1991, **253**, 879.
29. T. P. Martin, U. Näher, H. Schaber and U. Zimmermann, *J. Chem. Phys.*, 1994, **100**, 2322.
30. P. Nath and K. L. Chopra, *Thin Solid Films*, 1979, **58**, 339.
31. P. Nath, V. Dutta and K. L. Chopra, *Thin Solid Films*, 1979, **64**, 65.
32. S. Gaudet, C. Detavernier, A. J. Kellock, P. Desjardins and C. Lavoie, *J. Vac. Sci. Technol. A*, 2006, **24**, 474.
33. S. Dhar and V. N. Kulkarni, *Thin Solid Films*, 1998, **333**, 20.
34. S. Das and T. L. Alford, *Appl. Phys. Lett.*, 2013, **103**, 094104.
35. A. Kumar, A. Saxena, A. De, R. Shankar and S. Mozumdar, *RSC Adv.*, 2013, **3**, 5015.
36. M. Blosi, S. Albonetti, M. Dondi, C. Martelli and G. Baldi, *J. Nanoparticle Res.*, 2011, **13**, 127.
37. F. Petraki, V. Papaefthimiou and S. Kennou, *Org. Electron.*, 2007, **8**, 522.
38. D. Deng, Y. Jin, Y. Cheng, T. Qi and F. Xiao, *ACS Appl. Mater. Interfaces*, 2013, **5**, 3839.

39. J. Zhang, Y. Yuan, X. Xu, X. Wang and X. Yang, *ACS Appl. Mater. Interfaces*, 2011, **3**, 4092.
40. M. Grouchko, A. Kamyshny and S. Magdassi, *J. Mater. Chem.*, 2009, **19**, 3057.
41. N. A. Dhas, C. P. Raj and A. Gedanken, *Chem. Mater.*, 1998, **10**, 1446.
42. S. Panigrahi, S. Kundu, S. K. Ghosh, S. Nath, S. Praharaj, S. Basu and T. Pal, *Polyhedron*, 2006, **25**, 1263.
43. L. Guan, H. Pang, J. Wang, Q. Lu, J. Yin and F. Gao, *Chem. Commun.*, 2010, **46**, 7022.
44. A. Martucci, G. Brusatin and M. Guglielmi, *J. Sol-Gel Sci. Technol.*, 1998, **13**, 535.
45. U. Schubert and N. Hüsing, *Synthesis of Inorganic Materials*, Wiley, Weinheim, 3rd edn, 2012.
46. Y. Son, M. Park, Y. Son, J. S. Lee, J. H. Jang, Y. Kim and J. Cho, *Nano Lett.*, 2014, **14**, 1005.
47. J. Wirringa, R. Wartchow and M. Binnewies, *Z. Anorg. Allg. Chem.*, 2000, **626**, 1473.

Chapter 4:

1. U. Resch-Genger, M. Grabolle, S. Cavaliere-Jaricot, R. Nitschke and T. Nann, *Nat. Methods*, 2008, **5**, 763.
2. R. Hardman, *Environ. Health Perspect.*, 2006, **114**, 165.
3. L. Ruizendaal, S. Bhattacharjee, K. Pournazari, M. Rosso-Vasic, L. H. J. de Haan, G. M. Alink, A. T. M. Marcelis and H. Zuilhof, *Nanotoxicology*, 2009, **3**, 339.
4. N. H. Alsharif, C. E. Berger, S. S. Varanasi, Y. Chao, B. R. Horrocks and H. K. Datta, *Small*, 2009, **5**, 221.
5. D. J. Bharali, D. W. Lucey, H. Jayakumar, H. E. Pudavar and P. N. Prasad, *J. Am. Chem. Soc.*, 2005, **127**, 11364.
6. F. Wang and X. Liu, *J. Am. Chem. Soc.*, 2008, **130**, 5642.
7. M. Dasog, G. B. De los Reyes, L. V. Titova, F. a. Hegmann and J. G. C. Veinot, *ACS Nano*, 2014, doi: 10.1021/nn504109a.
8. M. A. Borek, S. Oktyabrsky, M. O. Aboelfotoh and J. Narayan, *Appl. Phys. Lett.*, 1996, **69**, 3560.
9. L. Krusin-Elbaum and M. O. Aboelfotoh, *Appl. Phys. Lett.*, 1991, **58**, 1341.
10. L. J. V. d. Pauw, *Philips Res. Rep. B*, 1958, **13**, 1.